UNIVERSITÉ DE SHERBROOKE
Faculté de génie
Département de génie mécanique

Le développement d'une méthode hybride pour accélérer les études paramétriques de systèmes vibroacoustiques plats et courbes avec un traitement acoustique attaché

Thèse de doctorat
Spécialité : génie mécanique

Kamal KESOUR

Sherbrooke (Québec) Canada

Juillet 2019

MEMBRES DU JURY

Noureddine ATALLA

Directeur

Raymond PANNETON

Évaluateur

Alain BERRY

Évaluateur

Luca ALIMONTI

Évaluateur

Andrea PARRINELLO

Évaluateur

RÉSUMÉ

Le bruit est devenu une partie intégrante de notre vie quotidienne, au point où il peut affecter notre santé et notre bien-être. C'est particulièrement vrai dans les différents secteurs de transport tels que l'automobile, le ferroviaire et l'aviation. Dans ces conditions, la méthode la plus pratique et la plus économique pour améliorer le confort acoustique consiste à modifier le trajet de propagation des ondes sonores et vibratoires en utilisant des composants dissipatifs placés entre la structure (p. ex. le fuselage) et la cavité acoustique (p. ex. la cabine). Ces composants dissipatifs, appelés traitement acoustique (TA), impliquent souvent des couches de matériaux poroélastiques qui ont d'excellentes performances acoustiques en hautes fréquences. Cependant, cette capacité d'absorption du son et des vibrations diminue considérablement dans la gamme des basses fréquences à cause de la longueur d'onde acoustique. Par conséquent, au début du processus de conception, des simulations numériques et des études paramétriques sont nécessaires pour identifier la configuration optimale de la multicouche acoustique. Les outils numériques traditionnels utilisés à ce stade manquent de précision (si l'efficacité est visée) ou sont prohibitifs sur le plan computationnel (si la précision est plutôt visée).

Récemment, un modèle hybride qui combine la flexibilité et la précision de la méthode des éléments finis (FEM) ainsi que l'efficacité et la précision de la méthode des matrices de transfert (TMM) a été présenté par Alimonti et al. Au cours de cette étude, un modèle qui permet de tenir compte de la réaction non locale des TA a été proposé, permettant ainsi de surmonter les limites des modèles à réaction locale. Cette méthode a montré sa précision, en particulier si le TA est modélisé comme fluide équivalent, ainsi que son efficacité face à la méthode FEM. Dans ce contexte, après une étude de la validité de la méthode, la présente thèse propose une extension pour des traitements et structures complexes (p. ex. structures courbes, cylindres...) tout en permettant de faciliter et d'accélérer avec une précision acceptable les études paramétriques lors de la phase de conception. La méthode développée utilise la procédure *Patch Transfer Functions* afin de coupler efficacement, à travers des surfaces élémentaires, les sous-domaines d'un système vibroacoustique donné. La présente technique est d'abord validée dans le cas de la transmission sonore à travers une structure plane où deux types de TA sont considérés. Ensuite, deux études paramétriques, utilisant le rayon de courbure de la structure et l'épaisseur du TA comme paramètres, sont réalisées afin d'évaluer l'effet de la courbure du TA sur la précision des modèles TMM classique. Par la suite, une extension du modèle TMM à réaction non locale pour les traitements acoustiques cylindriques est proposée et validée dans le cas d'un cylindre excité par une force ponctuelle. Finalement, une approche basée sur les éléments finis ondulatoires est proposée afin de prédire la perte par transmission à travers des structures multicouches périodiques. Cette approche permet de surmonter le caractère individuel et les expressions algébriques complexes utilisées dans le développement des modèles analytiques ainsi que d'exploiter la flexibilité de la méthode FEM.

Mots-clés : FEM, TMM, PTF, transmission, traitement acoustique, courbe, cylindre, cellule unitaire périodique.

À ma mère, à mon père
Tout est toujours parfait...

REMERCIEMENTS

Je tiens à exprimer mes sincères remerciements et ma gratitude à mon directeur de recherche, professeur Noureddine Atalla, pour m'avoir accordé sa confiance, pour m'avoir guidé, conseillé, soutenu et encouragé au cours de ces quatre dernières années. Je vous remercie aussi pour votre patience.

Je voudrais remercier les professeurs Raymond Panneton et Alain Berry d'avoir accepté d'évaluer ce travail. J'aimerais aussi remercier Luca Alimonti pour ses conseils si précieux et d'avoir accepté d'évaluer ce travail. Je remercie également Andrea Parrinello d'avoir accepté d'évaluer le présent ouvrage et pour les discussions et les commentaires pertinents sur la dernière partie de cette thèse.

Je tiens à remercier tous les membres du Groupe d'acoustique et vibrations de l'Université de Sherbrooke (GAUS) que j'ai rencontrés au cours de ces quatre années, particulièrement Ahmed Abbad, Farouk Maâboudalah, Karim Masmoudi, Raef cherif, Celse Kafui Amédin pour leurs amitiés et aides si précieuses.

À titre plus personnel, je remercie chaleureusement mes amis Othmane, Firdaous, Yassine, Said, Heidi, Patricia pour leur gentillesse, leur aide et leur humour. Je remercie aussi Eugénie et Sam pour les bons moments partagés (incluant le pain aux bananes).

Un remerciement spécial à mes parents, ma soeur, mes frères et toute ma famille pour leur soutien inconditionnel et leur patience sans limites tout au long de mes études doctorales.

Je remercie aussi mes beaux-parents pour leurs soutien et encouragement pendant ces quatre années.

Enfin toute cette aventure n'aurait pas été pareille sans Rose, ma chère et tendre épouse. Je te remercie d'avoir été à mes côtés, de m'avoir écouté et de m'avoir encouragé pendant toutes ces années.

TABLE DES MATIÈRES

LISTE DES FIGURES

LISTE DES TABLEAUX

LISTE DES ACRONYMES

Acronyme	**Définition**
PTF	Patch Transfer Functions
FEM	Finite Element Method
BEM	Boundary Element Method
WFEM	Wave and Finite Element Method
TMM	Transfer Matrix method
NLR-TMM	Non Locally Reacting Transfer Matrix Model
LR-TMM	Locally Reacting Transfer Matrix Model
GF	Green Functions
SP	Sound Package
NCT	Noise Control Treatment
TA	Traitement Acoustique

CHAPITRE 1

INTRODUCTION

Ce chapitre présente le contexte, les motivations et les enjeux de ce projet de recherche. Dans un premier temps, le contexte industriel et les motivations qui ont mené à ce projet sont présentés. Puis, la problématique scientifique est détaillée. Par la suite, les objectifs de ce projet ainsi que les contributions originales de la présente thèse sont listés. Enfin, ce chapitre se termine par un aperçu de l'organisation de la thèse.

1.1 Contexte industriel

Le bruit est devenu une partie intégrante de notre vie quotidienne, au point qu'il peut affecter notre santé et notre bien-être. C'est particulièrement vrai dans les différents secteurs de transport tels que l'automobile, le ferroviaire et l'aviation. Les industries du transport ont donc une multitude d'enjeux à relever : créer des moyens de transport qui prennent en compte le confort acoustique de ses passagers tout en permettant une mobilité écoresponsable. Pour réduire la consommation de carburant, exigée par les réglementations sur les émissions de gaz à effet de serre de plus en plus restrictives, les industries optent pour une conception légère de leurs véhicules. Ce type de conception peut entraîner des niveaux sonores intérieurs plus élevés et ainsi nuire au confort acoustique des passagers. De plus, dans de nombreux cas, l'atténuation du bruit à la source n'est pas envisageable. Dans ces conditions, la méthode la plus pratique et la plus économique pour améliorer le confort acoustique consiste à modifier le trajet de propagation des ondes sonores et vibratoires en utilisant des composants dissipatifs placés entre la structure (p. ex. le fuselage) et la cavité acoustique (p. ex. la cabine).

Ces composants dissipatifs, appelés traitement acoustique, traitement phonique ou traitement de contrôle du bruit, impliquent souvent des couches de matériaux poroélastiques qui ont d'excellentes performances acoustiques en hautes fréquences. Cependant, cette capacité d'absorption du son et des vibrations diminue considérablement dans la gamme des basses fréquences à cause de la longueur d'onde acoustique. Par conséquent, au début du processus de conception, des études paramétriques utilisant des simulations numériques sont nécessaires pour identifier la configuration optimale du traitement phonique. Les outils numériques traditionnels utilisés à ce stade, dans l'industrie, manquent de précision

(si l'efficacité est visée) ou sont prohibitifs sur le plan computationnel (si la précision est plutôt visée). De plus, les traitements acoustiques peuvent avoir différentes géométries (planes, courbes ou cylindriques) dépendamment de l'application souhaitée. En parallèle, les attentes des passagers sont en constante évolution et la durée de développement de produit est de plus en plus courte à cause de la concurrence et de la libération des marchés. Pour ces raisons, le développement d'un nouveau modèle d'études paramétriques, capable de répondre aux exigences de l'industrie en matière d'efficacité, de précision et de complexité est nécessaire. Le développement d'un tel modèle est la principale préoccupation de la présente thèse.

1.2 Problématique scientifique

L'intégration anticipée des traitements acoustiques dans le processus de conception est la clé pour un produit réussi. Il est donc important d'optimiser ces traitements, en particulier par l'agencement de multicouche. L'optimisation de leurs performances acoustiques nécessite une prédiction précise et rapide des indicateurs vibratoires et acoustiques des systèmes vibroacoustiques impliquant des structures, des cavités et des matériaux d'insonorisation sous différents types d'excitation (mécanique, acoustique et aérodynamique). D'une part, la méthode classique des éléments finis (FEM), possiblement couplée à la méthode des éléments de frontière, a prouvé sa fiabilité et sa précision dans des problèmes industriels réels. Cependant, ce type de méthode pourrait conduire à des modèles numériques importants en raison du grand nombre de degrés de liberté requis pour capturer avec précision le comportement dynamique du traitement acoustique (TA). Un maillage très fin est nécessaire parce que le TA implique généralement des matériaux très dissipatifs qui se caractérisent par des courtes longueurs d'ondes. De plus, une phase de maillage est requise pour chaque configuration du TA testé. Ce type de méthodologie nécessite une description détaillée de la géométrie ainsi que la définition des conditions aux limites qui peuvent être inconnues. D'autre part, la méthode analytique des matrices de transfert (TMM) est souvent préférée grâce à son efficacité et sa facilité d'utilisation. Toutefois, la TMM peut manquer de précision en raison des simplifications et des hypothèses inhérentes de son cadre analytique. Par conséquent, des outils numériques simplifiés et plus pratiques pour modéliser les systèmes vibroacoustiques complexes arbitraires sont nécessaires.

Récemment, un modèle hybride FEM-TMM qui combine la flexibilité et la précision de la méthode des éléments finis ainsi que la simplicité et l'efficacité de la méthode des matrices de transfert a été présenté par Alimonti et coll. [4]. Au cours de cette étude, un modèle qui permet de tenir compte de la réaction non locale des TA a été proposé, permettant ainsi de

surmonter les limites des modèles à réaction locale. Les auteurs ont démontré la précision de cette méthode, en particulier si le traitement phonique est modélisé comme fluide équivalent, ainsi que son efficacité face à la méthode FEM. Toutefois, l'utilisation de la TMM est basée sur l'introduction d'hypothèses fortes. En effet, le traitement de contrôle de bruit est supposé être (i) plat, (ii) homogène et (iii) latéralement infini. D'ailleurs, seulement l'effet de l'hypothèse (iii) sur la précision du modèle proposé a été étudié. Aussi, l'état de l'art a révélé que la méthode de sous-structuration *patch transfer functions* (PTF), permet de réduire considérablement les degrés de liberté du système vibroacoustique couplé. Ainsi, l'intégration de la méthode hybride FEM-TMM dans un cadre PTF permettra d'accélérer la résolution des systèmes vibroacoustiques couplés.

En conséquence, la motivation principale de la présente thèse est de développer une méthode hybride FEM-TMM dans un cadre PTF pour prédire le comportement dynamique de systèmes vibroacoustiques plats, courbes et cylindriques avec un traitement acoustique attaché. De plus, une attention particulière est dédiée à l'effet des hypothèses simplificatrices de la TMM sur la précision de la méthodologie FEM-TMM dans un cadre PTF.

1.3 Originalités

La principale originalité de ce projet de recherche est le développement et la validation d'une méthode hybride FEM-TMM-PTF de prédiction du comportement dynamique des systèmes vibroacoustiques plats, courbes et cylindriques avec un traitement acoustique attaché. Ceci permet d'accélérer les études paramétriques avec une précision acceptable et répondre ainsi à la réalité industrielle en termes de complexité géométrique.

La première originalité se manifeste par la combinaison des modèles des éléments finis des sous-systèmes maitres (structure et la cavité acoustique) avec un modèle TMM à réaction non locale du traitement phonique dans le cadre d'une procédure PTF.

La deuxième originalité est l'adaptation du modèle TMM à réaction non locale pour des traitements phoniques à géométrie courbe et cylindrique.

La troisième originalité est l'amélioration de l'efficacité du modèle TMM à réaction non locale permettant ainsi d'améliorer les performances de la méthode hybride FEM-TMM-PTF. Ceci est réalisé à travers l'intégration d'un critère de troncature dynamique permettant de considérer seulement les sources ayant une contribution significative à la réponse dynamique du traitement acoustique.

Finalement, la quatrième originalité consiste dans le développement d'un modèle basé sur les éléments finis ondulatoires pour prédire la transmission acoustique à travers des structures cylindriques multicouches.

1.4 Objectifs

L'objectif général de ce projet consiste à développer, implémenter et valider numériquement une méthode hybride FEM-TMM dans un cadre PTF pour les études paramétriques de systèmes vibroacoustiques plats, courbes et cylindriques avec un traitement acoustique attaché. Afin d'atteindre notre objectif général, nous organiserons notre travail autour de sept objectifs spécifiques :

1. Réaliser une revue de littérature sur les modèles numériques existants et évaluer le potentiel de la procédure PTF.
2. Valider la méthode FEM dans un cadre PTF et étudier la convergence de la procédure PTF dans le cas d'un système vibroacoustique plat ou courbe.
3. Valider la méthode hybride FEM-TMM dans un cadre PTF dans le cas d'un système vibroacoustique plat ou courbe.
4. Évaluer l'effet de la courbure du TA sur la précision des modèles basés sur la TMM.
5. Évaluer l'effet de l'épaisseur d'un TA courbe sur la précision des modèles basés sur la TMM.
6. Étendre le modèle TMM à réaction non locale à des traitements acoustiques cylindriques.
7. Proposer un critère de troncature pour améliorer l'efficacité du modèle TMM à réaction non locale.

1.5 Plan du document

Cette thèse est constituée de sept chapitres, soit une introduction, cinq chapitres et une conclusion générale. Les chapitres 3 et 4 sont des articles de journaux qui sont publiés ou soumis pour publication dans le cadre de ce projet de doctorat. Les chapitres 5 et 6 sont des articles de journaux en cours de soumission.

Le premier chapitre permet de situer le contexte de ce projet de recherche et de présenter ses motivations et ses enjeux. Le deuxième chapitre s'intéresse à l'état de l'art sur les méthodes existantes concernant la modélisation des systèmes vibroacoustiques avec un traitement acoustique en basses fréquences.

Le troisième chapitre contient les développements reliés aux objectifs spécifiques 2 et 3 dans le cas d'un système vibroacoustique plat. D'abord, le cadre théorique de la procédure PTF est présenté ainsi que celui des modèles basés sur la TMM, à savoir le modèle à réaction locale (LR-TMM) et le modèle à réaction non locale (NLR-TMM). Ensuite, la convergence de la procédure PTF est étudiée. La précision de la méthodologie FEM-TMM dans un cadre PTF est évaluée pour les problèmes de transmission acoustique à travers des structures planes à parois simple et double avec deux différents traitements de contrôle du bruit. Les résultats obtenus sont systématiquement comparés à trois modèles, à savoir les stratégies directes des FEM / BEM, et à deux approches de sous-structuration basées sur la modélisation du traitement acoustique par (i) le modèle LR-TMM et (ii) un modèle éléments finis. La méthode proposée est analysée pour voir si elle permet de prédire avec précision et efficacité le comportement dynamique des systèmes vibroacoustiques plats avec un traitement acoustique.

Le quatrième chapitre contient les développements reliés aux objectifs spécifiques 2, 3, 4 et 5 dans le cas d'un système vibroacoustique courbe. Dans un premier temps, le cadre théorique de la procédure PTF est présenté ainsi que celui des modèles LR-TMM et NLR-TMM. Ensuite, la convergence de la procédure PTF est étudiée. Puis, deux études paramétriques utilisant le rayon de courbure et l'épaisseur du traitement acoustique comme paramètres sont réalisées afin d'évaluer leurs effets sur la validité des modèles de la TMM.

Le cinquième chapitre propose une extension du modèle NLR-TMM à des traitements acoustiques cylindriques (objectif spécifique 6). Un critère de troncature pour améliorer l'efficacité du modèle NLR-TMM est présenté (objectif spécifique 7). Une coque cylindrique avec un traitement acoustique excitée par une force ponctuelle et couplée à une cavité acoustique est utilisée afin de valider le modèle proposé. Le NCT est constitué d'une couche de mousse de mélamine et d'une masse lourde. Les résultats sont systématiquement comparés à un modèle FEM exact. Dans les cas considérés, une attention particulière est portée à l'hypothèse selon laquelle le traitement acoustique est supposé plat, ce qui aurait potentiellement un effet négligeable sur la précision du modèle proposé.

Le sixième chapitre présente une approche différente pour calculer la transmission acoustique à travers des structures cylindriques multicouches. En effet, ce chapitre présente le développement et la validation d'un modèle basé sur les éléments finis ondulatoires (WFEM). Le modèle est validé avec des méthodes analytiques présentes dans la littérature dans le cas de la combinaison d'un cylindre infini avec un coeur en polymère et un coeur en matériau poroélastique (en mode sandwich). Ensuite, une étude sur l'effet du couplage entre le coeur poroélastique et les deux peaux du sandwich est présentée sous

une excitation en onde plane oblique et sous un champ diffus. L'approche développée permet de surmonter le caractère individuel et les expressions algébriques complexes utilisées dans le développement des modèles analytiques ainsi que d'exploiter la flexibilité de la méthode FEM.

Finalement, une conclusion générale sera présentée dans le septième chapitre, suivie des perspectives qui peuvent généraliser les différentes approches exposées dans la présente thèse.

CHAPITRE 2

État de l'art

Ce chapitre traite de l'état de l'art concernant les ouvrages scientifiques de référence sur lesquels s'appuient les travaux de ce projet de recherche. Les matériaux poroélastiques sont présentés, suivis par les méthodes existantes concernant la modélisation des systèmes vibroacoustiques. Ces derniers sont listés par type d'approche : analytique, numérique et hybride.

2.1 Les matériaux poroélastiques

Les matériaux poroélastiques présentent une solution passive largement utilisée pour la réduction du bruit grâce à leur efficacité acoustique et la faible masse ajoutée. Ces matériaux se composent, selon une description macroscopique, d'une phase solide formant le squelette du matériau et d'une phase fluide qui sature son réseau de pores. Dans notre cas, la phase fluide est de l'air. Comme le montre la figure 2.1, il existe deux types de pores : ceux qui correspondent aux pores fermés emprisonnés dans le squelette et ceux qui sont reliés entre eux, appelés pores ouverts. Le premier type, d'un point de vue mécanique, fait partie intégrante du squelette. Les bonnes performances acoustiques des matériaux poroélastiques proviennent des mécanismes de dissipation suivants : (i) les pertes visqueuses dues aux phénomènes d'interactions fluide-structure au niveau des pores (frottement de l'air contre le squelette), (ii) les effets de couplage thermique entre les deux phases (absorption de l'excès de chaleur du fluide par le squelette) et (iii) l'amortissement structural du squelette.

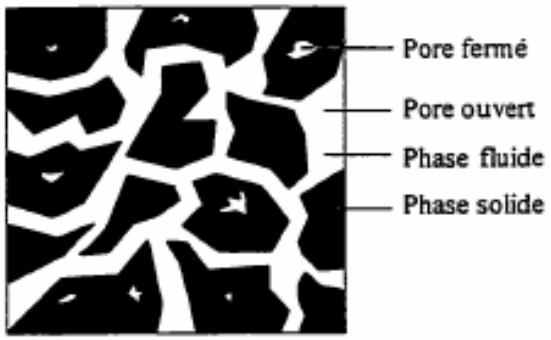

Figure 2.1 Composantes d'un matériau poreux[63]

Au cours des 70 dernières années, la nature multiphysique et la microgéométrie complexe des matériaux poreux ont fait l'objet d'une attention particulière donnant naissance à leur théorie actuelle. Les principaux fondements de la théorie de modélisation mathématique des matériaux poreux ont été introduits par Biot en 1956 [13, 14, 15]. Il a supposé l'existence d'un volume élémentaire représentatif, suffisamment petit devant la longueur d'onde des différentes ondes pouvant se propager dans le matériau. À travers cette description macroscopique, la théorie de Biot permet de prendre en compte les mécanismes de dissipation énumérés ci-dessus. La théorie de Biot considère la propagation de trois ondes le long du milieu poroélastique, à savoir deux ondes de compression et de cisaillement dans la phase solide et une onde de compression dans la phase fluide. Depuis son apparition, la théorie proposée par Biot a été améliorée et de nos jours, elle est largement utilisée pour décrire la propagation des ondes dans un matériau poroélastique.

Parmi les améliorations importantes apportées à la théorie de Biot, on trouve une nouvelle description des effets visqueux proroposée par Johnson et al. [37]. Ils ont introduit une longueur caractéristique visqueuse tenant compte de la dépendance fréquentielle des effets visqueux. De la même manière, Champoux et Allard [21] ont introduit une longueur caractéristique thermique qui tient compte de la dépendance fréquentielle des effets thermiques. En 1997, Lafarge et al. [47] ont introduit une nouvelle constante dans la formulation de l'expression du module de compression dynamique. Cette constante, nommée la perméabilité thermique statique, permet une modélisation encore plus précise des échanges thermiques entre le squelette et la phase fluide, en particulier dans les basses fréquences. Le modèle de Johnson-Champoux-Allard reste le plus utilisé par la communauté scientifique ainsi que par le secteur industriel. Pour une documentation complète de la théorie moderne de la poro-élasticité et son application au contrôle passif du bruit, le lecteur peut consulter l'ouvrage d'Allard et Atalla [8].

Le modèle de Biot permet une description rigoureuse et complète de la propagation des ondes acoustiques dans un milieu poroélastique. Cependant, son utilisation dans un code éléments finis nécessite des ressources informatiques importantes. La recherche de modèles optimaux (fiables et à faible cout) a mené les chercheurs à développer des approches simplifiées. Dans ce contexte, le modèle de Biot se réduit, dans le cas où le squelette peut être considéré comme rigide ou mou (*Limp*), à un fluide équivalent.

2.2 Méthodes de modélisation des matériaux poroélastiques en vibroacoustique

Dans cette partie, les méthodes les plus répandues de modélisation des systèmes vibroacoustiques avec des traitements phoniques en basses fréquences sont présentées. La première, l'approche analytique, est préférée au stade de la conception. La deuxième, numérique, est dédiée aux systèmes complexes à géométrie quelconque. Quant à la dernière, la méthode hybride, elle présente un compromis des deux précédentes méthodes.

2.2.1 Méthodes analytiques

Les méthodes analytiques présentent une alternative largement préférée durant le stade de conception grâce à leurs efficacités. À ce stade, les méthodes analytiques sont utilisées pour optimiser les performances acoustiques des structures multicouches à travers des études paramétriques à cout négligeable sur une large bande de fréquences. En dépit de son efficacité, cette classe de méthodes implique généralement l'introduction d'hypothèses fortes afin de faciliter la modélisation.

Dans le contexte de la méthode des matrices de transfert (TMM) [8], le système multicouche est supposé (i) homogène, (ii) plat et (iii) latéralement infini. La méthode TMM est valable sous l'hypothèse d'une onde plane. La matrice de transfert de chaque couche, dite locale, est obtenue en exprimant le vecteur des variables (défini à l'extrémité supérieure de la multicouche) en fonction du même vecteur (défini à l'extrémité inférieure de la multicouche). Ensuite, la matrice de transfert globale est calculée par multiplication des matrices locales obtenues en exprimant la continuité des contraintes et des vitesses dans chaque interface. La TMM est souvent employée pour prédire avec simplicité et efficacité les coefficients de transmission et d'absorption des structures multicouches.

Parmi les améliorations de la TMM, Rhazi et al. [73] ont proposé une correction de la taille finie pour étendre sa validité aux basses fréquences. Plus tard, une extension de cette méthode aux matériaux hétérogènes a été développée par Verdière et al. [81]. La matrice de transfert résultante de l'ensemble parallèle est également une matrice carrée de dimension 2×2 et donc elle peut être assemblée en série avec la TMM classique. Malgré que cette méthode est limitée à des stratifiés plats, elle est utilisée pour caractériser des traitements acoustiques à géométrie courbe. Ces derniers sont déroulés, considérés comme plats avec des dimensions équivalentes et utilisés pour alimenter les modèles basés sur l'approche de l'analyse statistique énergétique (SEA) [72].

En 2018, Coguenanff et Duval [25] ont proposé une matrice de transfert cylindrique en se basant sur plusieurs travaux antérieurs [54, 55]. La méthode est évaluée dans le cas d'un demi-cylindre avec un traitement phonique attaché. Ces résultats ont été comparés, en termes de perte par insertion, à ceux de la méthode des éléments finis et ceux obtenus par la mesure. Cette comparaison a montré une corrélation acceptable avec la méthode FEM/BEM sur une bande fréquentielle allant de 500 Hz jusqu'à 2500 Hz. Cette approche prometteuse devrait remplacer la TMM classique pour la modélisation du traitement phonique courbe dans le cadre de la méthode SEA. Toutefois, la méthode TMM reste non adaptée à la gamme des basses fréquences et aux excitations mécaniques à cause des hypothèses inhérentes liées à sa formulation analytique. Par conséquent, des modèles déterministes plus précis sont classiquement nécessaires dans la gamme des basses fréquences à cause du caractère modal des systèmes vibroacoustiques.

2.2.2 Méthodes numériques

Les méthodes numériques ont fait l'objet d'une grande attention grâce à leur aptitude à prédire le comportement dynamique de systèmes vibroacoustiques de forme quelconque. Elles sont largement utilisées dans l'industrie pour des applications vibroacoustiques. Parmi les méthodes numériques de discrétisation, il y a la méthode des éléments finis (FEM) et la méthode des éléments de frontière (BEM) qui sont principalement destinées à la modélisation des systèmes vibroacoustiques.

La principale différence entre ces deux approches se manifeste par le fait que la FEM nécessite une discrétisation de volume, tandis que la BEM requiert une discrétisation surfacique à cause des fonctions de Green (solution fondamentale) utilisées dans sa formulation. Bien que cela se traduit par une réduction de la taille des problèmes à résoudre, l'utilisation de la BEM devient plus avantageuse seulement dans le cas de problèmes impliquant de larges cavités ou pour des problèmes de rayonnement dans des domaines extérieurs non bornés. Cette limitation est expliquée par le cout de calcul des intégrales impliquées dans sa formulation. Pour cette raison, la méthode FEM est généralement préférée quant à la prédiction de la réponse dynamique des problèmes vibroacoustiques intérieurs (incluant des traitements phoniques).

Toutefois, l'utilisation de la méthode FEM pour la modélisation des matériaux poroélastiques peut s'avérer, même si elle est précise, très couteuse sur le plan computationnel. Cette limitation peut être justifiée par deux raisons. La première se traduit par l'utilisation du modèle de Biot pour obtenir une bonne précision [64] pour des configurations phoniques générales sur une large bande fréquentielle. De plus, leur modélisation avec la

formulation mixte ($u,\ p$) [11, 10] nécessite quatre degrés de liberté (DOFs) par noeud bien qu'elle soit plus efficace par rapport à d'autres formulations (p. ex. la formulation basée sur les déplacements [65]). La deuxième raison se manifeste par le besoin d'une discrétisation plus fine pour obtenir des résultats fiables. Ceci est dû aux longueurs d'onde courtes et aux mécanismes de dissipation ayant lieu à l'intérieur des matériaux poroélastiques. Dans cette classe de modélisation, un grand nombre de DOFs est nécessaire pour capturer la dynamique des traitements phoniques. Ce qui rend la modélisation des problèmes vibroacoustiques industriels incluant des traitements phoniques prohibitive sur le plan computationnel voir irréalisable malgré le progrès informatique.

Dans le but de trouver un compromis entre la complexité des phénomènes et la fiabilité ainsi que l'efficacité de la méthode, plusieurs formulations ont été proposées. Cependant, la méthode de sous structuration proposée par Hamdi et al. [36] reste la plus utilisée. Les traitements de contrôle du bruit sont tenus en compte dans un modèle éléments finis par des impédances d'interface. Ces impédances contiennent la masse, l'amortissement et la raideur ajoutés au système par le traitement acoustique. Une telle approche permet de réduire le nombre de degrés de liberté du système d'équations couplées en considérant que les DOFs des domaines structural et acoustique. Cependant, le calcul des impédances d'interface par un modèle EF complet, même s'il fournit de bons résultats en termes de précision, reste très couteux en termes de charge de calcul.

2.2.3 Méthodes hybrides

Des approches hybrides ont été proposées afin de surmonter les couts engendrés par l'utilisation de la FEM pour la modélisation des traitements phoniques. Dans un cadre éléments finis, des impédances acoustiques d'interfaces [49, 29], à cout négligeable, tenant compte de l'effet dynamique du traitement phonique peuvent être ajoutées à la surface acoustique traitée des domaines structuraux et acoustiques (c.-à-d. la structure principale et la cavité). Généralement, l'impédance d'interface est mesurée en testant un échantillon du traitement acoustique dans le tube de Kundt. D'une part, cette approche présente l'avantage de simplifier la modélisation et d'éviter l'identification des paramètres mécaniques et acoustiques du traitement acoustique. D'autre part, elle suppose implicitement que le comportement du traitement de contrôle du bruit est local, ce qui signifie que l'impédance du traitement multicouche ne dépend que des valeurs locales du déplacement et de la pression. Ce qui rend cette approche inapplicable aux traitements acoustiques pratiques (p. ex. traitement de type masse-ressort, multicouche ...).

Dans le même contexte, les méthodes hybrides éléments finis - matrice de transfert (FEM-TMM) ont été développées pour offrir un modèle analytique simple du traitement phonique. L'utilisation de la méthode TMM est soutenue par les courtes longueurs d'onde et aux mécanismes de dissipation élevés impliqués dans les traitements acoustiques malgré que les hypothèses d'un système plat et latéralement infini ne puissent pas être vérifiées en basses fréquences. Les avantages d'une telle hybridation sont doubles. Le premier, une réduction considérable du temps de calcul des impédances d'interfaces et aussi une réduction du nombre de DOFs par rapport à une modélisation par éléments finis standards. Tandis que le deuxième réside dans la simplicité de la TMM où le traitement acoustique est considéré comme «une boite noire» (c.-à-d. la phase de maillage n'est plus nécessaire). Toutes ces raisons font de la méthode hybride FEM-TMM, une méthode très convenable à la phase de conception où la configuration optimale du traitement phonique est recherchée.

Peu d'attention a été accordée aux modèles hybrides FEM-TMM dans la littérature. En effet, selon leur modèle d'impédance, ils peuvent être classés en modèles à réaction locale ou non locale. D'une part, le premier modèle TMM à réaction locale (LR-TMM) utilisé dans le cadre de la FEM a été proposé par Tournour et al. [80]. Les impédances d'interfaces du traitement ont été caractérisées par la méthode TMM en considérant une excitation par onde plane en incidence normale. Cependant, ce modèle reste limité à une excitation par onde plane et à des traitements acoustiques monocouches. Dans ce contexte, récemment, Caillet et al. [20] ont proposé un modèle LR-TMM avec des coefficients ajustés pour estimer les impédances d'interfaces du traitement phonique. Le nombre d'ondes en flexion k_f de la structure a été utilisé pour obtenir l'impédance à l'interface structure-traitement, tandis que les impédances sur les interfaces restant sont moyennées en utilisant un nombre d'onde k entre 0 et k_0. Avec k_0 est le nombre d'ondes de l'air. L'utilisation d'un tel modèle a montré une amélioration significative en termes de précision par rapport au modèle LR-TMM classique. Cependant, cet ajustement dépend de la nature de l'excitation et du traitement acoustique considéré.

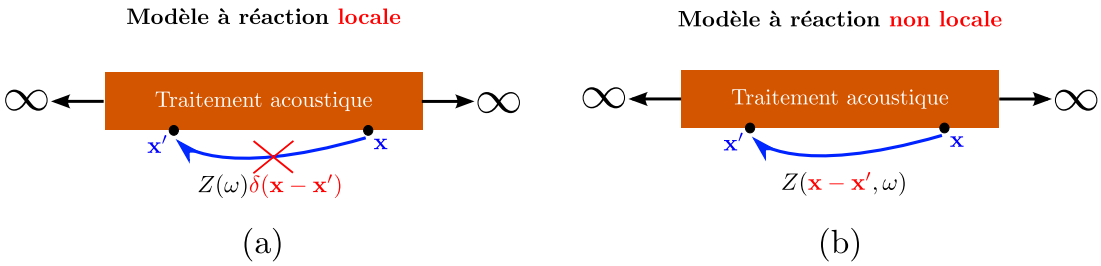

Figure 2.2 Impédance d'interface Z d'un traitement acoustique obtenue par un modèle TMM (a) à réaction locale et (b) à réaction non locale.

D'autre part, les modèles TMM à réaction non locale (NLR-TMM) nécessitent une formulation plus sophistiquée. Généralement, les impédances des interfaces sont considérées des fonctions de l'espace plutôt qu'une constante comme les modèles à réaction locale (voir Fig. 2.2). Shorter et al. [79] ont proposé un modèle qui prend en compte le comportement non local des traitements acoustiques. Elle a été appliquée pour une structure attachée à un traitement acoustique qui rayonne dans un domaine acoustique semi-infini. Cette approche suit la même méthodologie que celle proposée par Langley [48] pour le calcul de l'impédance en rayonnement d'une plaque non traitée. Ils ont utilisé une formulation intégrale faible d'un produit de convolution entre les sollicitations externes et des fonctions de Green (solutions fondamentales) dans le domaine du nombre d'ondes. Aussi, des fonctions de forme (pistons) ont été introduites pour approximer le déplacement à l'interface de la structure et du traitement acoustique. Ceci permet d'éviter le calcul exact de la transformée de Fourier inverse et par la suite d'augmenter l'efficacité du modèle proposé. Un autre modèle TMM à réaction non locale basé sur une approche intégrale similaire a été proposé par Courtois et al. [26], sauf que les fonctions de Green sont obtenues dans le domaine physique. Pour ce faire, la transformée de Fourier inverse est employée. Toutefois, cette méthodologie reste moins attrayante d'un point de vue numérique par rapport à une approche dans le domaine du nombre d'ondes. Ceci revient à l'utilisation de la transformée de Fourier inverse qui peut affecter et ralentir la convergence de l'approche proposée.

Récemment, Alimonti et al. [5, 6, 2, 3] ont proposé une méthode hybride FEM-TMM avec une étude théorique complète et détaillée sur son domaine de validité, sa précision et son efficacité par rapport à un modèle FEM des structures multicouches planes. Le modèle TMM à réaction non locale proposé permet d'obtenir les impédances du traitement phonique à ces deux faces (c.-à-d. aux interfaces avec le domaine structurel et acoustique) par le biais d'intégrales de convolution entre les perturbations externes et les fonctions de Green exprimées dans le domaine du nombre d'ondes. Les fonctions de Green sont estimées avec la TMM sous les hypothèses d'un traitement homogène, plat et latéralement infini. Les intégrales de convolutions bidimensionnelles sont réduites à des intégrales unidimensionnelles, sous la condition d'un traitement acoustique isotrope, en utilisant des fonctions de forme radialement symétriques. De plus, une correction de la taille finie basée sur la méthode des sources images (ISM) a été proposée et a montré, dans le cas d'un traitement phonique modélisé par un fluide équivalent, une précision comparable à celle de la méthode FEM. De plus, les auteurs ont proposé deux formulations basées sur les conditions de baffles aux deux extrémités latérales du traitement. Ils ont montré que les deux formulations sont équivalentes et que l'approche directe (celle qui ne demande pas d'inversion) doit être préférée. Ils ont constaté, dans une série d'articles, que leur modèle fournit une

amélioration considérable par rapport aux modèles à réaction locale trop simplifiés. En plus du gain en temps de calcul, le modèle proposé permet une simplification substantielle de l'intégration des traitements phoniques (un maillage tridimensionnel n'est plus nécessaire) dans les modèles par éléments finis. De plus, la méthode FEM-TMM développée par les auteurs est prometteuse.

2.2.4 Patch Transfer Functions

L'approche *Patch Transfer Functions* (PTF) est une procédure développée par Maxit et al. [58], à partir des travaux de Cacciolati et al. [19] sur les mobilités acoustiques. C'est une méthode de sous-structuration où chaque sous-système est considéré indépendamment. Les sous-systèmes sont considérés comme «une boite noire» et ils sont couplés à leurs interfaces commun à travers des surfaces élémentaires, appelées *patch*. Seules les variables/réponses normales moyennées sur les patchs sont considérées. Cette technique implique le calcul des matrices de mobilité ou d'impédance, appelées relations PTFs, de chaque sous-système. De plus, si le sous-système est excité, sa réponse découplée est également calculée. Une fois que les PTFs sont calculées, le couplage consiste à appliquer le principe de superposition à chaque sous-système et à écrire les relations de continuité entre les sous-systèmes aux surfaces de couplage en termes de la vitesse normale et de la pression.

L'approche PTF a été employée pour la caractérisation de plusieurs problèmes acoustiques et vibroacoustiques avec des traitements acoustiques. Morvan et al. [62] ont étudié sa convergence pour un problème acoustique incluant deux cavités. Ils ont conclu qu'une taille de patch supérieure à la moitié de la longueur d'onde acoustique est requise pour assurer sa convergence. La technique PTF a été utilisée par Chazot et al. [22, 23] et par Guyader et al. [35] pour prédire la perte par transmission dans le cas de l'air et d'un fluide équivalent remplissant la double paroi. L'impédance de rayonnement a été calculée efficacement par l'intégral de Rayleigh. Plus tard, Aucejo et al. [12] ont étudié la convergence de l'approche pour un problème de type plaque-cavité à couplage fort (c.-à-d. la cavité est remplie par de l'eau). Dans le même contexte, Maxit et al. [57] ont proposé une amélioration de l'approche pour accélérer sa convergence. Ils ont montré que la sous-structuration à l'extérieur du champ proche de la structure permet de réduire le nombre de patchs requis. Veronesi et al. [82] ont utilisé la technique PTF pour un système de type plaque-cavité avec un traitement phonique. Les PTFs du traitement acoustique ont été déterminées expérimentalement. Une telle méthode peut être d'une grande utilité, car les propriétés mécaniques et acoustiques du traitement acoustique n'ont plus besoin d'être caractérisées, surtout qu'elles peuvent être modifiées lors de l'assemblage. Afin d'améliorer

son efficacité, une méthode expérimentale réduite a été proposée par Albert et al. [1], où les PTFs sont déduites à partir des tests sur un seul patch. Toutefois, en pratique, ce type de méthodologie reste limité par la taille du patch qui contrôle sa convergence. Aussi, les effets non locaux peuvent être difficiles à mesurer en raison de la nature très dissipative du traitement acoustique, ce qui limite la précision de l'approche PTF expérimentale.

Cette technique modulaire permet un calcul indépendant des PTFs de chaque sous-système. Elle permet un calcul parallèle des relations PTFs. De plus, la caractérisation des sous-systèmes peut être réalisée à l'aide de la méthode la plus convenable : analytique, numérique (FEM, BEM,...) ou expérimentale. Elle conduit à des systèmes numériques symétriques pleins et de faibles dimensions, ce qui permet une résolution rapide du système final couplé. Finalement, elle peut faciliter et accélérer l'intégration des traitements acoustiques et par la suite l'identification de la configuration optimale dans un temps réduit.

2.3 Conclusion

D'un point de vue théorique, nous venons de voir que (1) l'approche analytique est facile à mettre en oeuvre et à appliquer, elle se base sur des hypothèses assez grossières ce qui limite sa validité en hautes fréquences. (2) La méthode FEM est d'une flexibilité et d'une précision remarquable, traitant ainsi des problèmes multiphysiques avec des géométries quelconques. Par contre, et comme nous l'avons fait remarqué dans la revue de la littérature, elle est très couteuse en termes de temps de calcul, surtout qu'elle requiert une phase précoce : le maillage. (3) La méthode hybride FEM-TMM, quant à elle, présente deux sous approches de modélisation du traitement acoustique :

- LR-TMM : elle est moins couteuse certes, mais peu fiable quant à la prédiction de la réponse dynamique des traitements acoustiques pratiques ;
- NLR-TMM : plusieurs études ont démontré le potentiel fort et le caractère attrayant de cette méthode ; non seulement par son temps de calcul qui est raisonnable, mais aussi pour sa simplicité et ses résultats pertinents dans le cas des systèmes plats.

(4) La PTF procède par la sous-structuration des systèmes. Le système couplé considère seulement les DOFs, la vitesse normale et la pression moyennés sur des surfaces élémentaires. Sa contribution principale réside dans la réduction considérable du nombre de DOFs du système couplé, ce qui rend cette technique attrayante, en particulier pour les problèmes de transmission acoustique.

L'ensemble des éléments bibliographiques nous ont permis de faire une synthèse globale de l'état actuel des techniques de modélisation des systèmes vibroacoustiques avec des traite-

ments acoustiques en basses fréquences, tout en mettant l'accent sur les inconvénients et le caractère ambitieux à développer de chaque méthode. C'est dans ce contexte que s'insère la présente thèse : le développement d'une méthode hybride pour accélérer les études paramétriques de systèmes vibroacoustiques plats, courbes et cylindriques avec un traitement acoustique attaché. Dans le cadre de l'approche proposée, la technique PTF est utilisée pour coupler efficacement les modèles éléments finis des domaines structuraux et acoustiques avec un modèle analytique TMM à réaction non locale du traitement acoustique. Dans le but d'ouvrir la voie à la conception et l'optimisation des traitements phoniques avec des modèles alliant précision, efficacité et flexibilité.

CHAPITRE 3

A hybrid patch transfer-Green functions method and its application to transmission through flat problems

Auteurs et affiliation :

K. Kesour : étudiant au doctorat, Université de Sherbrooke, Faculté de génie, Département de génie mécanique.

N. Atalla : professeur, Université de Sherbrooke, Faculté de génie, Département de génie mécanique.

Date d'acceptation : 4 mai 2018

État de l'acceptation : Version finale publiée

Revue : Journal of Sound and Vibration

Référence : [41]

Titre français : Une méthode hybride FEM-TMM-PTF pour résoudre les problèmes de transmission à travers des parois planes, simple et double, avec un traitement acoustique attaché.

Contribution au document : Dans cet article, d'abord, le cadre théorique de la méthode hybride, utilisant la technique de sous-structuration *patch transfer functions* pour coupler efficacement la méthode des éléments finis et la matrice de transfert, est présenté. Ensuite, la méthodologie est validée dans le cas de la transmission à travers des structures planes avec traitement acoustique.

Résumé français : Cet article présente et étudie les performances d'une méthode de sous-structuration basée sur la technique *patch transfer functions* (PTF) pour coupler efficacement la méthode des éléments finis des structures et des cavités à un modèle analytique à réaction non locale du traitement acoustique. Premièrement, l'approche est présentée, suivie d'une étude de convergence de la PTF pour définir un critère de maillage des surfaces élémentaires. Ensuite, la précision de la méthodologie proposée est évaluée pour les problèmes de transmission à parois simple et double avec deux différents traitements de contrôle du bruit. Les résultats obtenus sont systématiquement comparés avec trois modèles, à savoir les stratégies directes

des éléments finis / éléments de frontières (FEM / BEM), et à deux approches de sous-structuration PTF basées sur la modélisation du traitement acoustique par (i) un modèle à réaction locale et (ii) la FEM. On observe que la méthode proposée permet de prédire avec précision et efficacité le comportement dynamique des systèmes vibroacoustiques plats avec traitement acoustique.

Note : Dans cet article, le modèle TMM à réaction non locale est aussi appelé le modèle basé sur les fonctions de Green (GF).

3.1 Abstract

This paper presents and studies the performance of a sub-structuring method that employs a patch transfer approach (PTF) to couple the standard finite element schemes of the structures and cavities with a non-locally reacting analytical model of the sound package. First, the approach is presented followed by a convergence study to define a patch mesh criterion. Then, the accuracy of the proposed methodology is assessed for single and double wall transmission problems with two different attached noise control treatments. The obtained results are systematically compared to three models, namely full finite element/boundary element strategies (FEM/BEM), and to two sub-structuring approaches based on the modeling of the sound package by (i) a locally reacting model and (ii) FEM. It is observed that the proposed method predict accurately and efficiently the dynamic behavior of flat trimmed vibroacoustic systems.

3.2 Introduction

Passive noise control treatments (NCT), also called sound package [8], are widely used in different industries to dissipate energy of sound and vibration waves. Such acoustic components are usually multilayered and made up of several layers of highly dissipative materials, inserted between the structure and the acoustic domains. They are efficient at high frequencies, but perform poorly in the low frequency range (i.e. long wavelength). Therefore, it is highly demanded to enhance their vibroacoustical performance. Classical optimization processes, at low frequencies, use finite element/boundary element (FEM/BEM) strategies [9] ; they are, however, computationally expensive. Indeed, each layer of the sound package, for each tested configuration, must be carefully meshed at a preprocessing phase. Also, to correctly capture the behavior of the coupled trimmed vibroacoustic system, the NCT necessitate a refined mesh (up to 12 elements/wavelength for linear elements), because

of their highly dissipative and soft nature. Moreover, in the standard FEM strategies the global system must be remeshed and solved each time a sub-system is modified.

To overcome these limitations, several authors have proposed hybrid approaches wherein a simplified analytical model of the acoustic treatment is included in a finite element framework. Such strategies are inspired by the fact that a detailed description of the master systems (e.g. main structures and cavities), characterized by geometrical complexity and longer wavelengths, is always necessary for low/mid-frequency analysis. Therefore, this class of methods model the elastic and acoustic domains by classical FEM, while the subdomains with much shorter wavelengths (i.e. acoustic treatment) are modeled by using the Transfer Matrix method (TMM) [8] and thus avoids the time consuming meshing phase. The TMM relies on several assumptions, namely, the soft multilayer is assumed to be flat, homogeneous and laterally unbounded. Under these circumstances, two main classes arise among the proposed hybrid strategies. First, the local impedance model [80, 83] where the acoustic treatment is taken into account by its wall impedances calculated by means of the TMM or characterized experimentally. Such approaches can achieve a drastic reduction of the computational cost, but lacks accuracy, especially, if practical acoustic treatments involving complex layups, such as foam or fiber with heavy layers, are considered. Second, an impedance model based on an integral formulation (i.e., Green functions) has been proposed in order to capture the non-local behavior of the NCT [26, 79, 5, 6, 2]. For instance, Shorter and Mueller [79] coupled the FEM of a structure with a transfer matrix model of the sound package radiating into an unbounded fluid medium by considering a formulation in terms of self and mutual piston impedances. On the other hand, a hybrid FEM-TMM hybrid method was proposed recently by Alimonti et al. [5, 6, 2]. This hybrid methodology also employs an integral formulation to account for the dynamic response of the acoustic treatment, the latter is replaced by surface impedances added to the finite element domains of the structure and the cavity. These impedances are expressed in terms of convolution integral between external stresses and Green functions which are judiciously estimated by the TMM. The model neglects the reflected field contribution, since the sound package is assumed to be laterally unbounded in TMM. The effect of the latter assumption was analyzed in Ref. [2]. It was shown that direct field model, which neglects the reverberant field contribution emanating from the rigid lateral boundaries of the acoustic treatment may sometimes underestimate the radiated acoustic power and overestimate the absorption at low frequencies. In order to enhance the accuracy of the Green functions (GF) based model, the image source method was proposed by Alimonti and Atalla [3] to account for the reflected field. The latter was approximated only by the first and second reflections on the lateral boundaries of the NCT. Such approximation is

justified by the large dissipation nature of the acoustic treatment of a sufficiently large surface. Also, the impact of two different formulations based on baffling conditions of the acoustic treatment was assessed. It was observed that the two formulations give similar results. A systematic comparison with the finite element method was also used to demonstrate the validity, precision and numerical efficiency of the proposed methodology in different configurations involving a plate-cavity problem. In addition to the gain in computation time and the perfect matching with FEM solution a substantial simplification of the modeling of the problem is also performed.

On the other hand, to avoid the classical point to point coupling between subdomains used in the FEM-TMM hybrid method, the patch transfer function (PTF) approach can be employed to speed up the solution of the coupled problem. The latter method was developed by Maxit et al. [58] on the basis of the work of Cacciolati et al. [19] on acoustic mobilities. The PTF approach has been studied by several researchers. For instance, Ouisse et al. [62] used the PTF procedure to couple linear acoustic problems and proved its efficiency through a convergence study. Pavic et al. [67] used the PTF technique for noise source identification. Aucejo et al. [12] studied and accelerated the convergence of the approach in the case of heavy fluid-structure interaction by using the modal synthesis model with residual shapes to estimate the mobility and impedance (PTFs) relations of subsystems, Maxit et al. [57] proposed an improvement of the efficiency of the approach by structuring the structure-cavity system outside the near-field zone of the structure and by using a non-standard modal decomposition. Guyader et al. [35] and Chazot et al. [22, 23] used the PTF approach to solve a transmission loss problem for double wall configurations. The radiation impedance into an unbounded fluid domain was computed by means of Rayleigh's integral. Finally, Veronesi et al. [82] used the PTF technique for a plate-cavity system with attached acoustic foam, the PTFs relations of the foam were determined experimentally. In this context, the PTF method can be very useful because the mechanical and acoustical properties of the acoustic treatment can be modified during the assembly process, as well as, the boundary conditions which may be unknown. To improve the efficiency of the method, a reduced experimental method was proposed by Albert et al. [1], where PTFs of a spring-mass treatment are deduced from single-patch tests. However, in practice this class of methodology remains limited by the size of the patches, which controls the convergence of the approach. Also, non-local effects can be difficult to measure due to the dissipative nature of the acoustic treatment, which limits the accuracy of the experimental PTF approach.

In this paper, a hybrid approach based on the PTF method combining the FEM for the master systems and the GF model for the sound package is presented and used to solve transmission loss problems involving flat single and double wall configurations. The needed theoretical background of the GF methodology and the PTF is provided in section 3.3. Next, the principle of the PTF procedure and the used coupling schemes are presented for the considered cases. In section 3.4, the convergence of PTF schemes is assessed numerically and a criterion is proposed. Finally, the accuracy of the proposed methodology is assessed on various transmission problems for two acoustic treatment configurations (light foam and a foam with a heavy layer) by a systematic comparison with FEM. It is shown that the introduction of the GF model in the sub-structuring method allows a perfect matching with FEM/BEM solutions and a substantial simplification of the modeling of the problem. In addition, the presented examples corroborate the limitations of the widely used locally reacting impedance models. The case of a double wall with an empty cavity is also presented to show the limit of employing the classical TMM to represent the cavity.

3.3 Theory

The sub-structuring Patch transfer functions procedure is used to couple subsystems. First, the impedance and mobility surface relations are estimated using the classical FEM for the master systems (structure and the acoustic cavity) while the impedance matrix of the acoustic treatments backed by a rigid wall is characterized by three models : FEM, a locally reacting model and a Green Function based model. These three models will be presented and compared in this paper. Once each subsystem is characterized, continuity relations over elementary areas of the physical interfaces between subdomains are used to couple the domains to each other and to the exterior (excitation and receiver, semi-infinite fluids). In the next sections, the theory of the GF based model used to provide impedance relations of the noise control treatments is recalled. Also, the PTF coupling schemes and the transmission loss calculation using the PTF technique are provided.

3.3.1 Green functions based model

The analytical acoustic treatment model (i.e. Green functions based model) developed by Alimonti et al. [5, 6, 2, 3] aims to simplify the modeling of noise control treatments and to speed up its integration in finite element analysis of vibroacoustic systems. The dynamic response of the acoustic treatment is replaced by interface impedances added to the FE domains of the structure and cavity. These impedances are expressed in terms of convolution integral between the external loads (e.g. nodal displacement and stress)

and Green functions (fundamental solution). As a first approximation, the model was developed to take into account only the direct field contribution [2], where the acoustic treatment is assumed to be flat, homogeneous, isotropic and laterally unbounded (i.e the reflected field is neglected). Under this assumption, the TMM method is used to estimate judiciously and efficiently a set of Green functions. The Transfer Matrix is represented by a reduced 2x2 matrix since only the normal stresses σ and normal displacements u (i.e. normal velocities) are assumed continuous at the structure and/or cavity interfaces. The normal displacement and stress assumption assumes a "fluid" type of coupling with the structure, i.e. the NCT is not constrained to the structure (e.g. glued like a viscoelastic layer). The multilayer up can, however, be arbitrary, that is, it may include porous-elastic (Biot) layers. Indeed, when the first or last layers are porous-elastic or solid, the approach assumes that the system is decoupled through a thin air layer. This is not an intrinsic limitation of the model and can still account for coupling between the solid frame of the foam and the structure.

Two formulations can be adopted according to the baffle conditions. First, the direct (u,u) formulation considers that both ends of the sound package are inserted into an infinite rigid baffle as depicted in Fig. 3.1. Second, the mixed (u,σ) formulation, where the NCT is assumed to be baffled over the side A and unbaffled over the side B. Therefore, this formulation considers that side A (resp. B) is excited by a normal displacement u field (resp. normal stress load σ). This is the natural formulation when the NCT is attached to a structure over side A and its other side B is in contact with an acoustic domain (e.g. cavity, semi-infinite fluid). A detailed derivation of these two formulations can be found in Ref. [2].

In Refs. [2, 3] it was found that the baffling conditions matters only near to the lateral boundaries of the acoustic treatment. In consequence, different baffling conditions, i.e. the (u,σ) and (u,u) formulations, are expected to be equivalent for a typical sound package with a sufficiently large lateral dimension. Hence, the direct formulation is preferred to avoid expensive matrix inversion. Moreover, as the acoustic treatments are described using an impedance matrix in the PTF approach (see subsection 3.3.2), only the (u,u) formulation is recalled here. The position of each point over the interfaces A and B is defined by means of the planar coordinates $\mathbf{x} = (x, y)$. Under the assumptions mentioned above, the reaction vectors at sides A and B of the NCT due to normal displacement loads write

$$\begin{cases} \mathbf{R}_A(\omega) = \mathbf{D}_{AA}(\omega)\mathbf{a}(\omega) + \mathbf{D}_{AB}(\omega)\mathbf{b}(\omega) \\ \mathbf{R}_B(\omega) = -\mathbf{D}_{AB}(\omega)\mathbf{a}(\omega) + \mathbf{D}_{BB}(\omega)\mathbf{b}(\omega) \end{cases}, \tag{3.1}$$

where each component of the coefficient **a** (resp. **b**) in Eq.(3.1) is defined as the product of the area S_i associated with the i^{th} node of the discretized surface and the normal displacement u_A (resp. u_B) over side A (resp. over side B) :

$$\begin{cases} \mathbf{a}_i(\omega) = S_i u_A(\mathbf{x}_i, \omega) \\ \mathbf{b}_i(\omega) = S_i u_B(\mathbf{x}_i, \omega) \end{cases}. \tag{3.2}$$

The reaction vectors $\mathbf{R}_A(\omega)$ and $\mathbf{R}_B(\omega)$ at node i can be interpreted as an averaged (i.e. filtered) nodal normal stresses and they are defined as

$$\begin{cases} \mathbf{R}_{A_i}(\omega) = \int_{\mathbf{x}} \psi(|\mathbf{x} - \mathbf{x}_i|)\sigma_A(\mathbf{x}, \omega)dx \\ \mathbf{R}_{B_i}(\omega) = \int_{\mathbf{x}} \psi(|\mathbf{x} - \mathbf{x}_i|)\sigma_B(\mathbf{x}, \omega)dx \end{cases}, \tag{3.3}$$

where σ_A and σ_B refer to the normal stresses over sides A and B, respectively. The radially symmetric smoothing kernel $\psi(\mathbf{x})$, i.e. filter, satisfy the normalization condition $\int_{\mathbf{x}} \psi(\mathbf{x})d\mathbf{x} = 1$. On the other hand, each (i,j) element of the generalized matrices $\mathbf{D}_{mn}$, m=A or B and n=A or B, is defined such as

$$D_{mn_{ij}}(\omega) = D_{mn}(r_{ij}, \omega) = \frac{1}{2\pi} \int_0^{k_s} \hat{d}_{mn}(k, \omega) J_0(k r_{ij}) |\hat{\psi}(k)|^2 k dk, \tag{3.4}$$

$r_{ij} = |r_{ij}|$ is the Euclidean distance between the nodes x_i and x_j as depicted in Fig. 3.1, k is the wavenumber and $J_0(kr_{ij})$ is the Bessel function of zero order of argument kr_{ij}. The notation $\hat{f}(k)$ indicates the Hankel transform of the function $f(r)$. The filter $\hat{\psi}(k)$ is the Hankel Transform of $\psi(r)$ defined using the normalized jinc function, i.e. $\psi(r) = \frac{k_s^2}{2\pi} \frac{J_1(k_s r)}{k_s r}$. In the pass-band $(0,k_s)$, the filter $\hat{\psi}(k)$ behaves as an ideal filter (i.e. $\hat{\psi}(k)$=1). The maximum wavenumber k_s is defined by Nyquist criteria based on the minimum Euclidean distance $r_{min_{ij}}$ between the nodes of the mesh at a given NCT side.

The Eq. 3.4 is valid for acoustic treatment which are spatially homogeneous (i.e. isotopic). The fundamental kernels $\hat{d}_{mn}(k, \omega)$ represent the radially symmetric Fourier transform of the Green functions and they are efficiently estimated by means of the TMM according to the baffling conditions adopted in the (u, u) formulation. Hence, the $\hat{d}_{mn}(k, \omega)$ are the coefficient of the 2×2 reduced TMM between normal velocities V_T^A, V_T^B and normal stresses σ_T^A, σ_T^B, as shown in [2] and in Eq.3.19. It should be noted that a complete independent evaluation of $\hat{d}_{mn}(k, \omega)$ (resp. $D_{mn}(r_{ij}, \omega)$) can be handled for different couples (k, ω) (resp. (r_{ij}, ω)), making the approach suitable for parallel computing.

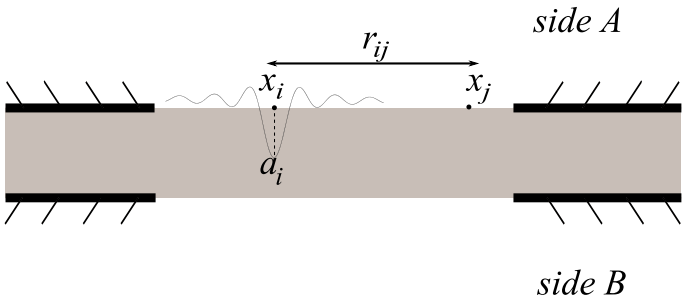

Figure 3.1 Presentation of the baffling conditions of the (u, u) formulation, the sound package is baffled at both ends. r_{ij} is the Euclidean distance between the point x_j (excited by a normal displacement using the jinc function) and the point x_i.

It was shown in [2] that the direct field model, regardless of the adopted formulation, is able to capture qualitatively the dynamic behavior of an acoustic treatment (i.e. felt, light foam, spring-mass treatment...) with rigid lateral boundaries. However, it is not accurate enough by comparing it to the FEM method where the direct field model may sometimes lead to an underestimation of the transmission and an overestimation of the absorption at low frequencies. Hence, the reflected field must be added. Therefore, the image source method (ISM) [68] is employed to retrieve the contribution of the reflected field emanating from the lateral boundaries of the sound package. This latter is assumed to have a polygonal geometry because only the reflections at straight edges can be performed by ISM method. Therefore, by considering the whole multilayer treatment behaves like an equivalent fluid and assuming perfect reflections at lateral edges, the reflected field is obtained by means of the direct field arising from successive virtual image sources. In addition, since the vibrational field emanating from the image sources is highly damped (i.e. the reflected field is of non-diffuse nature), in theory only few order reflections along the lateral edges are needed. Consequently, the reaction vectors over sides A and B, given by Eq. (3.5), are obtained by superposing the direct field $\mathbf{D}_{mn}$ and the reflected field $\mathbf{D}^q_{mn}$ responses. The reflected field $\mathbf{D}^q_{mn}$ is procured by means of the N_s virtual image sources of nodes at sides A and B of the acoustic treatment. The reader can find a comprehensive derivation of the methodology in Ref. [3]. Without loss of generality, we can write

$$\begin{cases} \mathbf{R}_A(\omega) = \Big[\mathbf{D}_{AA}(\omega) + \sum\limits_{q=1}^{N_s} \mathbf{D}^q_{AA}(\omega)\Big]\mathbf{a}(\omega) + \Big[\mathbf{D}_{AB}(\omega) + \sum\limits_{q=1}^{N_s} \mathbf{D}^q_{AB}(\omega)\Big]\mathbf{b}(\omega) \\ \mathbf{R}_B(\omega) = -\Big[\mathbf{D}_{AB}(\omega) + \sum\limits_{q=1}^{N_s} \mathbf{D}^q_{AB}(\omega)\Big]\mathbf{a}(\omega) + \Big[\mathbf{D}_{BB}(\omega) + \sum\limits_{q=1}^{N_s} \mathbf{D}^q_{BB}(\omega)\Big]\mathbf{b}(\omega) \end{cases}, \tag{3.5}$$

where $D^q_{mn_{ij}}(\omega) = D_{mn}(r^q_{ij}, \omega)$ as defined in Eq. (3.4) with r^q_{ij} is the distance between the q^{th} image of the node j and the receiver node i.

It should be pointed out that the reflected field effect of an acoustic treatment with a sufficiently large rectangular area, can be approximated by using only the first and second order of reflections (i.e. Ns=8). In the context of the used image-source approach, the finite size effect is only exact for equivalent fluids. In consequence, the proposed developments while "exact" for equivalent fluids (keeping in mind its other assumptions) are approximate for general layered media. Indeed, it was found in [3] that when the sound package contains a solid or a porous-elastic layer with non-negligible structural properties, the method captures only qualitatively the vibroacoustic behavior of the multilayer. As final remark, note that the Green functions based model allows a large computational gain while ensuring a good accuracy compared to the FEM. However, this computational gain intrinsically depends on the considered number of nodes of the mesh and on the number of image sources. Moreover, the validity of using few orders of reflections is based on the highly damped nature of NCT with sufficiently large surface. An example is presented later to show the limitation of this assumption.

3.3.2 Patch transfer functions

Patch transfer function is a sub-structuring approach which can be efficiently applied to predict the vibroacoustic response of linear complex systems coupled through their coupling surfaces (i.e. physical interfaces). Each interface is divided into elementary areas called patches, where a set of patch transfer function (PTFs), mobility and/or impedance relations, is computed for each patch and for each subsystem. Once the PTFs are computed, the coupling consists of applying the superposition principle to each subsystem and in writing the continuity relations between the subsystems over the coupling surfaces in terms of normal velocity and acoustic pressure.

The PTF technique allows a complete independent characterization of each subsystem using the most appropriate analytical, numerical (FEM, BEM, ...) or experimental method. Therefore, a parallel computation of the PTFs can be envisaged. Moreover, the PTF approach leads to small, symmetric systems fully populated, leading to a fast solution of the coupled problem. Also, if one subsystem is modified, only its own PTFs relations have to be upgraded. As a result, this approach can speed up and facilitate the integration of acoustic treatments, especially in the early stage of the design process, when a lot of configurations are tested with the same structural and acoustic domains (i.e. only acoustic

treatments need to be characterized for each configuration). Detailed derivations of the patch transfer function method can be found in Ref. [62, 12, 82].

In the following, the coupling schemes are described briefly for the three considered transmission problems (Fig. 3.3). Namely (i) baffled simply supported panel with attached light foam (ii) a baffled simply supported panel with attached light foam and heavy layer coupled to a niche and (iii) double panels filled with a light foam. In all the studied cases, the vibroacoustic systems are assumed to be embedded in an infinite rigid baffle and fluid loading is neglected. Since the acoustic treatment is represented by an equivalent fluid model, only normal components are involved in the continuity conditions at the interfaces between subsystems. The systems are excited by an oblique incidence acoustic plane wave. Next, the transmission loss calculation is described.

Configuration 1 : panel-foam system

The first system consists of a structure (i.e. panel) with attached sound package radiating into an unbounded semi-infinite fluid (SIF) domain (Fig. 3.3(a)). The coupled system is partitioned into three subsystems, namely (i) the structure (ii) the acoustic treatment and (iii) the unbounded fluid domain. The PTFs of each subsystem are defined at the coupling interfaces (i.e. physical interfaces), which are discretized into patches (see Fig. 3.2). The PTFs equations of each subsystem are briefly presented.

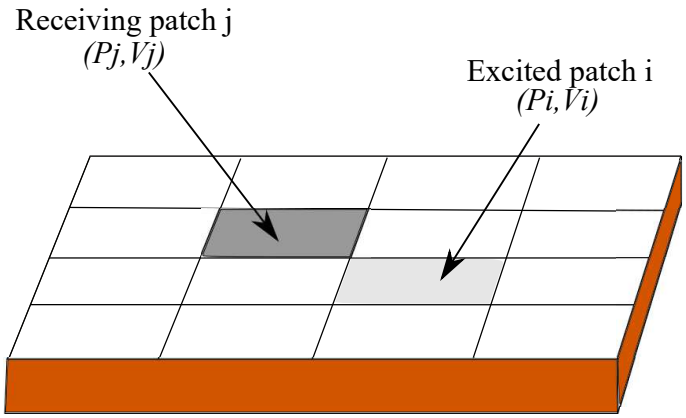

Figure 3.2 A generic interface of a sub-domain divided into patches.

The normal velocity of the panel $\mathbf{V}_S^A$ on the excited surface A is defined as the superposition of the in-vacuo panel averaged normal velocity $\tilde{\mathbf{V}}_S^A$ due to the external excitation and the averaged normal velocity $\mathbf{Y}_S\mathbf{P}_S^A$ due to the pressure caused by the acoustic treatment, that is

$$\mathbf{V}_S^A = \tilde{\mathbf{V}}_S^A - \mathbf{Y}_S\mathbf{P}_S^A, \tag{3.6}$$

where $\mathbf{Y}_S$ is a mobility matrix of size N_{patch} by N_{patch}. Each element $Y_{S_{ij}}$ of the mobility matrix $\mathbf{Y}_S$ is defined as the ratio of the arithmetic mean normal velocity $V_{S_i}^A$ on a receiving patch i and the arithmetic mean pressure $P_{S_j}^A = 1$ on an excited patch j, which reads

$$Y_{S_{ij}} = \frac{V_{S_i}^A}{P_{S_j}^A}. \tag{3.7}$$

The PTFs of the acoustic treatment (subsystem 2) can be expressed with an impedance matrix :

$$\left\{ \begin{array}{c} \mathbf{P}_T^A \\ \mathbf{P}_T^B \end{array} \right\} = \mathbf{Z}_T \left\{ \begin{array}{c} \mathbf{V}_T^A \\ \mathbf{V}_T^B \end{array} \right\} = \begin{bmatrix} \mathbf{Z}_T^{AA} & \mathbf{Z}_T^{AB} \\ \mathbf{Z}_T^{BA} & \mathbf{Z}_T^{BB} \end{bmatrix} \left\{ \begin{array}{c} \mathbf{V}_T^A \\ \mathbf{V}_T^B \end{array} \right\}. \tag{3.8}$$

In this equation, subscript A denote the side of the acoustic treatment in contact with the panel, and subscript B the side in contact with the SIF (transmission hole).

In the semi-infinite fluid (subsystem 3), the radiated pressure can be expressed as a function of the impedance radiation matrix and the normal velocity over the surface of the transmission hole (Fig. 3.3(a)).

$$\mathbf{P}_{SIF}^B = \mathbf{Z}_{rad} \mathbf{V}_{SIF}^B. \tag{3.9}$$

The continuity conditions for velocities and pressures at the interface A between the panel and acoustic treatment and at interface B over the transmission hole are :

$$\left\{ \begin{array}{l} \mathbf{P}^A = \mathbf{P}_S^A = \mathbf{P}_T^A \\ \mathbf{V}^A = \mathbf{V}_S^A = \mathbf{V}_T^A \\ \mathbf{P}^B = \mathbf{P}_T^B = \mathbf{P}_{SIF}^B \\ \mathbf{V}^B = -\mathbf{V}_T^B = \mathbf{V}_{SIF}^B \end{array} \right. , \tag{3.10}$$

where the subscript S stands for the panel, T for the treatment and SIF for the semi-infinite medium. These equations can be expressed in matrix form such as

$$\begin{bmatrix} \mathbf{I}_d & \mathbf{Y}_S & 0 \\ -\mathbf{Z}_T^{AA} & \mathbf{I}_d & \mathbf{Z}_T^{AB} \\ -\mathbf{Z}_T^{BA} & 0 & \mathbf{Z}_T^{BB} + \mathbf{Z}_{rad} \end{bmatrix} \left\{ \begin{array}{c} \mathbf{V}^A \\ \mathbf{P}^A \\ \mathbf{V}^B \end{array} \right\} = \left\{ \begin{array}{c} \tilde{\mathbf{V}}^A \\ 0 \\ 0 \end{array} \right\}. \tag{3.11}$$

Solving the linear system (3.11) provides the coupled velocities and pressures at interfaces A and B.

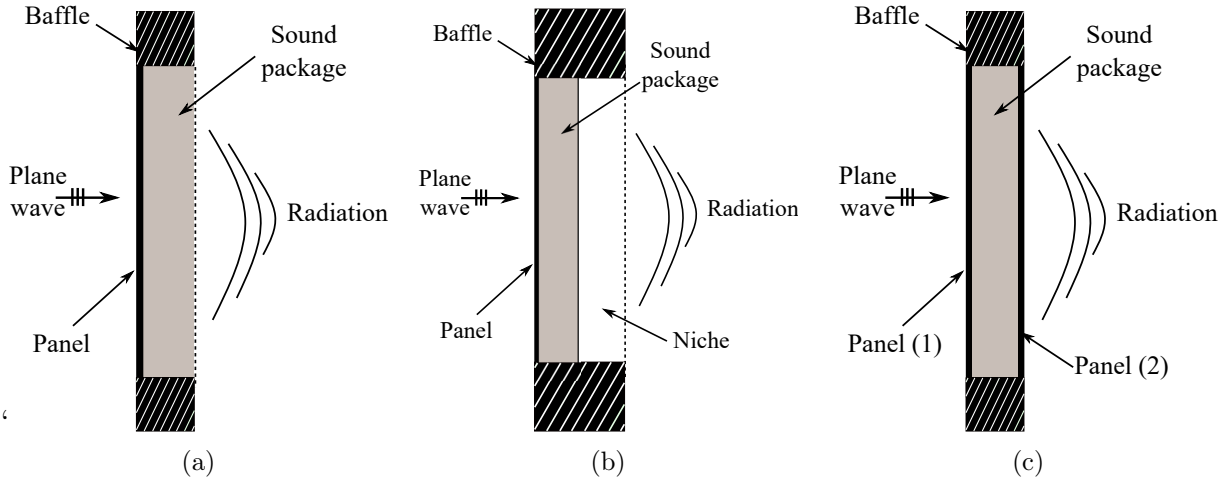

Figure 3.3 A schemes of the three studied configurations ; the sound package is made from either a foam or a foam-mass layer. (a) Configuration 1 (b) configuration 2 (c) configuration 3.

Configuration 2 : panel-foam/mass layer-niche system

The second system consists of a structure with attached sound package coupled to a niche and radiating into an unbounded fluid domain (Fig. 3.3(b)). The coupled system is partitioned into four subsystems, namely (i) the structure (ii) the acoustic treatment (iii) the niche and (iv) the unbounded fluid domain. The niche is coupled with the NCT over interface B and with the unbounded sub-domain over interface C. It is characterized by an impedance matrix Z_{Cav}, as well as the one used for the acoustic trim.

As a consequence, the response of the coupled system is given by the following set of equations :

$$\begin{bmatrix} \mathbf{I}_d & \mathbf{Y}_S & 0 & 0 \\ -\mathbf{Z}_T^{AA} & \mathbf{I}_d & \mathbf{Z}_T^{AB} & 0 \\ -\mathbf{Z}_T^{BA} & 0 & \mathbf{Z}_T^{BB} + \mathbf{Z}_{Cav}^{BB} & -\mathbf{Z}_{Cav}^{BC} \\ 0 & 0 & \mathbf{Z}_{Cav}^{CB} & -\mathbf{Z}_{Cav}^{CC} - \mathbf{Z}_{rad} \end{bmatrix} \begin{Bmatrix} \mathbf{V}^A \\ \mathbf{P}^A \\ \mathbf{V}^B \\ \mathbf{V}^C \end{Bmatrix} = \begin{Bmatrix} \tilde{\mathbf{V}}^A \\ 0 \\ 0 \\ 0 \end{Bmatrix}. \tag{3.12}$$

Solving the linear system (3.12) provides the coupled velocities and pressures at interfaces A, B and C.

Configuration 3 : panel-foam-panel system

In the case of the double wall filled with an acoustic treatment (Fig. 3.3(c)), the coupled system is divided into four subsystems, namely (i) the first panel (ii) the acoustic treatment (iii) the second panel and (iv) the unbounded fluid domain. The coupling equations are obtained using the superposition principle and continuity conditions on each patch of the coupling surfaces (A, B). The governing equations of the first panel and the acoustic treatment are already presented in the case of a simple wall configuration and by consequence the simplified governing equations for each subsystem are giving by :

- Panel (1)

$$\mathbf{V}^A = \tilde{\mathbf{V}}^A - \mathbf{Y}_{p1}\mathbf{P}^A. \tag{3.13}$$

- Acoustic treatment (first panel side)

$$\mathbf{P}^A = \mathbf{Z}_T^{AA}\mathbf{V}^A - \mathbf{Z}_T^{AB}\mathbf{V}^B. \tag{3.14}$$

- Acoustic treatment (second panel side)

$$\mathbf{P}^B = \mathbf{Z}_T^{BA}\mathbf{V}^A - \mathbf{Z}_T^{BB}\mathbf{V}^B. \tag{3.15}$$

- Panel (2)

$$\mathbf{V}^A = \mathbf{Y}_{p2}\mathbf{P}^B. \tag{3.16}$$

Here subscript $p1$ (resp. $p2$) stands for the first (resp. second) panel and subscript T stands for the acoustic treatment. Finally, the fully coupled problem can be described in a matrix form :

$$\begin{bmatrix} \mathbf{I}_d & \mathbf{Y}_{p1} & 0 & 0 \\ -\mathbf{Z}_T^{AA} & \mathbf{I}_d & \mathbf{Z}_T^{AB} & 0 \\ 0 & 0 & -\mathbf{Y}_{p2} & \mathbf{I}_d \\ -\mathbf{Z}_T^{BA} & 0 & \mathbf{Z}_T^{BB} & \mathbf{I}_d \end{bmatrix} \begin{Bmatrix} \mathbf{V}^A \\ \mathbf{P}^A \\ \mathbf{V}^B \\ \mathbf{P}^B \end{Bmatrix} = \begin{Bmatrix} \tilde{\mathbf{V}}^A \\ 0 \\ 0 \\ 0 \end{Bmatrix}. \tag{3.17}$$

Solving the linear system (3.17) provides the coupled velocities and pressures at interfaces A and B.

3.3.3 Estimation of the PTFs

As mentioned before, the PTFs can be calculated analytically, numerically or even identified experimentally. In this paper, they are derived from a classical FEM calculation. Since

the radiating face is flat and baffled, the radiation impedance $\mathbf{Z}_{rad}$ is based on Rayleigh's integral ; its expression and numerical estimation are given in Appendix A.

On the other hand, the impedances of the acoustic treatment, backed by a hard wall, are modeled by three strategies. Namely (i) FEM (ii) locally reacting model (TMM) and (iii) Green functions based model. In the following, only the PTFs equations of the TMM and the analytical Green functions based model (subsection 3.3.1) are presented.

Locally reacting model

In order to build the PTFs of a generic multilayer system, the transfer matrix model is adopted. Hence, the sound propagation in the infinite, homogeneous, flat multilayer system due to a plane acoustic wave at an incidence angle θ is represented by a 2x2 reduced transfer matrix [2]. The latter relates the normal variables on sides A and B of a multilayer system and is defined as

$$\left\{ \begin{array}{c} \sigma^A \\ V^A \end{array} \right\} = \begin{bmatrix} T^{AA}(k_t,\omega) & T^{AB}(k_t,\omega) \\ T^{BA}(k_t,\omega) & T^{BB}(k_t,\omega) \end{bmatrix} \left\{ \begin{array}{c} \sigma^B \\ V^B \end{array} \right\}, \tag{3.18}$$

where (σ^A,V^A) (resp. (σ^B,V^B)) are the normal stress and velocity on side A (resp. side B), $k_t = k_0 \sin(\theta)$ with k_0 the wavenumber in the free air and θ the incidence angle. Equation (3.18) is rearranged in the impedance matrix form such as

$$\left\{ \begin{array}{c} \sigma^A \\ \sigma^B \end{array} \right\} = \left\{ \begin{array}{c} -P^A \\ -P^B \end{array} \right\} = \begin{bmatrix} \hat{d}_{AA}(k_t,\omega) & \hat{d}_{AB}(k_t,\omega) \\ \hat{d}_{BA}(k_t,\omega) & \hat{d}_{BB}(k_t,\omega) \end{bmatrix} \left\{ \begin{array}{c} V^A \\ V^B \end{array} \right\}, \tag{3.19}$$

Since the direct use of the TMM is not able to take into account the inter-patch interactions, only the diagonal components of impedance matrices $\mathbf{Z}_T$ are calculated for each patch i (i.e. $i = [1, Npatches]$) using

$$\left\{ \begin{array}{l} Z_{T_{ii}}^{AA}(k_t,\omega) = -\hat{d}_{AA}(k_t,\omega) = -\dfrac{T^{AA}(k_t,\omega)}{T^{BA}(k_t,\omega)} \\ Z_{T_{ii}}^{AB}(k_t,\omega) = -\hat{d}_{AB}(k_t,\omega) = \dfrac{1}{T^{BA}(k_t,\omega)} = -Z_{T_{ii}}^{BA}(k_t,\omega)\ . \\ Z_{T_{ii}}^{BB}(k_t,\omega) = -\hat{d}_{BB}(k_t,\omega) = \dfrac{T^{BB}(k_t,\omega)}{T^{BA}(k_t,\omega)} \end{array} \right. \tag{3.20}$$

According to the angle of incidence θ, two models are compared : (i) normal incidence ($\theta = 0$, equivalently $k_t = 0$) and (ii) averaged incidence ($0 \leq \theta \leq \pi/2$).

Green functions based model

In order to build the PTFs impedance, the front and rear sides of a multilayer are discretized into rectangular patches using $n_x \times n_y$ nodes per patch as depicted in Fig. 3.4. Then, piston excitation is applied over each patch. The movement of the pistons is reproduced approximately by the jinc function to smooth out the piston displacement (eliminate discontinuities at the piston edges).

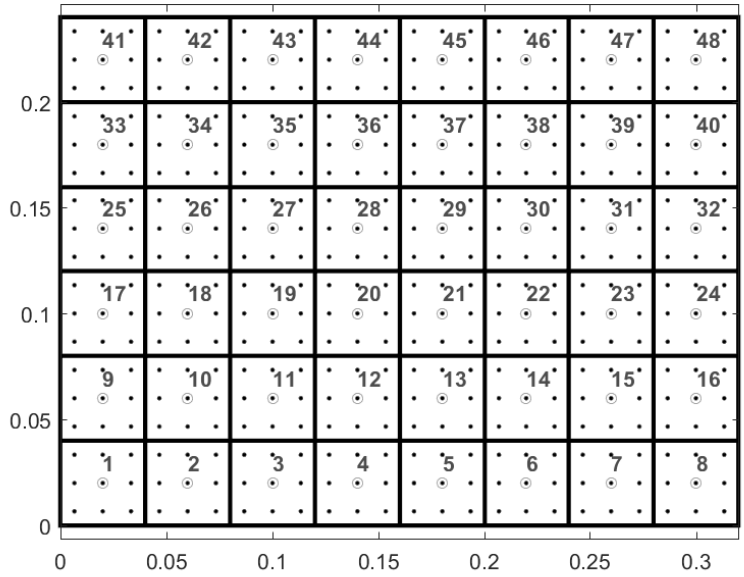

Figure 3.4 An example of the geometry of the surface of the sound package subdivided into 8×6 patches. The circles denote the centers of the pistons and the black dot the used mesh nodes considered in the GF model.

In the context of the (u, u) formulation [2], a boolean operator $\mathbf{V}_{in}$ is used to relate the nodal velocities $\mathbf{v}_{nodal}$ and the piston normal velocities $\mathbf{V}$, such as

$$\begin{cases} \mathbf{v}^A_{nodal} = \mathbf{V}_{in}\mathbf{V}^A \\ \mathbf{v}^B_{nodal} = \mathbf{V}_{in}\mathbf{V}^B \end{cases}, \tag{3.21}$$

where $\mathbf{v}_{nodal} = j\omega \boldsymbol{u}_{nodal}$ with $\boldsymbol{u}_{nodal}$ is the normal displacement vector used in the (u, u) formulation in section 3.3.1 and with $V_{in_{ij}} = 1$ if node i belongs to patch j. By consequence,

the solution at the nodes due to piston excitation is obtained by replacing Eq. (3.21) in Eq. (3.1), such as

$$\begin{cases} \mathbf{R}_A(\omega) = \mathbf{D}_{AA}(\omega)\mathbf{S}\mathbf{V}_{in}\mathbf{V}^A(\omega) + \mathbf{D}_{AB}(\omega)\mathbf{S}\mathbf{V}_{in}\mathbf{V}^B(\omega) \\ \mathbf{R}_B(\omega) = -\mathbf{D}_{AB}(\omega)\mathbf{S}\mathbf{V}_{in}\mathbf{V}^A(\omega) + \mathbf{D}_{BB}(\omega)\mathbf{S}\mathbf{V}_{in}\mathbf{V}^B(\omega) \end{cases}. \tag{3.22}$$

The average pressure acting on each piston is obtained by averaging the nodal solutions $R_{A_i,B_i}(\omega)$ over each patch. Thus, to get the pistons pressures a mapping operator $\mathbf{V}_{out}$ is used to perform the desired averaging :

$$\begin{cases} \mathbf{P}^A = -\mathbf{V}_{out}\mathbf{R}_A^A \\ \mathbf{P}^B = -\mathbf{V}_{out}\mathbf{R}_B \end{cases}. \tag{3.23}$$

The minus sign comes from the fact that $\mathbf{P} = -\mathbf{R}$. In this paper, a moving average is used such that $V_{out_{ij}} = S_j/S_p$ if node j belongs to patch i, with S_p being the piston area and S_j the area of node j. Therefore, $V_{out_{ij}} = 1/S_p V_{in_{ij}}$. Hence, the Eq.3.22 can be written such as,

$$\begin{cases} \mathbf{P}^A = -\mathbf{V}_{out}\mathbf{D}_{AA}(\omega)\mathbf{S}\mathbf{V}_{in}\mathbf{V}^A(\omega) - \mathbf{V}_{out}\mathbf{D}_{AB}(\omega)\mathbf{S}\mathbf{V}_{in}\mathbf{V}^B(\omega) \\ \mathbf{P}^B = \mathbf{V}_{out}\mathbf{D}_{AB}(\omega)\mathbf{S}\mathbf{V}_{in}\mathbf{V}^A(\omega) - \mathbf{V}_{out}\mathbf{D}_{BB}(\omega)\mathbf{S}\mathbf{V}_{in}\mathbf{V}^B(\omega) \end{cases}, \tag{3.24}$$

which can be rearranged in an impedance matrix form to give

$$\begin{Bmatrix} \mathbf{P}^A \\ \mathbf{P}^B \end{Bmatrix} = \begin{bmatrix} \mathbf{Z}_T^{AA} & \mathbf{Z}_T^{AB} \\ -\mathbf{Z}_T^{AB} & \mathbf{Z}_T^{BB} \end{bmatrix} \begin{Bmatrix} \mathbf{V}^A \\ \mathbf{V}^B \end{Bmatrix}. \tag{3.25}$$

The different sign of the extra-diagonal term is due to the fact that the piston velocity is positive in the thickness coordinate direction for both sides A and B.

3.3.4 Transmission loss calculation

The transmission loss is given by

$$TL = 10\log\left(\frac{\Pi_{inc}}{\Pi_{rad}}\right), \tag{3.26}$$

where Π_{inc} denote the incident sound power and Π_{rad} the transmitted power.

The incident sound power for a plane wave excitation with an incident angle θ and with an amplitude P_{inc} is given by :

$$\Pi_{inc} = \frac{P_{inc}^2 S \cos(\theta)}{2\rho_0 c_0}. \tag{3.27}$$

On the other hand, the radiated sound power Eq. (3.28) is calculated by the PTF method from the patch area Si , patch normal velocities V_{n_i} and radiated patch pressures P_{rad_i} of the surface in contact with the SIF :

$$\Pi_{rad} = \frac{1}{2} \sum_{i=1}^{N} Re\{V_{n_i}^* P_{rad_i} S_i\}, \tag{3.28}$$

where the superscript * indicates the conjugate of the complex normal velocity and N is the number of patches.

3.4 Validation

The purpose of this section is to validate numerically the proposed methodology for transmission through simple and double wall (DWL) configurations with attached noise control treatment. The validation is done by a systematic comparison with full classical FEM/BEM solution (reference) using an in-home code (NOVAFEM). Before presenting the comparisons, various patch sizes are considered in a convergence study to define the optimum patch size that allows a good accuracy of the PTF approach with low computational effort. The ability of the PTF approach to retrieve the coupled response is analyzed when the PTFs of the sound package are computed using three different methods. Namely, classical FEM, Green functions based model corrected by means of ISM and the locally reacting model. The examples in this paper are limited to flat vibroacoustic systems.

3.4.1 Optimum patch size

This section aims at defining the optimum patch size by investigating the convergence of the PTF approach using classical FEM schemes that is, the impedance matrix $\mathbf{Z}_T$ of the trim is also calculated by FEM to eliminate any bias introduced by the TMM or GF methods. For the sake of conciseness, only the case of a baffled simply supported double wall filled with a porous material radiating into an unbounded acoustic domain is presented. The double wall is made up from two «same» aluminum panels with area

$0.32 \times 0.24\ m^2$ and thickness of 2 mm. The inner cavity is 20 mm thick and filled with melamine foam (see Table 3.2 for the material properties). The response of the system excited by an oblique plane wave of an incident angle $\theta = 45°$ is considered up to 1 kHz. The foam is assumed to be decoupled from the two walls and is thus modeled by the limp model [64], i.e. the stiffness of the frame is neglected. The finite element model of the panels uses 32×24 four-noded shell elements and the acoustic foam is meshed by $32 \times 24 \times 5$ eight-noded equivalent fluid (i.e. limp) elements. As explained in the section 3.3.2, the whole system is divided into four subsystems, namely the first panel, the acoustic treatment, the second panel and the unbounded acoustic domain. The interfaces between subsystems are discretized into rectangular patches, as shown in Fig. 3.4 and table 3.1. Equations (3.9), (3.17) and (3.26) are used to compute the transmission loss of the coupled system (referred to as PTF[FEM] in the results). The same FEM mesh is used in the reference simulation (direct response of the coupled system).

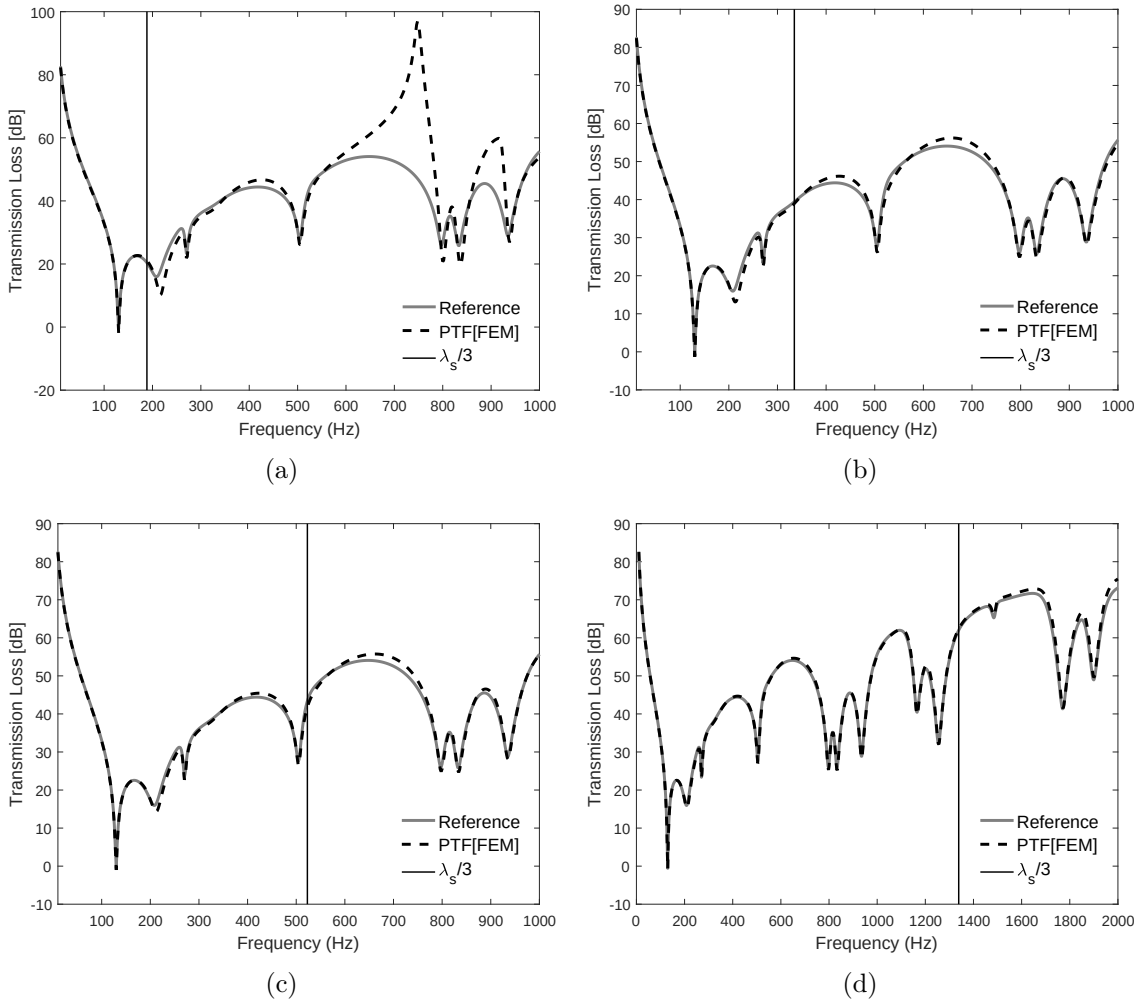

Figure 3.5 Transmission Loss of the double wall panel. The DWL system is acoustically excited by a plane wave 45°/0°. A 2 cm melamine foam is placed between the panels. Effect of the patch size on the accuracy of the presented sub-structuring approach. The interfaces are discretized into different patches mesh (a) 3×2, (b) 4×3, (c) 5×4, (d) 8×6.

The transmission loss obtained by the PTF approach is compared to the reference in Fig. 3.5 for various patch sizes (listed in table 3.1). As expected the patch size should be small enough to get better matching between the PTF response and the reference one. However, as the patch size decreases, the computational cost increases. It is observed that the PTF method converges when the patch size is less than or equal to one third of the smallest wavelength λ of the uncoupled panel and acoustic treatment, computed at the maximal frequency of the range of interest. Therefore, the patch size must respect the convergence criteria $\lambda_s/3$ as indicated by the black dashed vertical lines. Beyond these lines, the PTF approach responses start diverging from the reference solution. This is more

conservative compared to the classical $\lambda/2$ criterion used by previous authors. Table 3.1 shows the maximal convergence frequency for different meshing criteria for the plate and cavity.

	Patch size (cm^2)	Criterion					
		$\lambda_a/6$	$\lambda_a/4$	$\lambda_a/2$	$\lambda_s/4$	$\lambda_s/3$	$\lambda_s/2$
Mesh 8×6	4×4	1425	2138	4277	753	1338	3012
Mesh 6×5	5.33×4.8	1069	1604	3208	423	753	1694
Mesh 5×4	6.4×6	891	1336	2673	294	522	1176
Mesh 4×3	8×8	712	1069	2138	188	334	753
Mesh 3×2	10.66×12	475	712	1425	83	148	334

Tableau 3.1 Maximal convergence frequency based on different meshing criteria using structural and acoustical wavelength λ_s and λ_a, respectively.

Figure 3.6 shows the relative error ϵ on the transmission loss estimation obtained using the PTF approach for different patch sizes (the same frequency step is used in all calculation). The relative error ϵ is defined by $\frac{|TL_{Ref}-TL_{PTF}|}{|TL_{Ref}|}$, where TL_{Ref} denote the TL obtained by the reference solution and TL_{PTF} denote the sub-structuring PTF approach. It is clear that the relative error is higher in the case where the patch size is large and decreases slowly with patch size. The maximal error observed at 130 Hz is due to the fact that the value of the transmission loss is close to 0 at this frequency. Note that the mesh using 8×6 patches give the best accuracy where the relative error is under 1.5% almost in all the frequency range, except at peaks where it can be greater (i.e. up to 5%). In order to ensure convergence of the PTF approach with a good accuracy and to facilitate the analysis, the 8×6 patches mesh is considered in the following validation study of the PTF-GF methodology.

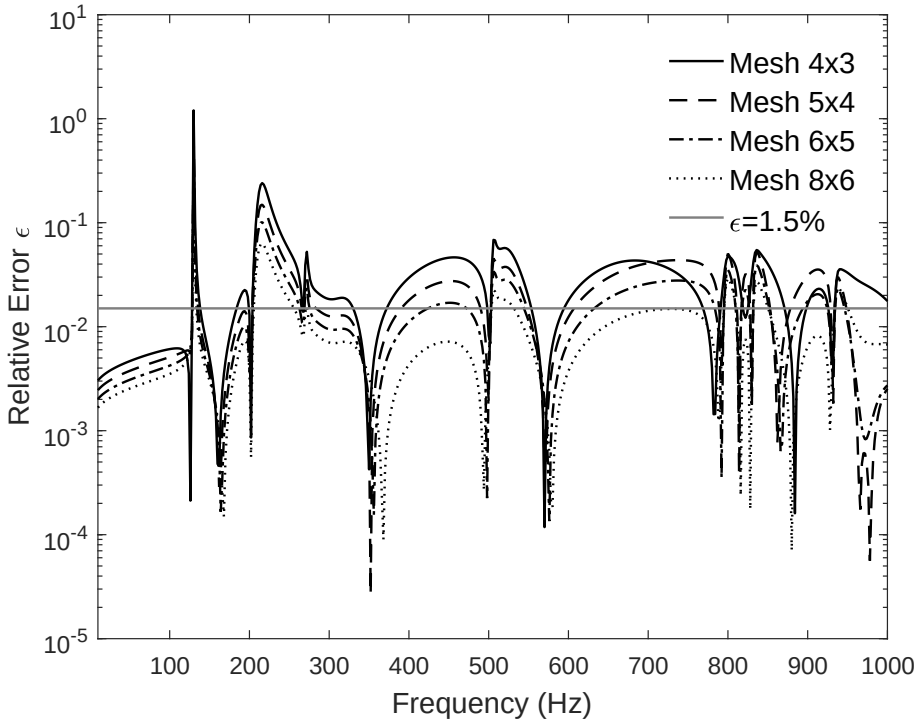

Figure 3.6 Relative error in the Transmission Loss of the double wall panel obtained by the PTF approach.

3.4.2 Assessment of the PTF-GF approach

The proposed method is assessed in two types of transmission problems (see Fig. 3.3). The first consist of two single wall configurations with attached sound package, namely (i) panel with attached limp foam (referred to as light treatment) radiating into an unbounded fluid and (ii) panel with spring-mass treatment radiating into semi-infinite medium throughout a niche. The second considers a double wall configuration. This latter configuration is the same as in the convergence study. In all the studied cases, the same mechanical and acoustical properties of the panel and the light acoustic treatment as in the convergence study are considered with a similar FE modeling. Hence, the PTFs of the subsystems (i.e. panel and foam) remain valid and are used in all the studied cases. The GF based model uses a nodal mesh where each patch is meshed using 9 nodes for all the studied NCT.

In the following case studies, the proposed hybrid methodology where the PTFs of the NCT are computed by GF based model is compared to PTF calculations based on the modeling of the acoustic treatment either by an FE model or locally reacting strategies (TMM). Also, the response of the coupled vibroacoustic systems is systematically compared with full FEM/BEM the reference solution. It should be pointed out that the structure and

Materials	Properties	
	Mechanical	Acoustic
Aluminum	density=2742 kg/m^3 Young's modulus=69 GPa Poisson's ratio=0.33 damping factor=0.01	
Melamine	density=8.8 kg/m^3 Young's modulus=80 kPa Poisson's ratio=0.4 damping factor=0.17	porosity=0.99 resistivity=10900 kg/m^3s tortuosity=1.02 viscous length=100 μm thermal length=130 μm
Heavy layer	density=1.5 kg/m^2 Young's modulus=1 MPa Poisson's ratio=0.3 damping factor=0.5	
Air		density=1.21 kg/m^3 speed of sound=342.2 m/s

Tableau 3.2 Materials used in the numerical simulations.

the acoustic niche are modeled by classical FE schemes. For clarity, the compared models are :

◦ Reference : Classical coupled FEM/BEM approach wherein all the subsystems are modeled using FEM and the radiation from the transmission hole is modeled using BEM.

◦ PTF[FEM] : Exact classical FE model for all domains included in a sub-structuring PTF framework.

◦ PTF[GF] : Green functions based model for the sound package and assumption of infinite extent layer included in a sub-structuring PTF-FEM framework.

◦ PTF[GF(Ns=X)] : GF based model for the sound package accounting for the contribution of the reflected field using ISM by considering X image sources (ex. X=8 when first and second reflections are considered)

◦ PTF[TMM(0°)] : Locally reacting model for the sound package with the assumption of infinite extent and normal incidence.

◦ PTF[TMM(avg.)] : Locally reacting model for the sound package with the assumption of infinite extent averaged over 100 incidence angles between 0° and 90°.

Configuration 1 : panel-foam system

The first system consists of a 2 cm thick melamine attached to a 2 mm thick baffled aluminum panel. The system is excited by a plane wave with the angle of incidence 45°/0° and the semi-infinite termination is applied over the acoustic treatment side. The transmission loss (TL) of the system is thus retrieved by means of Equations (3.9), (3.11) and (3.26)–(3.28). Figures 3.7 and 3.8 show a comparison of the TL predicted by full FEM/BEM, sub-structuring PTF approach based on FEM, local reaction and Green functions models. The TL (Fig. 3.7) is perfectly predicted by the PTF[FEM], while the physics is captured by the PTF[TMM(0°)] and PTF[GF]. However, the PTF[GF] curve slightly overestimate the TL above 500 Hz while the TMM based local model with normal incidence slightly underestimates it above 700 Hz. These discrepancies are due to the fact that PTFs impedance of the foam are computed using only the direct field (infinite extent assumption).

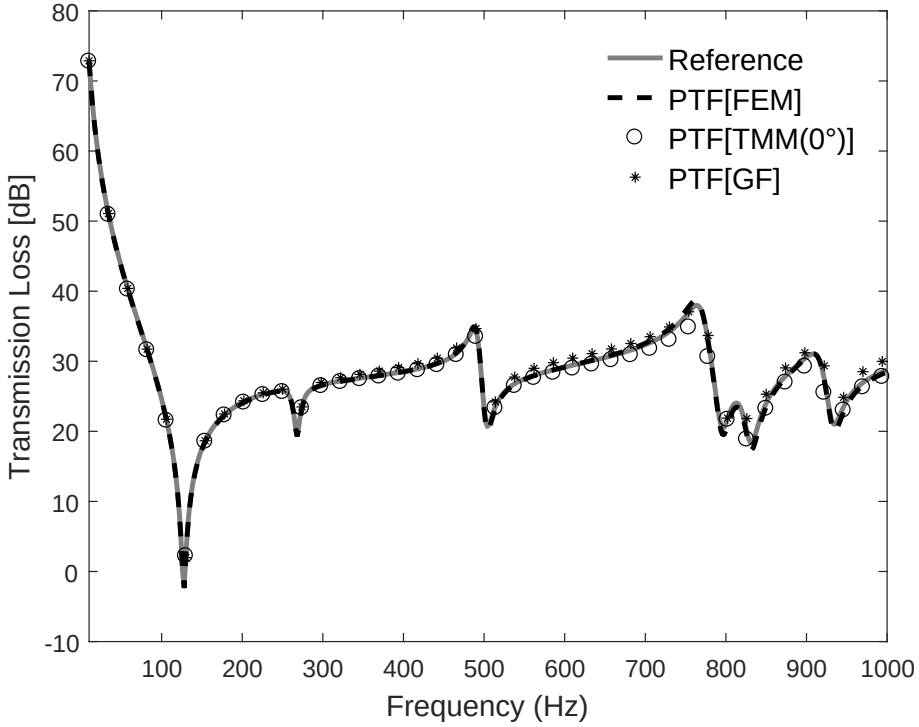

Figure 3.7 Transmission loss of simply supported panel excited by a 45°/0° plane wave and attached to 2 cm thick melamine.

Indeed as shown in Fig. 3.8, the accuracy of the response of the system predicted by GF based model included in PTF-FEM framework is enhanced when the reflected field is added by means of ISM with first and second order of reflections (i.e. Ns= 8 image sources). As expected, similar remark can be made when the averaged TMM is used to characterize the sound package compared to the TMM with normal incidence. This is due to the fact that

the complex velocity distribution over the panel does not resemble to a normal incident plane wave field. Still, the locally reacting TMM model with normal incidence is accurate enough and thus normal incidence impedance measurements can be used in simulations involving equivalent fluid like behaving simple monolayer sound packages (e.g. light foam or fiber).

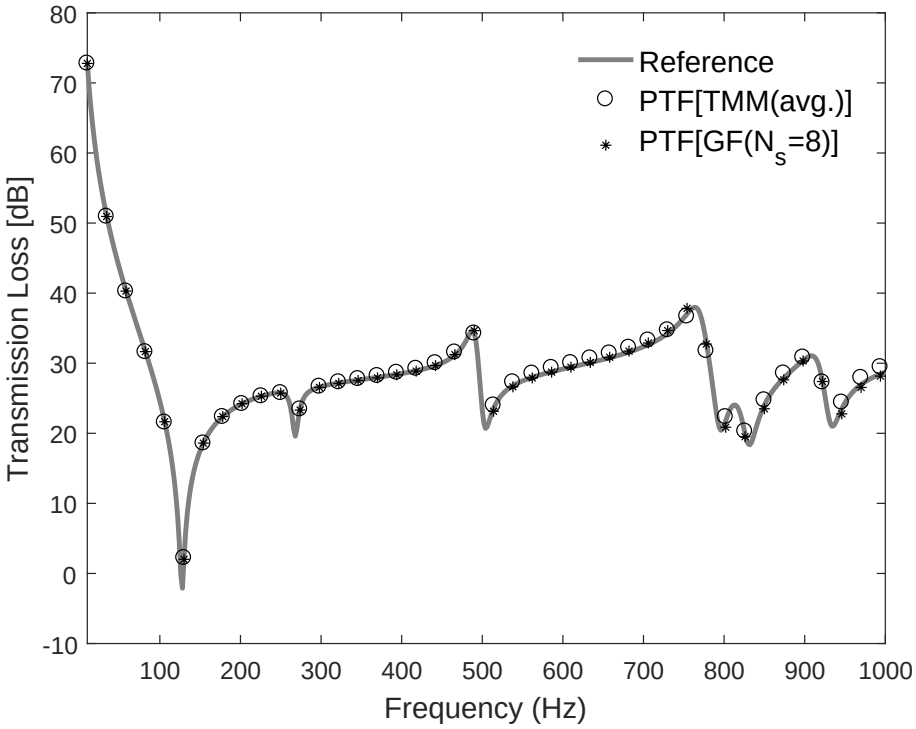

Figure 3.8 Transmission loss of simply supported panel excited by a 45°/0° plane wave and attached to 2 cm thick melamine.

Overall, it should be noted that, for the considered system, the analytical GF solution based on infinite acoustic treatment is approximating almost perfectly the behavior of the actual coupled system. However, the latter is enhanced by the corrected analytical solution and the averaged TMM over the considered frequency range. In consequence, and for the sake of conciseness only the averaged TMM and the corrected GF based model will be assessed in the remaining cases.

Configuration 2 : panel-foam/mass layer-niche system

The second system consists of a 2 mm thick simply supported aluminum panel with attached sound package coupled to a niche (cavity) of 20 cm of thickness. The latter is radiating into an unbounded fluid. The acoustic treatment involves a 2 cm thick melamine foam, and a 1.5 kg/m^2 heavy layer. The finite element model of the master subsystems (i.e.

plate and niche) consists of 32×24 four-noded shell elements and $32 \times 24 \times 6$ eight-noded fluid elements. On the other hand, the layers of the acoustic treatment are meshed by 5 eight-noded limp elements for the melamine foam while the heavy layer is modeled as a solid with 1 eight-noded element through the thickness. The transmission loss is presented in Fig. 3.9. It is obvious that all the considered methodologies are in good agreement below 150 Hz. Also, it can be observed a perfect correlation is obtained between the PTF[FEM] curve and the reference over the whole frequency range corroborating the accuracy of the PTF sub-structuring approach and the used meshing criterion for the patches size. On the other hand, the PTF based on TMM(avg.) is not able to capture the physics of the coupled system especially around the double wall (mass-spring-mass) resonance of the system. This can be explained by the fact that the inter-patch interactions and the reverberant field are not supported in locally reacting models which are important due to the presence of a heavy layer. On the other hand, the PTF[GF(Ns=8)] is providing a good prediction of the response of the coupled system over the entire frequency range except between 150 and 400 Hz, where the peak of the DWL resonance associated with the acoustic treatment takes place. In this frequency range, the finite size effect is important and in consequence more image sources have to be used in the ISM to retrieve the reverberant field emanating from the boundary of the sound package. This is confirmed in Fig. 3.10 when 24 image sources are used in the PTF-GF approach. Perfect correlation is observed.

To conclude, this configuration highlighted the importance of taking into account the inter-patch interactions in PTFs relations and confirmed the limitations of locally reacting models. On the other hand, the accuracy of GF based model is confirmed despite the small surface area of the studied system. Because of the latter, the few image sources assumption is no longer valid and more images were required (i.e. 24 image sources) in order to retrieve the exact behavior of the considered acoustic treatment.

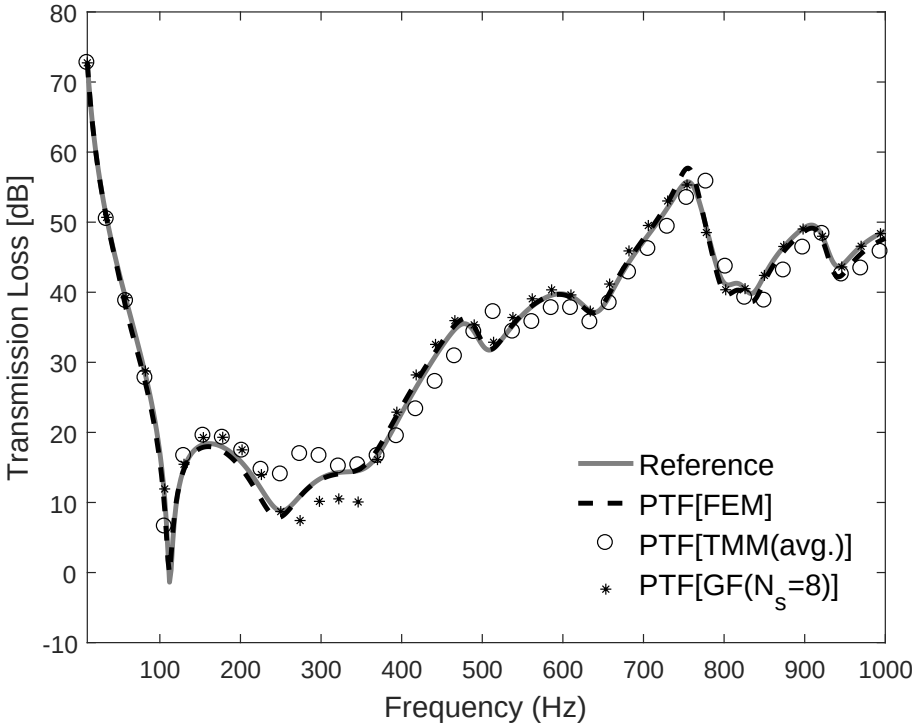

Figure 3.9 Transmission loss of a baffled simply supported aluminum panel with attached sound package coupled to 20 cm thick niche. The sound package involves 2 cm thick melamine foam with a 1.5 kg/m^2 heavy layer on top.

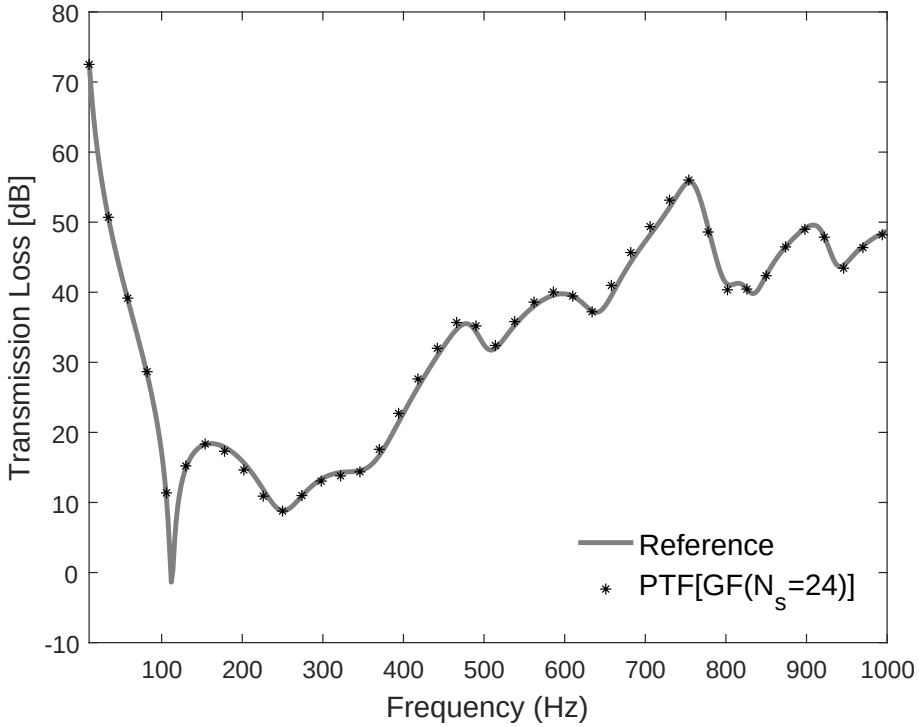

Figure 3.10 Transmission loss of a baffled simply supported aluminum panel with attached sound package coupled to 20 cm thick niche. The sound package involves 2 cm thick melamine foam with a 1.5 kg/m^2 heavy layer on top.

Configuration 3 : panel-foam-panel system

To round off the current validation, the radiation of simply supported aluminum double panels into an unbounded fluid is considered. 2 cm thick limp melamine foam is placed between the panels. A detailed description of the system and its FE model can be found in the convergence study subsection 3.4.1. The TL is reported in Fig. 3.11 and 3.12. The results are similar to the previous configuration. The PTF-TMM is not able to capture fully the physics of the problem. On the other hand, PTF-GF with the correct number of image sources predict perfectly the TL of the system.

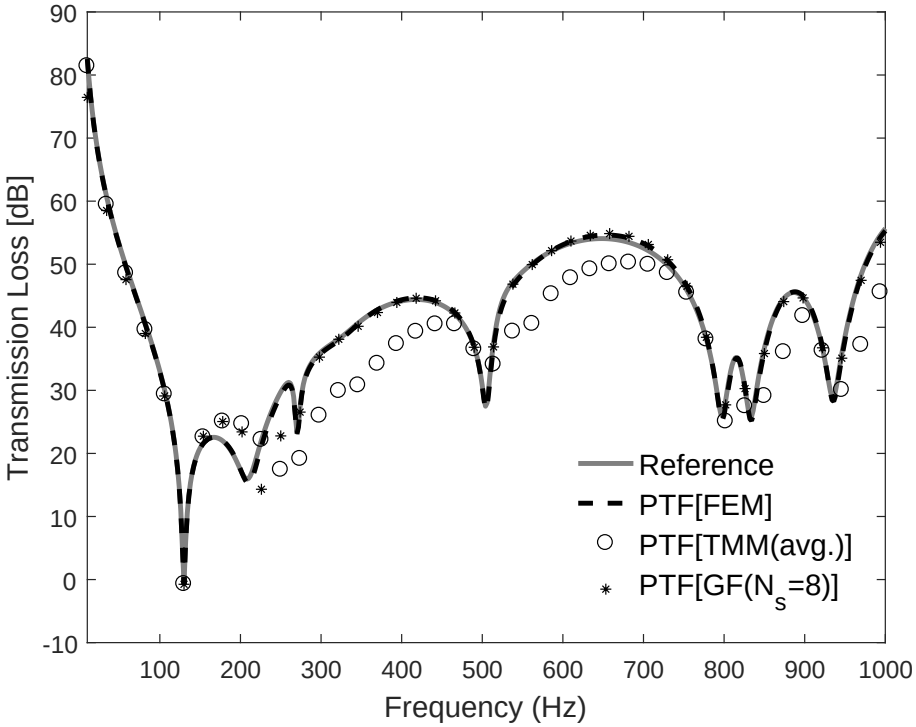

Figure 3.11 Transmission loss of simply supported aluminum double panels into an unbounded fluid. A 2 cm thick limp melamine foam is placed between the panels.

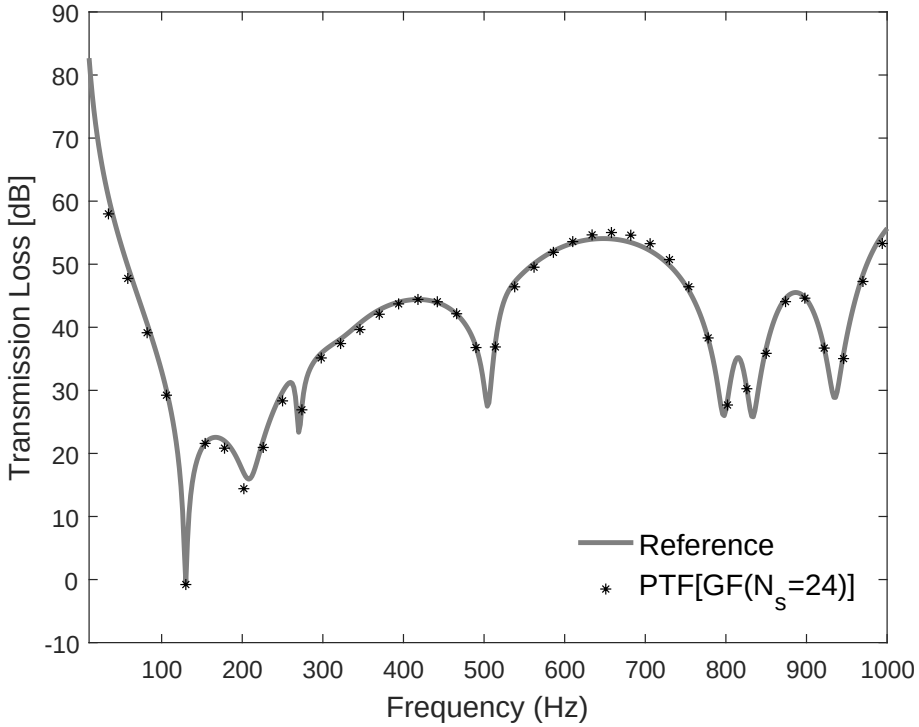

Figure 3.12 Transmission loss of simply supported aluminum double panels into an unbounded fluid. A 2 cm thick limp melamine foam is placed between the panels.

Finally to show the limitation of using the TMM in the PTF-GF approach, a more challenging configuration of the double panels case is considered by replacing the melamine foam with an acoustic cavity filled with air. A loss factor of 0.05 is considered for the acoustic cavity (i.e. $\eta_a = 0.05$). The finite element model used for the double panels remains the same and the cavity is modeled by $32 \times 24 \times 2$ eight-noded fluid elements. Figure 3.13 shows that the curves of the PTF[FEM] and the reference are in a good agreement over the whole frequency range. Its obvious that the averaged TMM is not able to capture the modal behavior of the rigid acoustic cavity due to the infinite lateral assumption. Also the GF based model corrected by means of ISM up to the fourth order of reflections (i.e. Ns=24 image sources) isn't able to capture fully the physics of the rigid acoustic cavity. Such low damped acoustic medium requires in theory an infinite number of reflections in order to capture accurately its modal behavior.

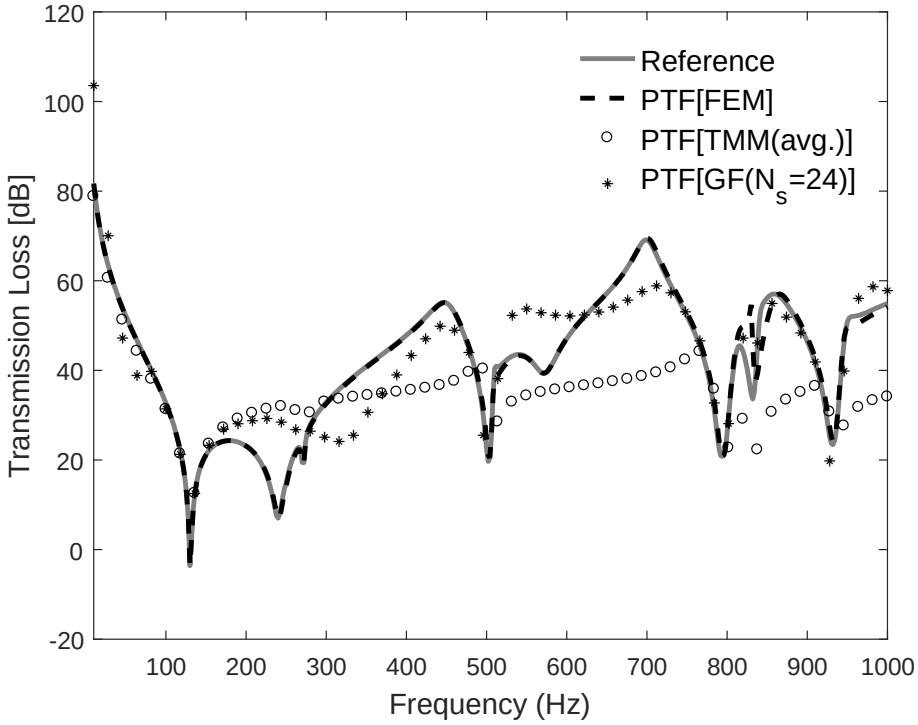

Figure 3.13 Transmission loss of simply supported aluminum double panels into an unbounded fluid. 2 cm thick acoustic cavity is placed between the panels.

Indeed, an enhancement of the accuracy of the GF based model is observed when the order of reflections is increased ; Fig. 3.14 presents the example using 8280 image sources. However, even if the physics is fully captured, the method still depict some differences with the reference especially around the double wall resonance frequency, i.e. 242 Hz. Therefore, the use of the GF based model to characterize such modal driven behavior is not realistic and requires a prohibitive computational time and resources.

Note that the use of such relatively high loss factor $\eta_a = 0.05$ within the cavity is done on purpose to show that even with this high damping, the GF based on the TMM is not able to describe correctly the «empty» cavity modal controlled behavior. Therefore, is expected that smaller loss factors lead to more discrepancies while higher one improve accuracy (almost perfect agreement using $\eta_a = 0.50$). Of course, once an absorbing material fills the cavity, the method becomes accurate. This is a limitation of the TMM and not the GF approach. On the other hand, using modal based TMM [73, 74] to estimate the Green's kernels can be easily employed to characterize such modal acoustic medium. And of course this configuration can also be handled accurately using a simple PTF model wherein the cavity is defined by its analytical or FE derived impedance, as was for the niche in configuration 2.

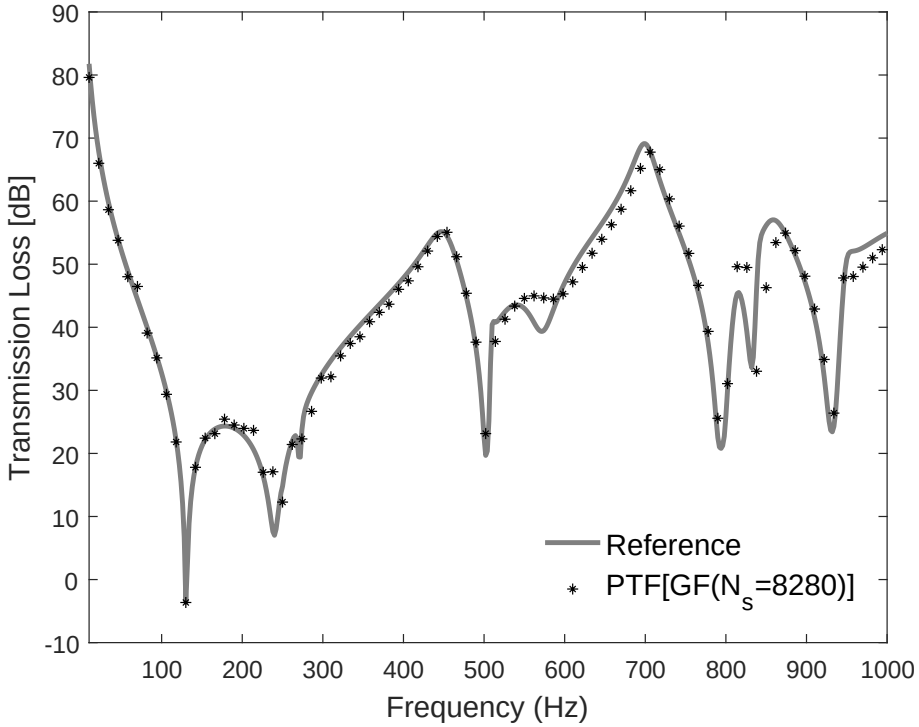

Figure 3.14 Transmission loss of simply supported aluminum double panels into an unbounded fluid. 2 cm thick acoustic cavity is placed between the panels.

As a final remark, note that while a formal comparison of the computational efficiency of the methods is not presented here, one can argue that the PTF-GF method is highly efficient. While the PTF approach needs an initial effort in order to compute the PTFs relations of master systems, these PTFs can take advantage (i) of the parallel aspect of the approach, (ii) the geometrical symmetry of the system and (iii) the different FE mesh that could be used in each subsystem in order to reach the convergence. Moreover, the simplified acoustic treatments model is about 10 times faster than classical FE methods as shown in Ref.[3] and provides a considerable simplification since meshing of the sound package is not needed. Finally, the radiation impedance is evaluated analytically, which avoid expensive integral calculations. All these advantages corroborate the efficiency of the proposed methodology, especially for parametric studies.

Also, it should be pointed out that the number of image sources is a critical point for the computational efficiency of the GF based model, and is recommended to consider as little as possible. This is plausible since the sound package is a highly dissipative medium. However, as shown along the paper the GF based model corrected by means of the ISM need up to the fourth order of reflections (i.e. Ns=24) due to the small area of the used acoustic treatments. Therefore, a decrease of the computational efficiency of the GF based

model is expected. In order to enhance the efficiency, a truncation rule (see Ref.[3]) can be used in order to stop image sources generation process when the vibrational field of virtual sources does not reach the trimmed area nodes inside the physical surface of the acoustic treatment S. The truncation rule is based on the mean free path r_c and a considered tolerance ϵ, such as

$$r_{ij} < \epsilon r_c, \tag{3.29}$$

with

$$r_c = \frac{\pi S}{p}, \tag{3.30}$$

where S is the area of the acoustic treatment and p its perimeter. It was shown in Ref.[3] that for a $\epsilon = 1$ good results are obtained and the error between the obtained results with the GF based model and the reference is near to zero. However, this truncation rule was not used in this article because the main objective was to demonstrate the accuracy of such methodology in a PTF framework. In future, the truncation criteria should be studied and a clear tolerance criterion should be identified depending on the surface dimension of the acoustic treatment. Then, it can be employed to improve the efficiency of the GF based model.

3.5 Conclusion

In this paper, the PTF approach has been used to couple the finite element method with an analytical model of the sound package. The noise control treatment model is based on the Green functions formalism with the TMM assumptions, i.e. homogeneous, flat, infinite extent (i.i. only the direct field is taken into account), and isotropic treatments. The contribution of the reflected field of the acoustic treatment is assumed to be of a non-diffuse nature and it has been taken into account by means of ISM, which is intrinsically limited to polygonal areas. A preliminary analysis was performed to assess the convergence of the PTF approach based on classical FEM. It was shown that a patch mesh criterion of $\lambda_s/3$ is necessary to predict reliably and accurately the dynamic behavior of vibroacoustic systems with attached control noise treatment. Another powerful numerical aspect is the independent characterization of each subsystem and by consequence only the PTFs relations of the modified subsystem have to be upgraded. Then, the performances of the proposed approach have been assessed for different transmission problems (i.e. simple and double wall configurations) with different attached acoustic treatments (light and spring-mass treatments). The results were systematically compared with full FEM/BEM

solution, a locally reacting model and a sub-structuring PTF approach wherein FE is used to calculate the PTFs relations.

It has been found that the GF based model, corrected with the proper number of image sources to account for the reflected field at the sound package lateral edges, matches extremely well the reference solution for all studied configurations. On the other hand, as expected, the locally reacting model is limited to simple single wall configurations with light sound packages. Finally, the proposed method provides an accurate and fast prediction of the behavior of flat trimmed vibroacoustic systems, especially at the early stage of the design process where a dozen of acoustic treatment are tested with the same structure and cabin. The curvature effect is the subject of ongoing research.

CHAPITRE 4

Validity of TMM models for the prediction of the effect of curved sound packages

Auteurs et affiliation :

K. Kesour : étudiant au doctorat, Université de Sherbrooke, Faculté de génie, Département de génie mécanique.

L. Alimonti : Ph. D. en génie mécanique, ESI US R&D North America, 12555 High Bluff Drive, 92130, San Diego, USA

N. Atalla : professeur, Université de Sherbrooke, Faculté de génie, Département de génie mécanique.

Date d'acceptation : Soumis pour publication le 28 janvier 2019

État de l'acceptation : -

Revue : Journal of Sound and Vibration

Référence : -

Titre français : Commentaires sur la validité des modèles basés sur la matrice de transfert pour la prédiction de l'effet des traitements phoniques courbes.

Contribution au document : Cet article contribue à la thèse en évaluant la validité des modèles TMM pour tenir compte de l'effet des traitements phoniques courbes dans des systèmes vibroacoustiques. Une étude quantitative à travers deux études paramétriques est présentée.

Résumé français : Dans cet article, nous évaluons la validité de l'utilisation de la méthode de la matrice de transfert (TMM) pour tenir compte de l'effet des traitements phoniques courbes dans les systèmes vibroacoustiques. Pour ce faire, une méthode de sous-structuration basée sur l'approche *Patch Transfer Functions* est utilisée pour coupler efficacement la Méthode des Éléments Finis (FEM) standard de la structure et de la cavité acoustique avec le modèle du traitement acoustique. Trois modèles de traitement du contrôle du bruit sont comparés, à savoir (i) un modèle TMM à réaction locale, (ii) un modèle TMM à réaction non locale, et (iii) la FEM. Le modèle FEM prend en compte la courbure du traitement pour prédire son comportement dynamique tandis que les modèles TMM simplifiés supposent que le traitement phonique est plat (c.-à-d. le traitement est déroulé), homogène et latéralement infini. De

plus, ces résultats sont systématiquement comparés à une méthodologie complète par éléments finis/éléments de frontières (FEM/BEM). La précision et les limites de l'adoption de l'approximation du traitement acoustique plat (*unwrapped*) utilisée dans les modèles de la TMM sont démontrées dans deux études paramétriques. Le premier considère le rayon de courbure du système comme un paramètre alors que l'épaisseur SP est constante. La seconde considère l'épaisseur du traitement comme un paramètre alors que le rayon de courbure du système est fixé. Pour les configurations considérées, la première étude paramétrique permet de conclure que la courbure du SP n'affecte pas le comportement dynamique du système en raison de sa grande dissipation et qu'il peut être pratiquement supposé plat. Toutefois, la deuxième étude paramétrique montre que l'épaisseur du traitement peut affecter la précision des modèles TMM.

Note : -

4.1 Abstract

In this paper, the validity of using the Transfer Matrix Method (TMM) to account for the effect of curved noise control treatments in vibroacoustic systems is assessed. For this purpose, a sub-structuring method that employs a Patch Transfer Functions (PTF) approach is used to efficiently couple standard Finite Element Method (FEM) of the structure and the acoustic cavity with the sound package model. Three models of the noise control treatment are compared, namely (i) a locally reacting model, (ii) a non-locally reacting model based on the TMM, and (iii) a FEM. The FEM model considers the actual curved geometry of the SP in order to estimate its dynamic behavior while the simplified TMM based models assume the SP to be flat (i.e. unwrapped if curvature is present), homogeneous and of infinite lateral extent. In addition, these results are systematically compared to a full Finite Element/Boundary Element Methodology (FEM/BEM). The accuracy and the limitations of adopting the unwrapped approximation in TMM based models are shown through two parametric studies. The first considers the radius of curvature of the system as a parameter while the SP thickness is constant. The second considers the thickness of the SP as a parameter while the radius of curvature of the system is held fixed. For the considered configurations, the first parametric study allows to conclude that the curvature of the SP does not affect the dynamic behavior of the system due to its large dissipation and softness and it can be practically assumed flat. However, the second parametric study shows that the thickness of the curved SP may affect the accuracy of the TMM based models.

4.2 Introduction

Noise has become an integral part of our daily lives, to the point that it can affect our health and well-being. This is particularly true in the different types of transport such as automobiles, trains and airplanes. Therefore, transportation industries have a double challenge to create a means of transport that takes into consideration the acoustic comfort of its passengers while allowing an eco-responsible mobility. To reduce fuel consumption, industries are opting for a lightweight design for their vehicles, which could lead to higher interior noise levels. Under these circumstances, the most practical and cost-efficient method to improve their acoustic efficiency is by changing the propagation path of the sound and vibration waves by using dissipative components placed between the structure (e.g. fuselage) and the acoustic cavity (e.g. cabin).

Such dissipative components, also called sound package (SP), often involve poroelastic layers which have excellent acoustic performances in the high-frequency range. However, this ability to absorb sound and vibration decreases considerably in the low-frequency range (i.e. long wavelength) where the energy emitted by the sources can be highly important. Therefore, in the early stage of the design process, numerical simulations are necessary to identify the optimal configuration of the sound package. Traditional numerical tools used at this stage either lack accuracy (if efficiency is targeted) or are computationally prohibitive (if accuracy is rather targeted). For instance, the classical Finite Element Method (FEM) possibly coupled with Boundary Element Method (BEM) [9] have proved to give good and reliable results in real industrial problems. However, this class of methods could lead to very large numerical models due to the large number of degrees of freedom required in order to capture accurately the dynamic behavior of the SP. This very fine mesh is required because the SP involves (i) soft, i.e. short wavelength, and (ii) very dissipative materials. In addition, the meshing phase is required for each configuration of the SP. Moreover, this class of methodologies necessitates a detailed description of the geometry and of the boundary conditions of the multilayer which may be unknown. Also, if one subsystem (e.g. SP, panel, cavity) or the excitation is modified the whole coupled system must be re-meshed and resolved. Therefore, more practical and simplified numerical tools for modeling SP are often needed.

In this context, several strategies have been proposed in order to overcome the computational burden of conventional methods. On the one hand, much attention was devoted to transmission loss and absorption problems involving flat trimmed panels [80, 83, 6, 2, 3, 41]. For instance, Alimonti et al. [6, 2, 3] proposed a non-locally reacting model based on the Transfer Matrix Method (TMM) [8] allowing to overcome the limitations of the locally

reacting techniques. The non-local behavior of the SP is obtained by an integral formulation that employs the Green functions of the flat, homogeneous and laterally unbounded SP. Under these assumptions, the Green functions are estimated by the TMM for a given boundary condition at the two faces of the SP. Moreover, it should be pointed out that almost perfect prediction of the response of the coupled system of a flat trimmed panel-cavity system was achieved when the reflected field of the acoustic treatment is retrieved by means of the Image Source Method (ISM) [3]. The ISM correction works only for a fluid, otherwise it is only an approximation. Moreover, in order to improve the efficiency of classical hybrid methodologies, Kesour and Atalla [41] used the simplified non-locally reacting model based on the TMM to describe the dynamic behavior of the SP combined with a FEM model of the structure and cavity in a Patch Transfer Functions (PTF) framework [62, 22, 82]. It should be noted that the PTF technique allows an independent characterization of subsystems that makes the approach suitable for parallel computation. Moreover, the PTF approach leads to a small complex symmetric system fully populated, leading to speeding up the solution of the coupled problem. And since the approach is fully modular, only the PTFs relations of the modified subsystem have to be upgraded. For these reasons, the PTF technique allows to speed up parametric and optimization studies making them possible in realistic times and compatible with the efficiency requirements of the industry.

If, on the one hand, the literature of flat SP models is very rich, the same cannot be stated for curved SP. In classical implementations [32, 75, 76], the effect of the flat sound package (i.e. unwrapped if curvature is present) is provided by the TMM and is used to correct the vibroacoustic indicators of the bare structure. For instance, Mejdi et al. [60] investigated the validity and accuracy of using locally reacting TMM model for prediction of the transmission loss through clamped curved panels lined with a light foam layer modeled as an equivalent limp fluid. This simplified model was able to capture the physical behavior in the case of three configurations of curved panels of different radius of curvature involving only light foam treatment. However, more discrepancies were observed in the low-frequency domain where the results tend to follow the bare panel curves. Another way to integrate the unwrapped flat SP characterized by TMM within a curved panel-cavity system consists of using hybrid methodologies [7, 40, 39]. Alimonti and Gardner [7] studied the case of moderately curved trimmed plate radiating in the air while excited by a force point. The FEM is used to describe the curved plate while the SP is unwrapped and assumed to be flat. The SP is modeled using the simplified non-locally reacting model based on TMM. Indeed, these obtained results indicate that for this high radius of curvature, the treatment can be practically assumed flat. These results suggest using unwrapped SP

approximation is acceptable for structures with a high radius of curvature (i.e. low ring frequency). However, such approximation becomes questionable in the case of low radius of curvature systems.

Recently, in Ref. [25] a curved TMM was proposed for infinite (non reverberant) trimmed cylinders excited by an oblique plane wave. It is based on the work of Magniez et al. [54, 55]. The proposed methodology was validated in the case of a trimmed half-cylinder where a good correlation was observed with the FEM/BEM approach, except at low frequency where discrepancies are present (i.e. due to the use of a TMM of a full free cylinder). In this context, the current paper proposes a methodology that aims to simplify the introduction of curved SP and proposes a more general method valid for various configurations of structures and SP (i.e. since is based on a hybrid FEM-TMM approach) and for various mechanical and acoustical excitations. In addition, this paper studies the validity of using TMM based models to account for the effect of curved SP attached into a curved structure-cavity system. For this purpose, a sub-structuring method that employs a patch transfer approach is used to couple efficiently a standard finite element schemes of the structure and the acoustic cavity with the sound package modeled using three methods, namely, (i) a locally reacting model, (ii) a non-locally reacting model and (iii) a FEM. First, the theory behind the PTF approach and the TMM based models is summarized. Then, the accuracy of using a non-locally reacting model based on TMM for a flat trimmed panel-cavity system is recalled while the limitations of the locally reacting models based on TMM are confirmed. Next, a parametric study involving several radii of curvature is considered in order to show the validity of using an unwrapped approximation to account for the effect of curved SP. Such approximation may be justified by the softness and large dissipation taking place in the poroelastic layers involved in the SP. The considered SP involves a foam layer with a mass-layer on top. Finally, a parametric study using the thickness of the SP as a parameter is conducted for curved shell-cavity system excited by point force. This latter parametric study allows to investigate the effect of the thickness of the SP as well as the strong and weak coupling between the structure and the mass-layer.

4.3 Theory

In this section, the theory behind the PTF approach is recalled briefly. Then, the coupled equations of the studied systems are presented. Next, the methodologies used to estimate the patch transfer functions relations (PTFs) of the subsystems and the calculation of the vibroacoustic indicators of interest are described.

4.3.1 Patch Transfer Functions

The PTF approach is a sub-structuring method where each subsystem is considered independently and its coupled interface is subdivided into patches (using a proper criterion). Only the averaged normal variables/responses over patches are considered. As a result, this technique involves the calculation of patches mobility or impedance matrices, also called PTFs relations, of the subsystem. In addition, if the subsystem is excited, then the uncoupled response is also computed. The PTFs may gather relations between excited and receiving patches belonging to the same or to different interfaces of the same subsystem.

The studied vibroacoustic problem involves a curved or a flat structure with attached SP coupled to an acoustic cavity that radiates into a semi-infinite fluid (SIF) (see Fig. 4.1). Hence, the coupled system is divided into four subsystems, namely (i) the structure (ii) the acoustic treatment (iii) the cavity and (iv) the SIF. The sound package is coupled over one side (i.e. interface 1) to the structure and over the other side (i.e. interface 2) to the cavity. The latter is radiating into a SIF through a transmission hole (i.e. interface 3) assumed to be inserted into infinite rigid baffle. The PTFs relations of each subdomain are defined over the coupling interfaces which are discretized into N_p patches, as depicted in Fig. 4.2.

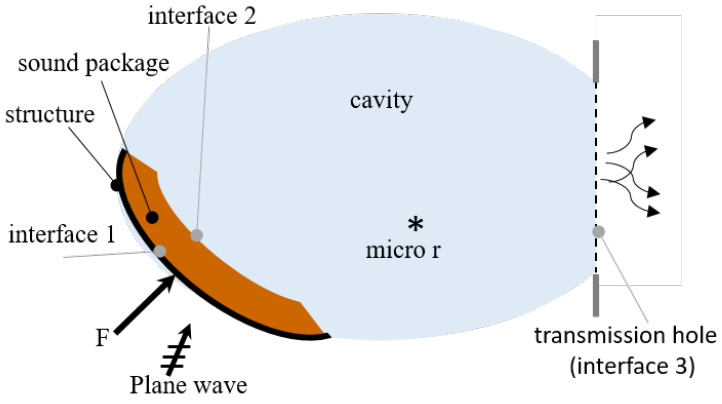

Figure 4.1 General vibroacoustic problem involving a trimmed structure-cavity system .

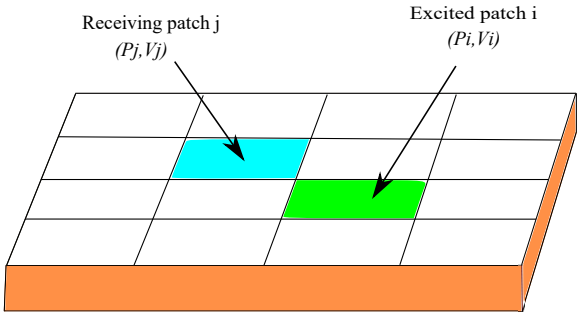

Figure 4.2 A generic interface of a sub-domain divided into patches.

Hence, once the PTFs relations of subdomains are computed the superposition principle can be applied to each subdomain. Then, coupling conditions are used to couple the subsystems leading to the following coupled system of equation [40],

$$\begin{bmatrix} \mathbf{I}_d + \mathbf{Y}^S\mathbf{Z}_{11}^{SP} & \mathbf{Y}^S\mathbf{Z}_{12}^{SP} & 0 \\ -\mathbf{Z}_{21}^{SP} & -\mathbf{Z}_{22}^{SP} + \mathbf{Z}_{22}^{Cav} & -\mathbf{Z}_{23}^{Cav} \\ 0 & \mathbf{Z}_{32}^{Cav} & -\mathbf{Z}_{33}^{Cav} - \mathbf{Z}^{rad} \end{bmatrix} \times \begin{bmatrix} \mathbf{V}_1 \\ \mathbf{V}_2 \\ \mathbf{V}_3 \end{bmatrix} = \begin{bmatrix} \tilde{\mathbf{V}}^S \\ 0 \\ 0 \end{bmatrix}, \tag{4.1}$$

where only the structure is assumed to be excited by an external load. In Eq. (4.1), $\mathbf{I}_d$ is the unit matrix of dimensions $N_p \times N_p$. The superscript S stands for the structure, SP for the sound package and Cav for the acoustic cavity. $\mathbf{Y}^S$ is the structure mobility matrix. Its entries Y_{ij}^S are defined as the ratio of the arithmetical mean normal velocity $\langle V_i \rangle$ over a receiving patch i and the mean pressure $\langle P_j \rangle = 1$ Pa of an excited patch j while using a pressure release condition over the other patches, i.e. $\langle P_{i \neq j} \rangle = 0$ Pa. $\tilde{\mathbf{V}}^S$ is a mobility vector of the in-vacuo structure due to the external excitation. The $\mathbf{Z}_{mn}$ (m, n=1, 2 or 3) is an impedance matrix. Its entries $Z_{mn_{ij}}$ are defined as the ratio of the mean pressure $\langle P_{m_i} \rangle$ over a receiving patch i belonging to an interface m and the mean normal velocity $\langle V_{n_j} \rangle = 1$ m/s of an excited patch j belonging to an interface n while blocking the other patches, i.e. $\langle V_{n_{i \neq j}} \rangle = 0$ m/s. Detailed derivations of the theory of the PTF technique can be found in [62, 1, 41].

4.3.2 Vibroacoustic indicators calculation

Solving the linear system (4.1) provides the patches normal velocities at interfaces 1, 2 and 3 for the coupled system. Therefore, the averaged quadratic velocity of the structure can be obtained by,

$$\left\langle \mathbf{v}^2 \right\rangle = \frac{1}{2S} \sum_{i=1}^{N_p} \mathbf{V}_{1_i} \mathbf{V}_{1_i}^* S_i, \tag{4.2}$$

with S_i is the area of patch i and S is the total area. The radiated power Π_{rad} can be expressed as a function of the radiated patch pressure P_{3_i}, patch normal velocities V_{3_i} at interface 3 and the patch area S_i :

$$\Pi_{rad} = \frac{1}{2} \sum_{i=1}^{N_p} Re\{\mathbf{P}_{3_i} \mathbf{V}_{3_i}^* S_i\}. \tag{4.3}$$

Since the radiated pressure is related to normal velocity by the radiation impedance, such as $\mathbf{P}_3 = \mathbf{Z}^{rad}\mathbf{V}_3$. Therefore, the Eq. (4.3) can be rewritten as :

$$\Pi_{rad} = \frac{1}{2} \sum_{i=1}^{N_p} Re\{(\mathbf{Z}^{rad}\mathbf{V}_{3_i})\mathbf{V}_{3_i}^* S_i\}, \tag{4.4}$$

where the superscript * indicates the conjugate of the complex normal velocity and N_p is the number of patches. Hence, the Transmission Loss (TL) can be simply computed as $TL = 10 \log\left(\frac{\Pi_{inc}}{\Pi_{rad}}\right)$, where Π_{inc} denote the incident sound power.

4.3.3 Calculation of the subsystems PTFs relations

In this part, the modeling of each subsystem is described. A very attractive aspect of the PTF approach consists of the possibility of providing the transfer functions between patches (PTFs) by using methods of different kinds (i.e. analytical, numerical or experimental). In this paper all the PTFs relations of the structure and cavity are computed using the classical FEM except for the mobility vector $\tilde{\mathbf{V}}^S$ of the in-vacuo structure due to an acoustic excitation. In the case of a curved structure, the mobility vector is obtained in two steps. First, a case of the rigid structure is considered in order to obtain the parietal pressure (i.e. blocked pressure) on the rigid surface by solving a scattering problem (using a BEM approach). Then, the nodal solutions (i.e. displacement) are calculated using the blocked pressure as excitation over the panel elements. On the other hand, since the ra-

diating interface (i.e. transmission hole) is flat and assumed to be inserted into infinite rigid baffle, the radiation impedance $\mathbf{Z}^{rad}$ is derived from a quick analytical estimation of Rayleigh's integral ; its expression and derivation are given in Ref.[22].

In order to study the validity of the unwrapped approximation, the SP is modeled using three methods, namely (i) a standard FEM model considering the real geometry of the SP (e.g. flat, curved or cylindrical), (ii) a locally reacting method based on the TMM (referred to as LR-TMM) and (iii) a non-locally reacting model based on the TMM (referred to as NLR-TMM).

Non-locally reacting based TMM model

The non-locally reacting model based on the TMM aims to simplify the modeling of noise control treatment. The model considers that the effect of geometric details, such as curvature and lateral dimensions, can be neglected. Such simplification can be justified by the highly dissipative and soft nature of these components. Hence, the acoustic treatment is assumed to be flat (i.e. unwrapped if curvature is present), homogeneous, isotropic and of an infinite lateral extent. Under these circumstances, the TMM is used to provide the Green functions for a given set of baffle condition at the two ends of the SP. Therefore, the nodal transfer function between an excited node x_i and a receiving node x_j is expressed as a convolution integral based on the Green functions, see Eq. (4.6). This model is referred to as a direct field model because of the infinite lateral extent assumption used in the TMM, i.e. the finite size effect is neglected. In the following, the simplified Green functions based model is briefly presented. The reader may refer to Ref. [2] for a detailed derivation.

It is worth mentioning that the non-locally reacting model only allows to account for the continuity of normal displacements (i.e. velocities) and stresses (i.e. pressures) at the structure and cavity interfaces. This limitation is due to the use of a 2x2 reduced transfer matrix that relates normal velocities and pressures over the two ends of SP, see Ref. [2] for more details. Since the PTFs relations of the SP are described using an impedance matrix form, the two ends of the SP are assumed to be inserted in an infinite rigid baffle (i.e. the normal displacement is null outside the trimmed surface). Moreover, the front and rear sides of the unwrapped multilayer are discretized into rectangular patches using $n_x \times n_y$ nodes per patch as depicted in Fig. 4.3 and a nodal velocity excitation is applied over each node. In the PTF framework, the impedance matrix of the baffled-baffled unwrapped acoustic treatment is given by (with $m = 1, 2$ and $n = 1, 2$) [41] :

$$Z_{mn}^{SP} = V_{out} D_{mn} A_n V_{in}, \tag{4.5}$$

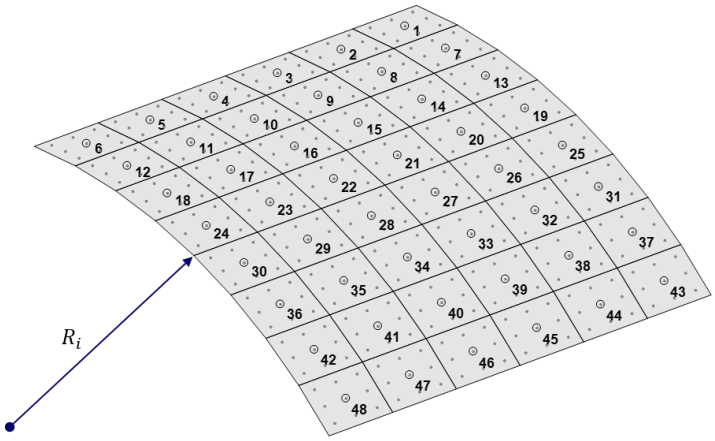

Figure 4.3 An example of the geometry of the curved surface of the sound package subdivided into 6×8 patches. The circles denote the centers of the patches and the dot the used mesh nodes considered in the NLR-TMM model.

where, V_{in} and V_{out} represent mapping operators used to perform the desired averaging, namely, $V_{in_{ij}} = 1$ and $V_{out_{ji}} = A_i/A_{p_j}$ if node i belongs to patch j. A_n is a diagonal matrix gathering the area associated with each node. The nodal matrices $\mathbf{D}_{mn}$ are given by the following integral

$$D_{mn}(r_{ij}, \omega) = \frac{1}{2\pi} \int_0^\infty d_{mn}(k, \omega) J_0(k r_{ij}) |\hat{\psi}(k)|^2 k dk, \tag{4.6}$$

where r_{ij} is the geodesic distance between the nodes x_i and x_j as depicted in Fig. 4.4 and for curved system is defined such as $r_{ij} = \sqrt{l_{ij}^2 + s_{ij}^2}$. k is the wavenumber and $J_0(kr_{ij})$ is the Bessel function of zero order of argument kr_{ij}. The notation $\hat{f}(k)$ indicates the Hankel transform of the function $f(r)$. The Green functions d_{mn} represent the transfer coefficient of the reduced transfer matrix between normal velocities $V_{1,2}$ and pressures $P_{1,2}$ (equivalently, stresses $\sigma_{1,2} = -P_{1,2}$) over the two ends of SP in the wavenumber domain. The filter $\hat{\psi}(k)$ is the Fourier transform of the normalized radially symmetric jinc function $\psi(r)$, defined a $\psi(r) = \frac{k_s^2}{2\pi} \frac{J_1(k_s r)}{k_s r}$. Thus, the filter $\hat{\psi}(k)$ is assumed to behave as an ideal filter (i.e. $\hat{\psi}(k)$=1).

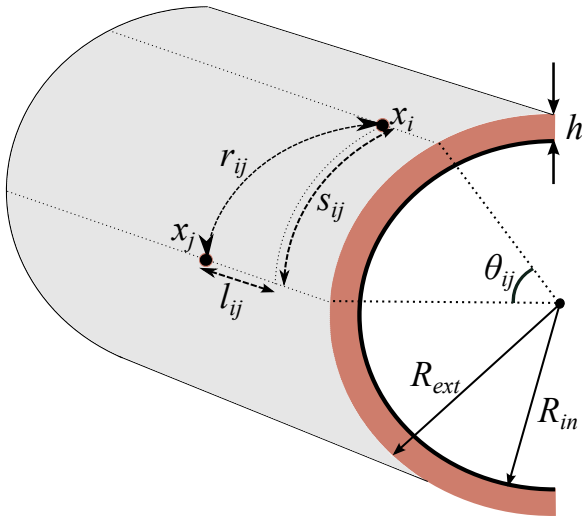

Figure 4.4 Example of the geodesic distance r_{ij} between nodes i and j lying on a curved trimmed interface.

It should be mentioned that for flat noise control treatment, we have $D_{12} = -D_{21}$. However, for curved thick SP this equality is no longer valid since the arc length is not the same at the two ends of the SP (i.e. equivalently the geodesic distance $R_{ext}\theta_{ij} > R_{in}\theta_{ij}$). Nonetheless, in the case of SP with a thickness h smaller compared to the radius of curvature R_{ext}, these entries can be considered approximately equal $D_{12} \approx -D_{21}$. Hence, the geodesic distance used to estimates transfer functions D_{mn} can be computed on the mid surface of the SP, defined by its radius $R_{mid} = R_{ext} - h/2$. This approximation may be justified by the fact that in real applications, the thickness of the SP is often very small compared to the radius of curvature of the system. Therefore, this approximation is used throughout this paper.

Moreover, to enhance the accuracy of the NLR-TMM model, the Image Source Method (ISM) [3] can be used to retrieve the reflected field from the lateral edges of the SP. Therefore, a finite size correction is considered by means of N_s additional mirror images of the sources (i.e. excited nodes). An example is given in Fig.4.5 when only the first and second order of reflections (i.e. $N_s = 8$) are taken into account in the reflected field. A detailed description is given in [3]. In the following, it will be referred to as NLR-TMM-ISM.

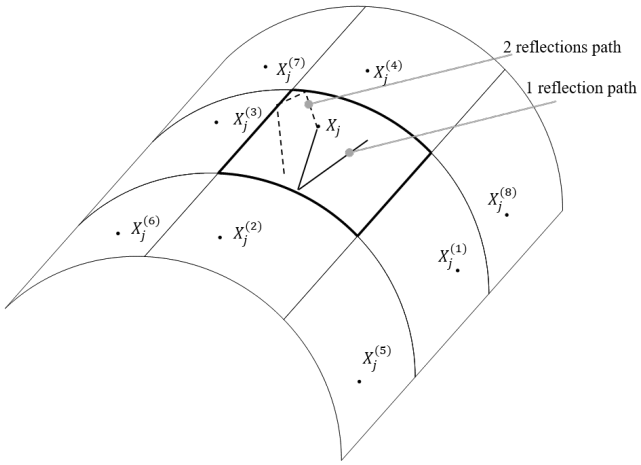

Figure 4.5 An example of the lattice pattern of the virtual sources associated with the generic source located at X_j inside the trimmed surface of SP in bold black lines. The Image lattice is accounting for up to two consecutive reflections.

Locally reacting TMM model

The locally reacting model takes into account the effect of the infinite unwrapped (i.e. flat) sound package in a locally reacting sense by means of the frequency-dependent coefficients of its reduced transfer matrix written in an impedance form. Thus, the diagonal elements of the impedances $\mathbf{Z}_{mn}^{SP}$ matrix of the acoustic treatment are defined such as $Z_{mn_{ii}}^{SP}(\omega) = d_{mn}(k, \omega)$.

Three models are derived from the LR-TMM, namely :

- a normal incidence model, referred to as LR-TMM($k = 0$), with $Z_{mn_{ii}}^{SP}(\omega) = d_{mn}(k = 0, \omega)$

- an averaged incidence model, referred to as LR-TMM(avg.), with $Z_{mn_{ii}}^{SP}(\omega) = \langle d_{mn}(k, \omega) \rangle_{k_0}$ where $d_{mn}(k, \omega)$ is averaged for k between 0 and k_0

- a more elaborated model, referred to as LR-TMM(avg./k_f), based on the flexural and acoustic wavenumber of the infinite flat structure and the cavity, respectively, defined such as :

$$\begin{cases} Z^{SP}_{11_{ii}}(\omega) = d_{11}(k_f, \omega) \\ Z^{SP}_{12_{ii}}(\omega) = \langle d_{12}(k, \omega) \rangle_{k_0} = -Z^{SP}_{21_{ii}}(\omega) \cdot \\ Z^{SP}_{22_{ii}}(\omega) = \langle d_{22}(k, \omega) \rangle_{k_0} \end{cases} \tag{4.7}$$

where k_0 is the acoustic wavenumber in the free air and k_f is the structural flexural wavenumber. In Ref. [20] it was found that the LR-TMM(avg./k_f) model with tuned coefficients was able to provide better predictions compared to the LR-TMM with normal incidence for the studied cases.

Remarks

At the design phase, it's a common practice to use simple flat, curved or cylindrical system. Thus, the primary effort to compute the PTFs of all subsystems can be decreased by exploiting the symmetry of such simple geometry. In this paper, the PTFs of the flat and curved system are derived by exciting only 1/4 of the total number of patches while averaging normal vibroacoustic variables over all the other patches. Next, the PTFs matrix of the subsystem is reconstructed by exploiting the symmetry of the problem.

4.4 Results

This section is concerned with the assessment of the validity of using an unwrapped acoustic treatment approximation in NLR-TMM and LR-TMM models. The studied cases consist of a SP, involving a 19 mm melamine foam and a 1 mm thick mass-layer on top, placed between a 2 mm thick steel shell and an acoustic cavity filled with air (see Table 4.1). The melamine foam layer is modeled as an equivalent limp fluid [64] while the mass-layer as a solid. The first case aims to recall the validity and accuracy of the modeling of such complex SP by NLR-TMM model in a flat system (i.e. $R_{ext} = \infty$). Next, three half-cylinder configurations with different radius of curvature ($R_{ext} = 0.5m$, $R_{ext} = 0.25m$ and $R_{ext} = 0.1m$) are considered in order to investigate the influence of the unwrapped approximation as a function of curvature on the vibrational response of the structure and the Transmission Loss (TL). Finally, a parametric study is conducted using the thickness of the SP as a parameter while the radius of curvature of the system is held fixed. Both flat and curved structures are clamped along the edges and are excited by an

oblique plane wave with an incident and heading angle (45°,0°). Three models included in a PTF framework are compared where the sound package is modeled by (i) an NLR-TMM model, (ii) a locally reacting model and (iii) a FEM model. The Green functions d_{mn} used in TMM based models are obtained from the unwrapped SP while the FEM model considers the actual curved geometry of the SP. The obtained results are systematically compared to a full FEM/BEM [9] provided by an in-house code (NOVAFEM). In the case of a curved structure excited by a plane wave, the exact FEM/BEM solution requires two steps. First, the scattering problem, where the master structure is considered as an acoustically baffled rigid object, is solved in order to estimate the blocked pressure acting on the master structure in the emission domain. Then, in the second step the TL of the coupled system is obtained by solving a fully coupled model where the structure, the SP and its cavity are modeled by a standard FEM while the radiation from the transmission hole and the blocked pressure over the elastic domain on the excitation side are modeled using the BEM. In the PTF framework, all the interfaces between subsystems are discretized into patches respecting a convergence criterion of 3 patches per wavelength $\lambda/3$ which is more conservative compared to a $\lambda/2$ criterion employed by previous authors. The smallest wavelength of the uncoupled panel and cavity is referred to as λ. In the studied frequency range, the structural wavelength λ_s is the smallest. Such a conservative criterion aims to ensure results with better accuracy and to minimize errors introduced by the PTF approach. In fact, this will facilitate the analysis of the results and isolate the effect of the unwrapped approximation.

The compared methodologies are summarized in the following. The Reference solution is obtained by a full FEM/BEM while the subsystems in the PTF approach are modeled by :

- Acoustic excitation : BEM
- Structure : FEM
- Cavity : FEM
- Radiation impedance : analytical calculation using Rayleigh's integral
- SP (unwrapped) : LR-TMM versus NLR-TMM
- SP (curved) : FEM

4.4.1 Flat trimmed system

The first system concerns the sound transmission loss through a flat baffled clamped steel panel with attached sound package coupled to 10 mm thick cavity. The steel shell panel is 2 mm thick and covers all the cavity and its area is of about 0.6×0.5 m^2. The finite element model of the shell and the cavity uses 60×54 4-noded shell elements and

Tableau 4.1 Materials used in the numerical simulations.

Materials	Properties	
Steel	density=7800 kg/m^3 Poisson's ratio=0.3125	Young's modulus=200 GPa damping factor=0.01
Melamine	density=8.8 kg/m^3 Poisson's ratio=0.4 porosity=0.99 tortuosity=1.02 thermal length=130 μm	Young's modulus=80 kPa damping factor=0.17 resistivity=10900 kg/m^3 viscous length=100 μm
Mass layer	density=1.5 kg/m^2 Poisson's ratio=0.3	Young's modulus=1 MPa damping factor=0.5
Air	density=1.21 kg/m^3	speed of sound=342.2 m/s

$60\times54\times1$ eight-noded fluid elements, respectively. The FE mesh along the thickness of the melamine foam layer and the mass layer involves 10 and 1 Hexa-8 elements, respectively. The used materials properties are shown in Table 4.1. As explained in the section 4.3.1, the whole system is divided into four subsystems, namely the first panel, the SP, the rigid walled parallelepiped cavity and the unbounded acoustic domain. Since the convergence of the PTF technique is controlled by the patch size, the interfaces between sub-systems are meshed using 20×18 patches according to the criterion $\lambda/3$ in order to ensure the convergence up to 2400 Hz. In this configuration, the reference problem as well as the mobility vector $\tilde{\mathbf{V}}^S$ of the in-vacuo structure due to the acoustic excitation is solved in one step, because the blocked pressure that excites the flat panel corresponds to twice the incident pressure (i.e. the diffraction problem is not needed).

The mean quadratic velocity of the flat panel and the TL are depicted in Figs. 4.6 and 4.7, respectively. It can be observed that the NLR-TMM model follows almost perfectly the reference. Small discrepancies are observed between 200-400 Hz due to the double wall resonance. These small errors disappear when the reflected field is retrieved by means of ISM using early reflections. As a result the NLR-TMM-ISM model provides a perfect prediction of the structure vibrational response and the TL compared to the PTF(FEM) and the reference. On the other hand, the classical locally reacting models fail around the double wall (DWL) resonance. Indeed, the LR-TMM(avg./k_f) model in Eq. (4.7) fails totally to capture the physics below 500 Hz whereas above this frequency its response is improved to the point of providing an almost perfect approximation of the reference. This can be explained by the fact that the used k_f of the structure is not a good guess

for the k_f of the coupled response. And is mainly due to the strong coupling between the structure and the mass-layer. However, at higher frequencies, the mass acts as a mechanical filter and the structure behaves as if the mass were not present (i.e. the used k_f is a good approximation for the coupled response). The LR-TMM[$k = 0$] model with normal incidence overestimates the TL and the quadratic velocity. The results show that the NLR-TMM model is able to capture the dynamic behavior accurately of complex lay-up over the whole frequency range and suggest that costless locally reacting models such LR-TMM(avg./k_f) may be used in the higher portion of the spectrum.

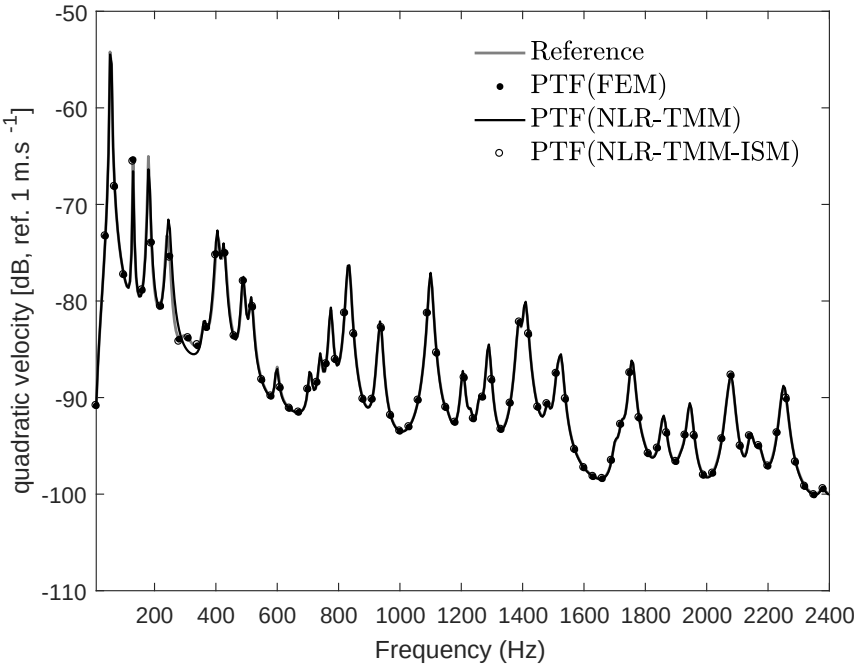

(a)

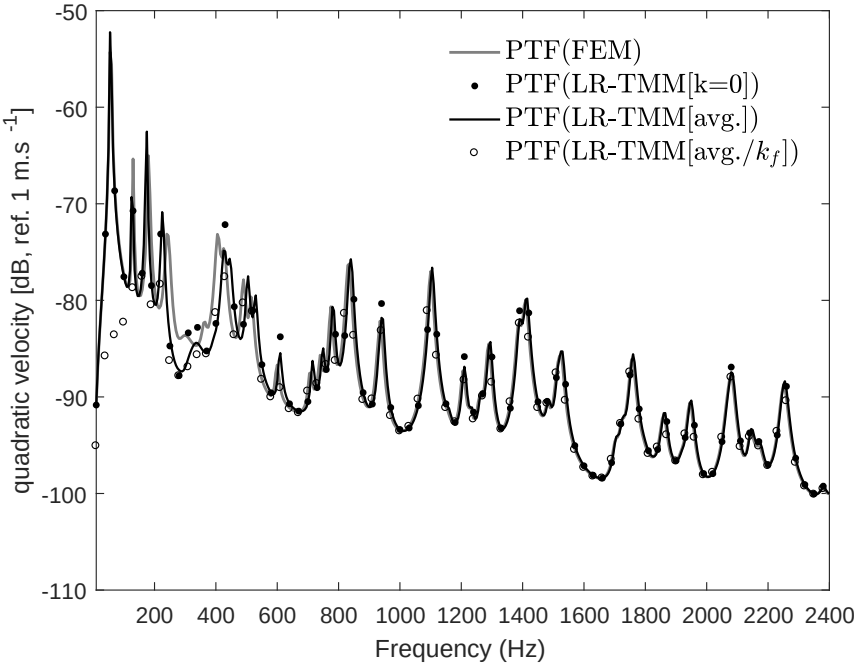

(b)

Figure 4.6 Quadratic velocity of the baffled clamped steel panel. Results relative to the flat system.

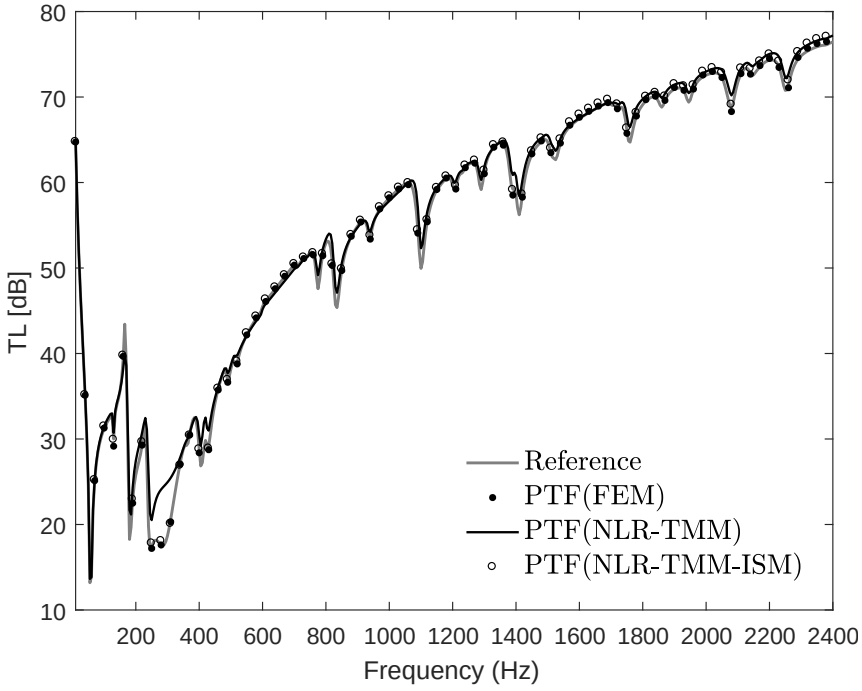

(a)

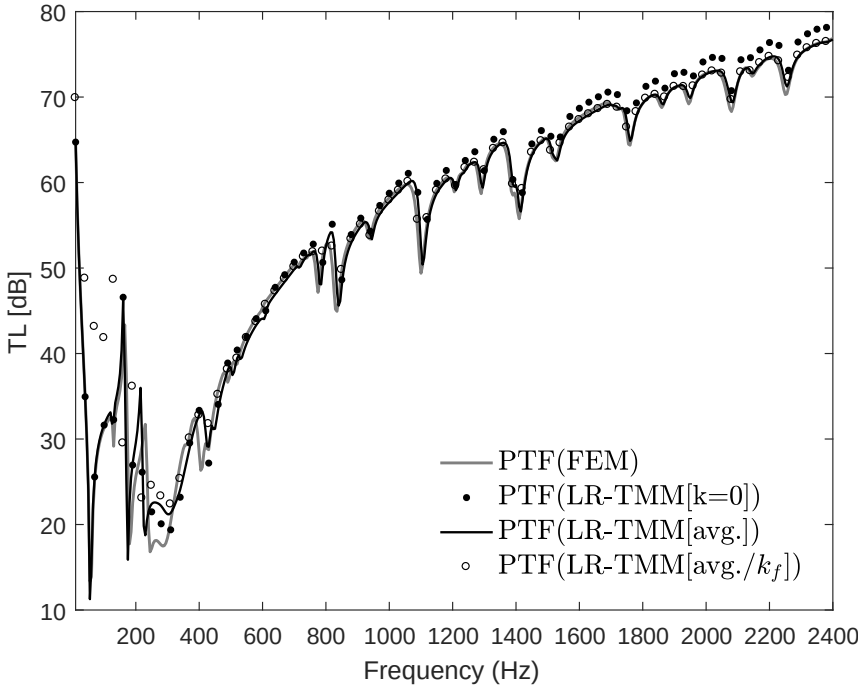

(b)

Figure 4.7 Transmission loss through the baffled clamped steel panel-cavity system with attached spring-mass treatment. Results relative to the flat system.

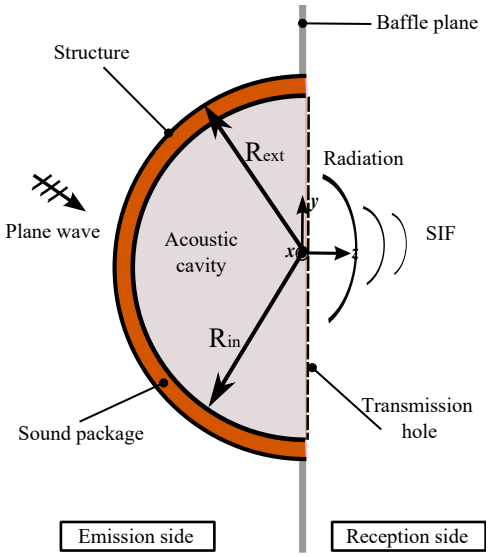

Figure 4.8 Geometry of the clamped half-cylinder structure with attached sound package coupled to a cavity. The system is excited by an oblique plane wave (45°,0°) and radiating into a SIF through the transmission hole. The ends of the cavity and the sound package are considered acoustically rigid.

4.4.2 Curved trimmed system : radius of curvature effect

This section intends to study the validity of using TMM based models (i.e. unwrapped approximation) to account for the effect of curved SP. For this purpose, three clamped half-cylinder with different radii (i.e. R_{ext}=0.5 m, R_{ext}=0.25 m and R_{ext}=0.1 m) and of a length of $L_x = 0.6m$ are considered. The lateral sides of the system (i.e. the bulkheads of the cavity and the SP) are considered as acoustically rigid. The radiation of the lateral faces of the sound package into the SIF is neglected. Hence, the system radiates only through the transmission hole as depicted in Fig. 4.8. In the PTF framework, the interfaces of subsystems are discretized into patches to ensure convergence up to 2000 Hz. The FEM mesh respects the condition $\lambda/9$ for the three configurations in the reference solution. First, a convergence study is conducted for the configuration with R_{ext}=0.5 m in order to show how the patch size affects accuracy and the convergence of the PTF approach in the case of trimmed curved system. Then, the validity and accuracy of the unwrapped approximation is investigated in detail for a spring-mass SP with a constant thickness $h = 20mm$. The vibroacoustic indicators of interest are the averaged quadratic velocity of the panel and the sound transmission loss. In addition, in order to give the reader a clear idea about the accuracy of the compared models, the relative difference of decibels of coupled responses is also added.

Figs. 4.9 and 4.10 show, respectively, the mean quadratic velocity and the TL through the trimmed half-cylinder cavity system with a radius of curvature of about R_{ext}= 0.5 m (i.e. the theoretical ring frequency is at 1690 Hz). Two discretizations of interfaces into patches according to $\lambda/2$ and $\lambda/3$ are compared. As expected, it is observed that the accuracy is enhanced when the number of patches increases, i.e. equivalently the patch size decreases. Therefore, the criterion $\lambda/3$ provides almost prefect prediction compared to the reference while the $\lambda/2$ curves exhibit more errors (see Fig. 4.10(b)), especially above 1300 Hz which represents the convergence limit according to the $\lambda/3$ criterion. However, these errors remain acceptable as the primary effort within the PTF technique can be reduced by half if $\lambda/2$ criterion is used instead of $\lambda/3$. Indeed, one of the two criteria could be used depending on the desired accuracy. However, since the main focus of this paper is the validity of the unwrapped approximation, the $\lambda/3$ criterion is used in order to minimize errors introduced by the PTF approach.

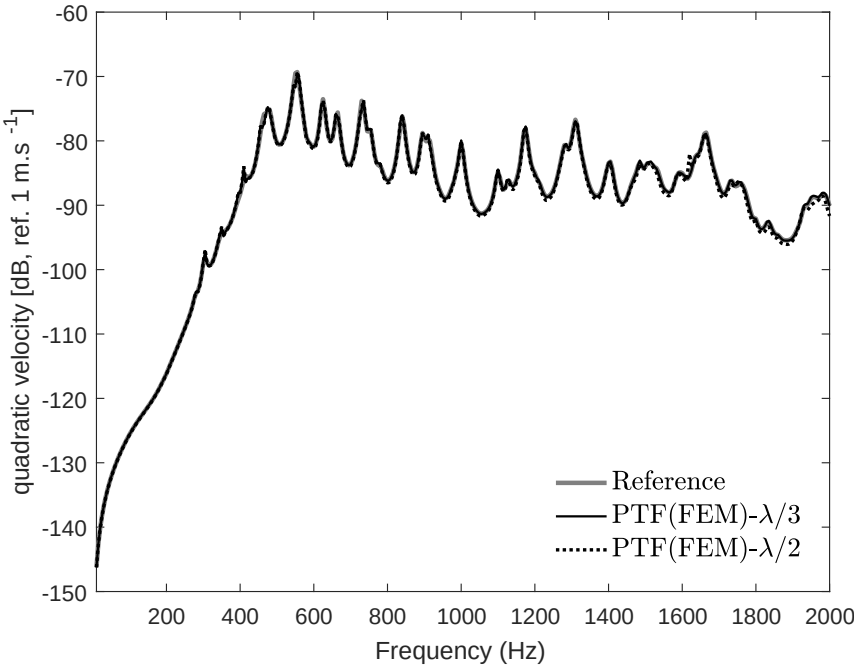

Figure 4.9 Quadratic velocity of the clamped half-cylinder shell. Results relative to the convergence study of the curved panel with radius of curvature R_{ext}=0.5m.

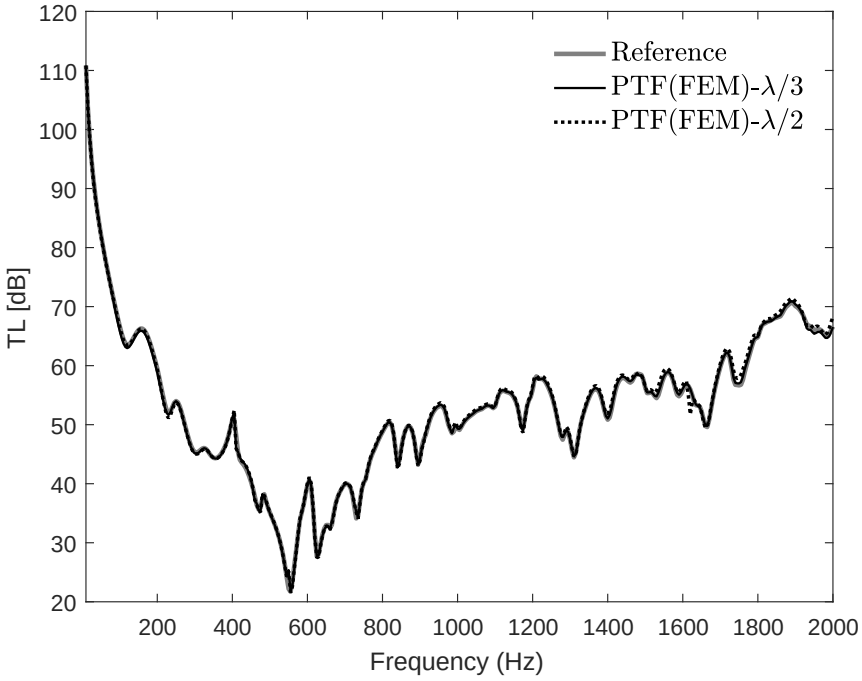

(a)

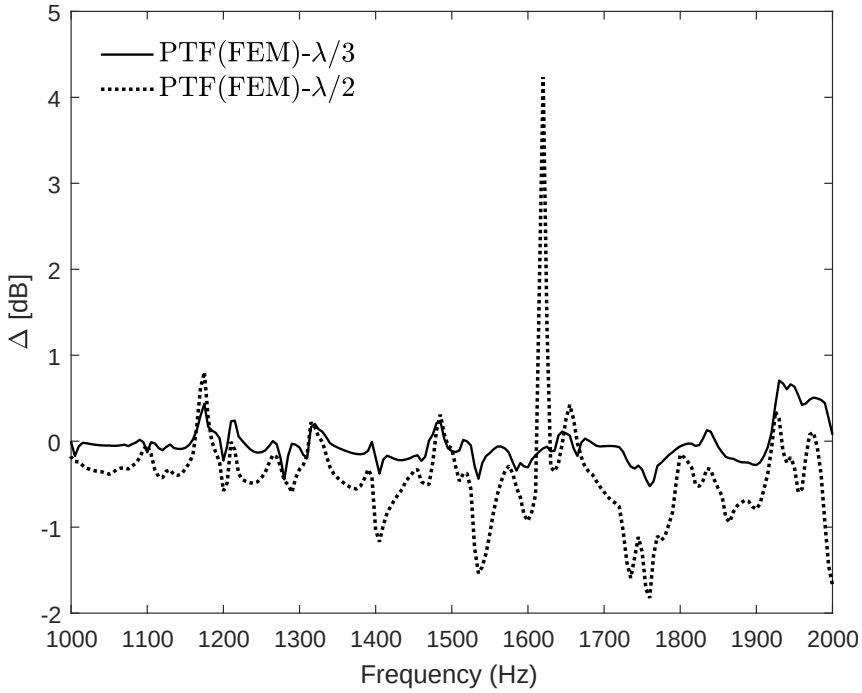

(b)

Figure 4.10 (a) Transmission loss through a trimmed clamped half-cylinder cavity system (b) the relative difference between the reference and the PTF(FEM) responses from 1 kHz up to 2 kHz. Results relative to the convergence study of the curved panel with a radius of curvature R_{ext}=0.5m.

Fig. 4.11 presents the TL when the TMM based models using the unwrapped approximation are compared to the PTF(FEM) model that considers the curved geometry of the SP. In the NLR-model three equivalent surfaces were considered where the geodesic distance r_{ij} in Eq. 4.6 is computed using three radii, i.e. $R_{ext} = 0.5m$, $R_{in} = 0.48m$, $R_{mid} = 0.49m$. It was found that the three configurations yield almost to the same prediction for this high radius of curvature with $20mm$ thick SP. However, it's expected that the effect of the equivalent unwrapped length will be more visible if the ratio of the SP thickness and the external radius increases. For the sake of conciseness only the results obtained by the geodesic distance r_{ij} with $R_{mid} = 0.49m$ are presented. As expected, Fig. 4.11(a) shows that the NLR-TMM model is not able to capture the physic accurately around the double wall resonance. This is mainly due to the strong coupling at the aforementioned resonance and the importance of the finite size, due to the presence of the mass-layer. Nevertheless, the qualitative behavior of the reference solution is always captured. More importantly, the prediction is enhanced when the reflected field is retrieved by means of ISM using the first and second order of reflections where almost a perfect agreement with the PTF(FEM) curve is noticed. However, due to the unwrapped approximation an underestimation of about 0.3 dB over the studied spectrum is observed as reported in Fig. 4.12(a). It should be noted that the two non-locally reacting models predict accurately the quadratic velocity compared to the PTF(FEM). However, these results are not shown here for the sake of conciseness.

On the other hand, again the less accurate model is the LR-TMM model with normal incidence as depicted in Fig. 4.11(b). In addition to the frequency resonance shift, the model is overestimating the TL. These results are improved when averaged models are used. Indeed, the model using the flexural and acoustic wavenumber of the infinite flat structure and the cavity, respectively, LR-TMM(avg./k_f) allows for the best approximation among the locally reacting models with some discrepancies greater than 2 dB between 200 Hz and 700 Hz. It should be pointed out that the same conclusions were made in the predictions of the quadratic velocity of the curved panel. However, the averaged models yield to similar results far from the double wall resonance of the trim. Therefore, for an acoustic excitation the LR-TMM[avg.] model can be used instead of the LR-TMM(avg./k_f) in the case of more complicated and non-homogeneous structures where the flexural wavenumber of the structure is hard to estimate. Nonetheless, in what follows only the LR-TMM(avg./k_f) model will be used.

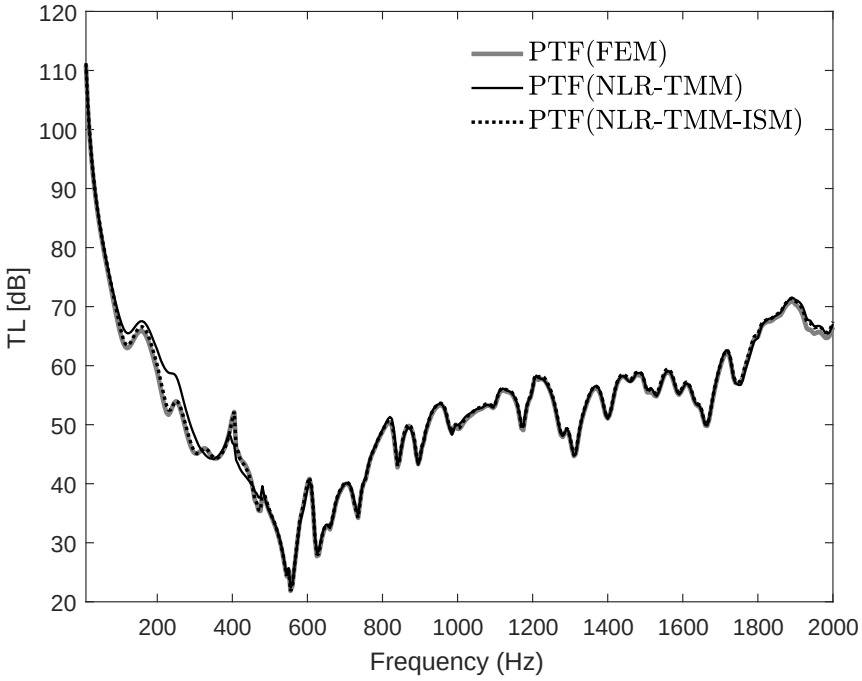

(a)

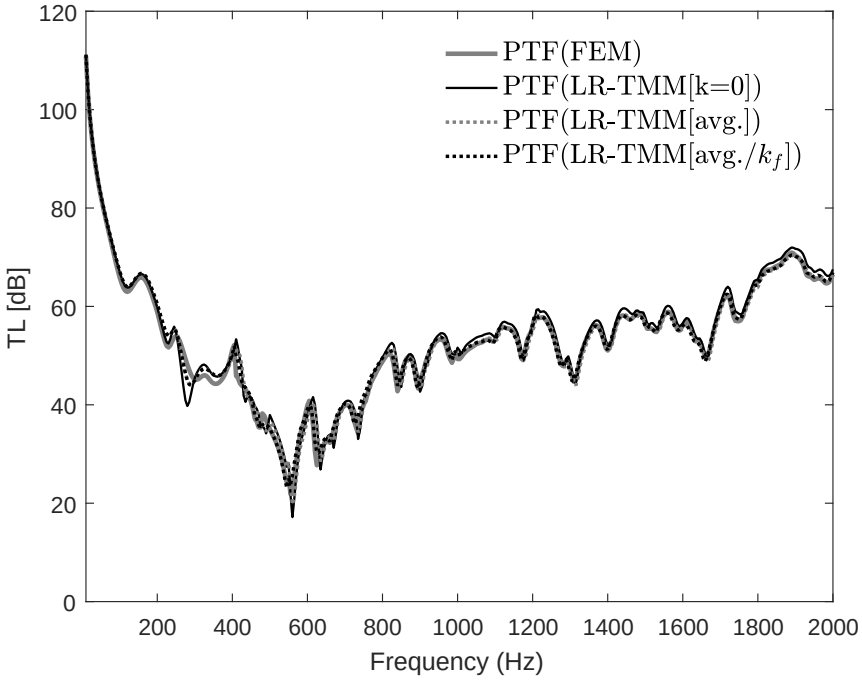

(b)

Figure 4.11 Transmission loss through a trimmed clamped half-cylinder cavity system. Results relative to the comparison between PTF(FEM), LR-TMM and NLR-TMM with and without finite size correction (R_{ext}=0.50 m).

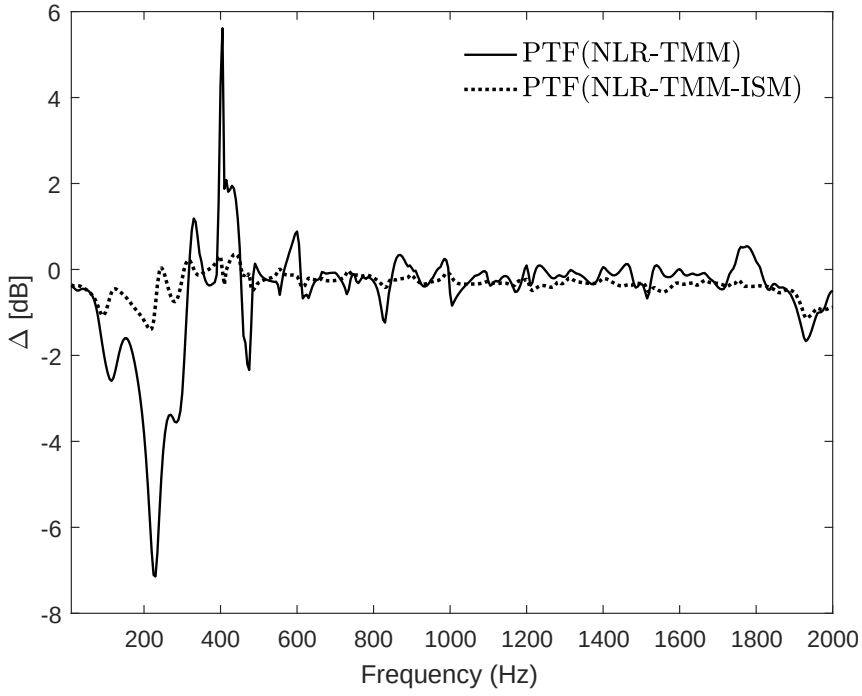

(a)

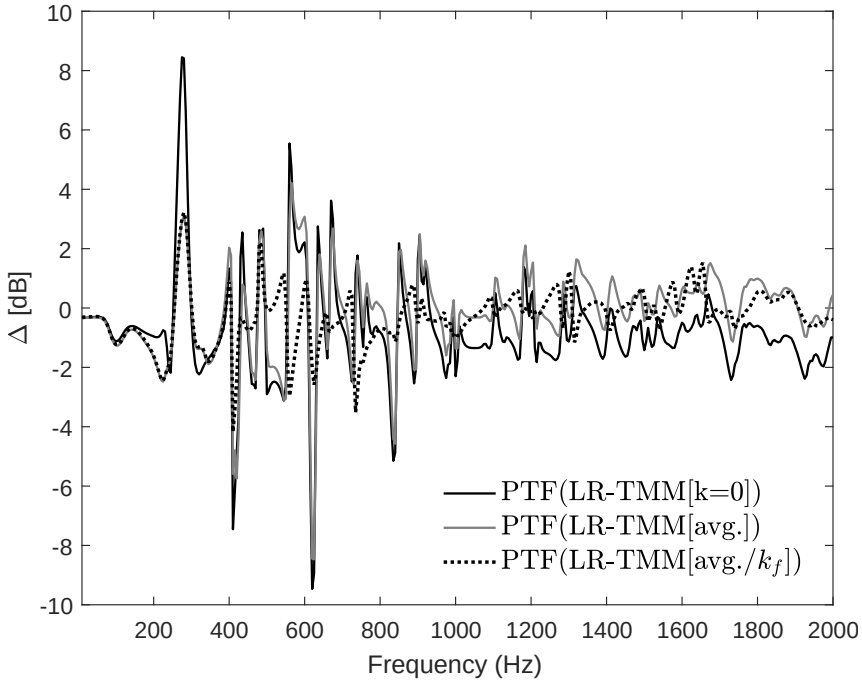

(b)

Figure 4.12 Error on the Transmission loss through a trimmed clamped half-cylinder cavity system. Results relative to the comparison between PTF(FEM) and TMM based models (R_{ext}=0.50 m).

These observations are confirmed in Figs. 4.13 and 4.14 where the TL through the curved panel with a radius of curvature $R_{ext} = 0.25m$ is depicted. The ring frequency is 3400 Hz. In this case, while the NLR-TMM model continues to have issues around 300 Hz, the LR-TMM[(avg./k$_f$] model compares well with the PTF(FEM) with a few discrepancies between 300 and 800 Hz of maximum of about 4 dB. This reveals that the effect of the reflected field is crucial to capture the indirect coupling effect between the panel and the cavity. This is confirmed again since the NLR-TMM-ISM model is in a good agreement with the reference curve. However, the TL before 200 Hz is slightly overestimated (i.e. 0.7 dB) by all the TMM based models due to the unwrapped approximation. For assurance, Fig. 4.13 shows that the PTF(FEM) model result is in a good agreement with the reference solution.

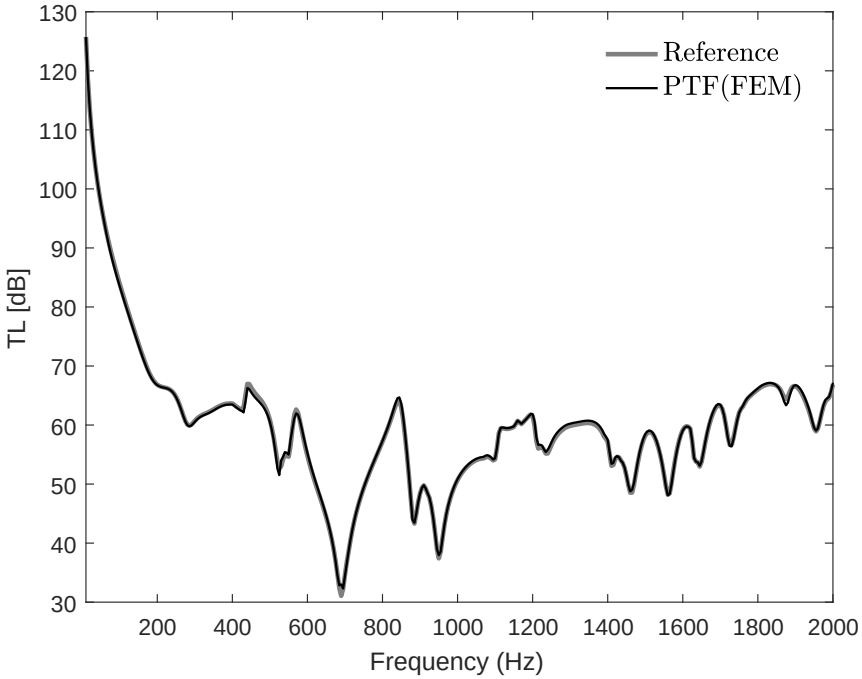

Figure 4.13 Transmission loss through a trimmed clamped half-cylinder cavity system. Results relative to the comparison between PTF(FEM) and reference (R_{ext}=0.25 m).

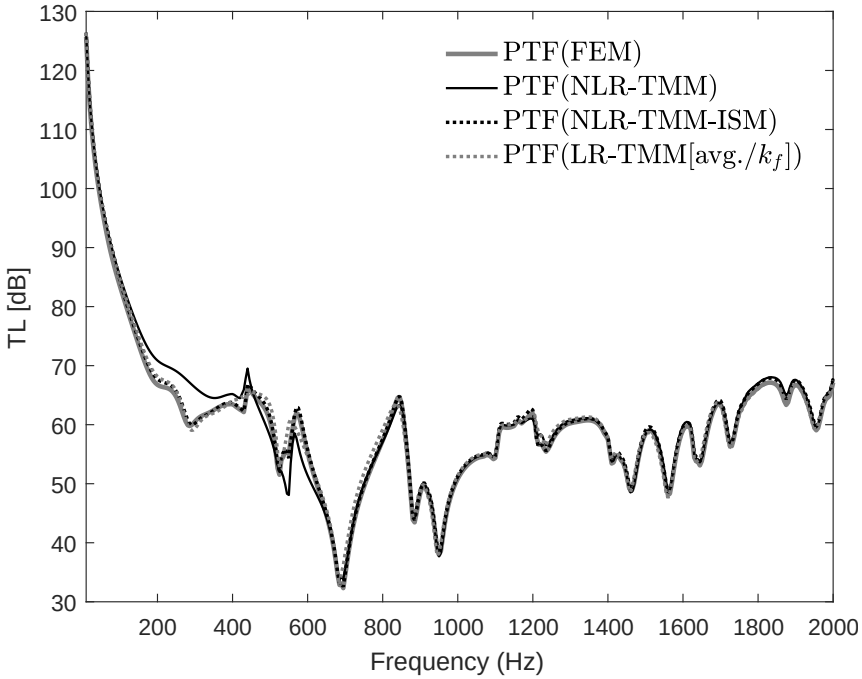

Figure 4.14 Transmission loss through a trimmed clamped half-cylinder cavity system. Results relative to the comparison between PTF(FEM), LR-TMM and NLR-TMM with and without finite size correction (R_{ext}=0.25 m).

The third investigation concerns a strongly curved trimmed panel with a small radius of curvature $R = 0.1m$ of a ring frequency at 8480 Hz. The PTF(FEM) model follows very well the reference TL as presented in Fig. 4.15. On the other hand, in Fig. 4.16 all the approximated methods are able to capture the physics of the coupled system with different accuracy except the non-locally reacting based on TMM model without correction which has issues around the double wall resonance. Indeed, due to the unwrapped approximation used within TMM based models the TL is overestimated more than in previous cases. However, such overestimation remains acceptable in the case of NLR-TMM model above the aforementioned resonance and over the whole studied frequency range when the reflected field is added (i.e. an averaged error less than 2 dB is observed). In this case, the reflected field was retrieved from up to the fourth order of reflections due to the small size of the unwrapped length of the equivalent surface. In addition, it should be pointed out that it was found that the unwrapped length of the equivalent surface affects accuracy of the results. Indeed, when the radius R_{ext} at the interface panel-SP (i.e. $R_{ext} = 0.1m$) is considered less errors were recorded on the quadratic velocity of the panel while the TL is more overestimated and vice versa if the radius R_{in} at the interface SP-cavity (i.e. $R_{in} = 0.08m$) is used instead. For this reason, a good accuracy trade-off can be obtained by using the mid radius R_{mid} keeping the same computational effort as in flat case.

However, enhancement of the accuracy can be obtained if the impedance components are computed at each interface using the radius of curvature of the interface.

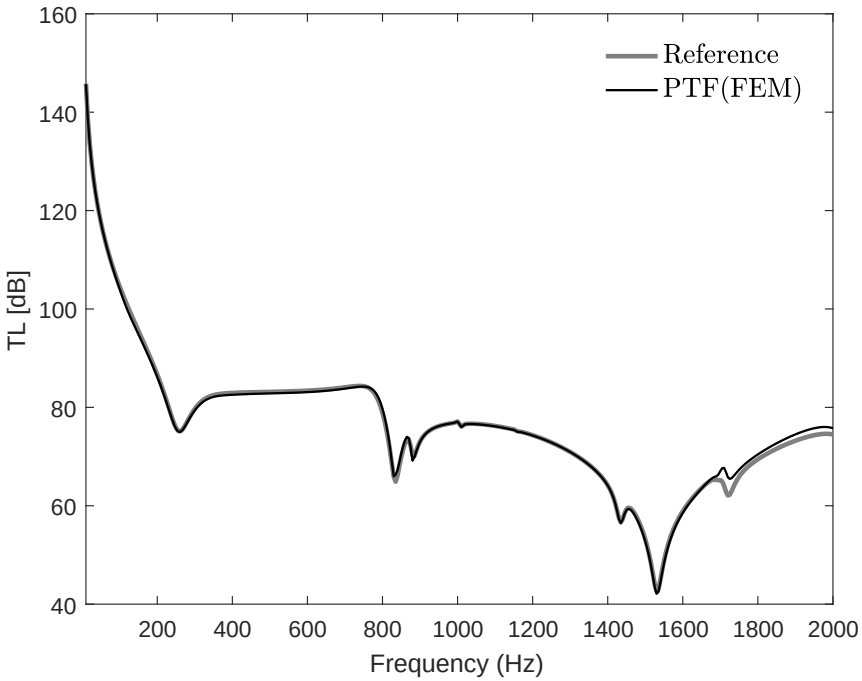

Figure 4.15 Transmission loss through a trimmed clamped half-cylinder cavity system. Results relative to the comparison between PTF(FEM) and reference (R_{ext}=0.10 m).

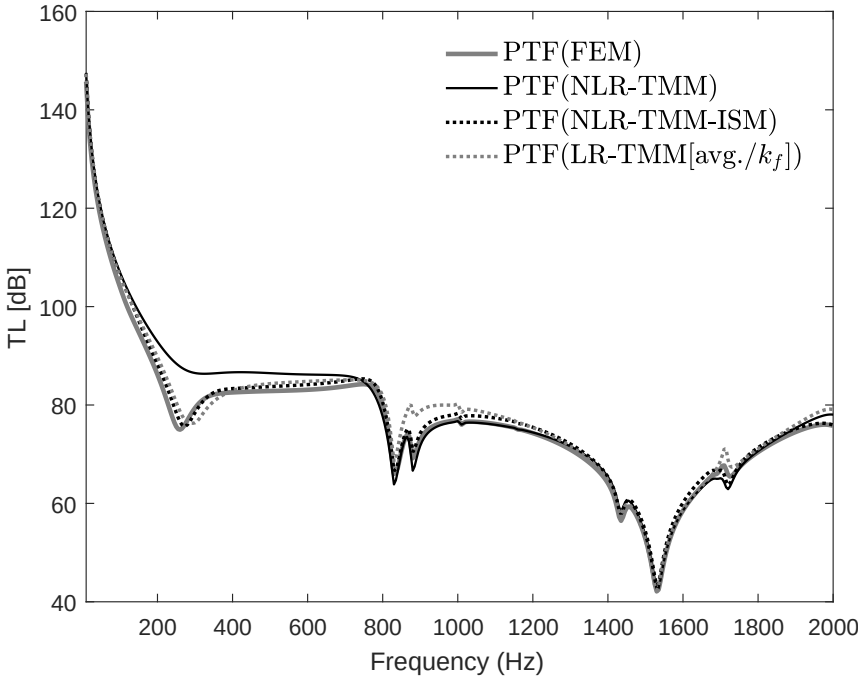

Figure 4.16 Transmission loss through a trimmed clamped half-cylinder cavity system.Results relative to the comparison between PTF(FEM), LR-TMM and NLR-TMM with and without finite size correction (R_{ext}=0.10 m).

The parametric study results suggest that for the considered systems and excitation (acoustic), locally reacting model with tuned coefficients (i.e. LR-TMM(avg./k_f)) and more sophisticated simplified models like NLR-TMM model can be used to approximate the dynamic behavior of complex SP with quite a good accuracy. However, the best overall approximation was always obtained by the NLR-TMM-ISM approach. Indeed, this study shows that even for a strongly curved trimmed panel, the SP effect is still correctly captured by TMM based models. That is, the inherent assumption of using a flat noise control treatment approximation is acceptable ; the curvature effect is mainly governed by the master structure.

4.4.3 Curved trimmed system : SP thickness effect

In this section a parametric study using the SP thickness as a parameter is conducted. This parametric study aims to show the validity of using the TMM (i.e. unwrapped assumption) to estimates the Green's functions d_{mn}. Moreover, a mechanical excitation is selected to show accuracy for these types of excitations. For this purpose, three different values for the thickness h of SP are used, namely (i) h=20 mm, (ii) h=40 mm and h=100 mm, while the radius of curvature of the system is held fixed R_{ext}=0.5 m. The foam layer thickness h_f is increased while the mass-layer thickness h_m is considered to be constant,

i.e. h_m=0.001 m. The structure is made of 2 mm thick steel, clamped along its edges and excited by a normal point force along the z-axis at (0.3, 0.0, -0.5) m, as depicted in Fig. 4.17. The same acoustic trim is used which involves a melamine foam modeled as limp with a mass-layer on top. The acoustic cavity is filled with air. Materials properties are shown in Table 4.1. According to the criterion $\lambda/3$, the interfaces of subsystems are meshed by 48 and 18 patches in the circumferential and length directions. The FEM mesh in the reference respects the criterion $\lambda/9$. The vibroacoustic indicators of interest are the averaged quadratic velocity of the structure and the radiated power.

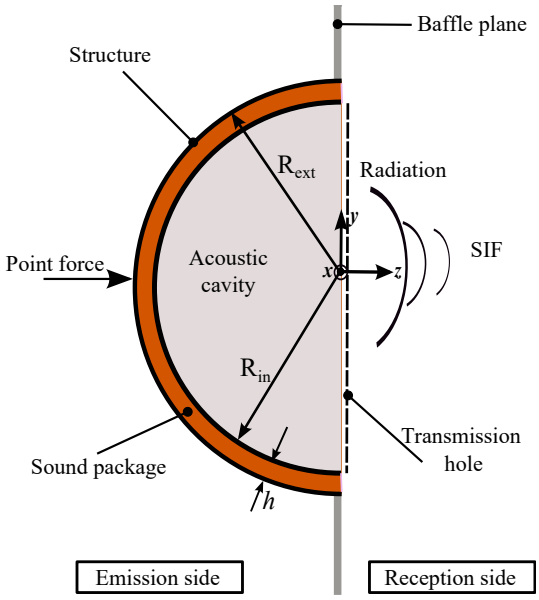

Figure 4.17 Geometry of the curved structure with attached sound package coupled to a cavity. The system is mechanically excited by a normal point force along the z-axis at (0.3, 0.0, -0.5) m. The ends of the cavity and the sound package are considered acoustically rigid.

Let's define a ratio noted as b between the thickness of the SP h and the radius of curvature of the system R_{ext}, e.i. $b = \dfrac{h}{R_{ext}}$. The first case concerns the 20 mm thick SP, i.e. b = 4%. For the sake of conciseness, the reference solution is not presented since a perfect prediction is obtained by PTF(FEM) as shown in the previous section. The compared PTF models prediction of the averaged quadratic velocity of the structure is depicted in Fig. 4.18. It is observed that the NLR-TMM models with and without finite size effect are in good agreements with the PTF(FEM). On the other hand, the LR-TMM[avg./k_f] model exhibit discrepancies around the double wall resonance due to the strong coupling between the structure and the mass-layer. However, at higher frequencies the prediction of the aforementioned LR-TMM model is enhanced.

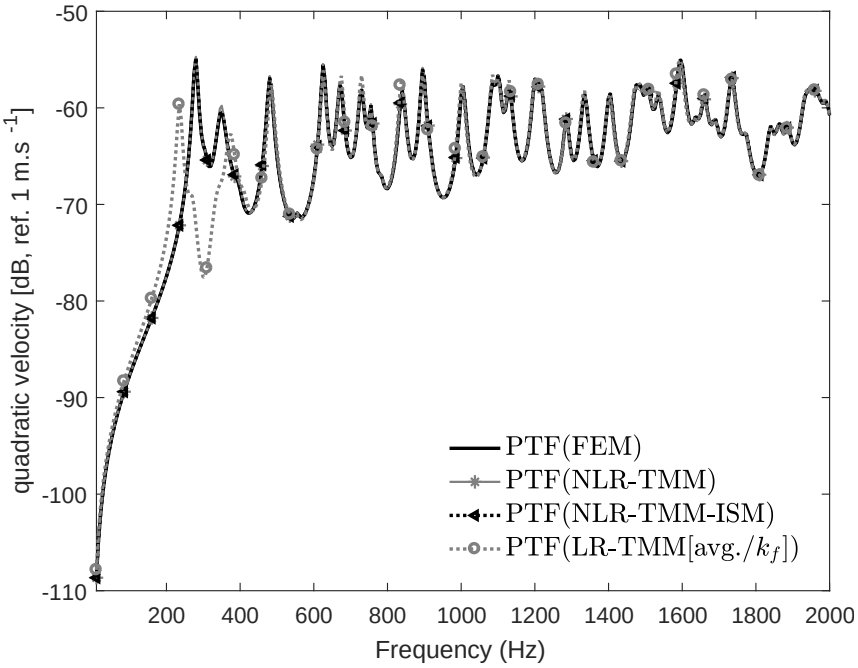

Figure 4.18 quadratic velocity of the trimmed curved structure excited by a point force. Results relative to the comparison between PTF(FEM), LR-TMM and NLR-TMM with and without finite size correction ($b = 4\%$).

Fig. 4.19 shows the radiated power through the trimmed curved panel when the ratio $b = 4\%$. It is observed that the non-locally reacting model based on the TMM without finite size correction exhibits few errors around the thickness resonance of the SP due to the presence of the mass-layer. Of course, the predictions of the aforementioned model are enhanced when the finite size effect is taken into account. Meanwhile, the LR-TMM model has much more issues especially around the DWL resonance as explained before.

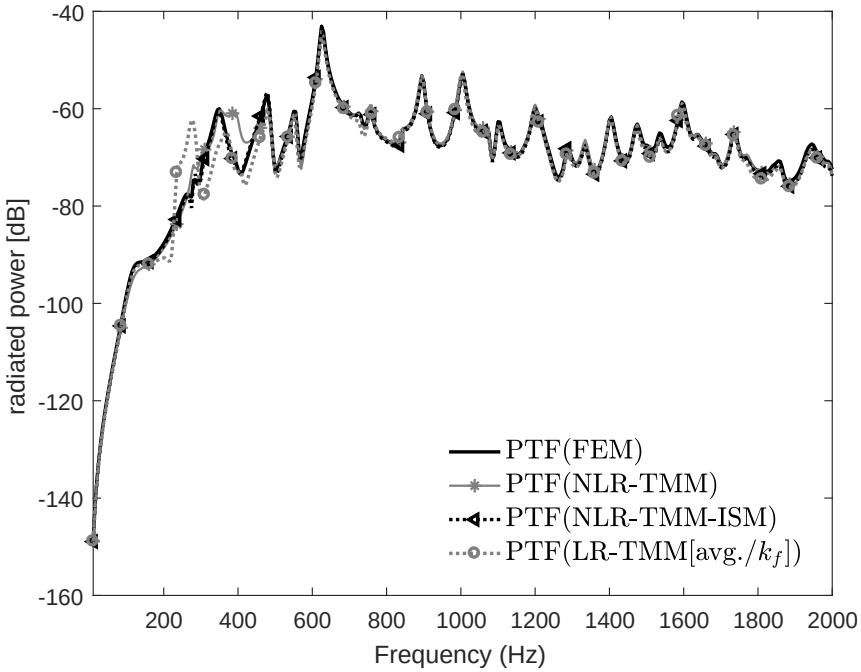

Figure 4.19 Radiated power through the trimmed curved structure excited by a point force. Results relative to the comparison between PTF(FEM), LR-TMM and NLR-TMM with and without finite size correction ($b = 4\%$).

The second tested SP thickness is of about $h = 40mm$. The vibroacoustic indicators are depicted in Figs. 4.20- 4.21. It can be noticed that the coupled response prediction by the LR-TMM model is enhanced, especially for the quadratic velocity. This is explained mainly by the fact that the spring-mass resonance is moved at lower frequency ; above it the coupling between the structure and the mass-layer is less strong in this case (i.e. the melamine foam layer is of about $39mm$). This reveals that in the case of weak coupling this locally reacting model can provide good predictions. In other words, the flexural wavenumber of the structure dominates in the case of low coupling. This is confirmed in Fig. 4.22 when a fair approximation of the structural response is observed in the case of $b = 20\%$, i.e. the SP is made of $99mm$ melamine foam layer and $1mm$ mass-layer. However, the same enhancement cannot be stated for the radiated power where errors are still observed around the SP thickness resonance. Hence, The NLR-TMM model with ISM correction, while costly, remains the best approach.

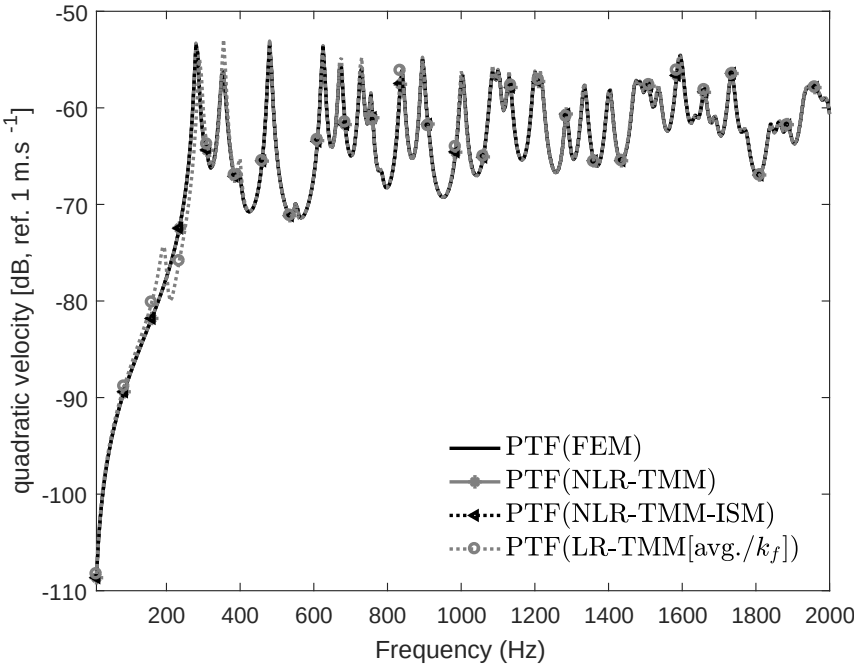

Figure 4.20 quadratic velocity of the trimmed curved structure excited by a point force. Results relative to the comparison between PTF(FEM), LR-TMM and NLR-TMM with and without finite size correction ($b = 8\%$).

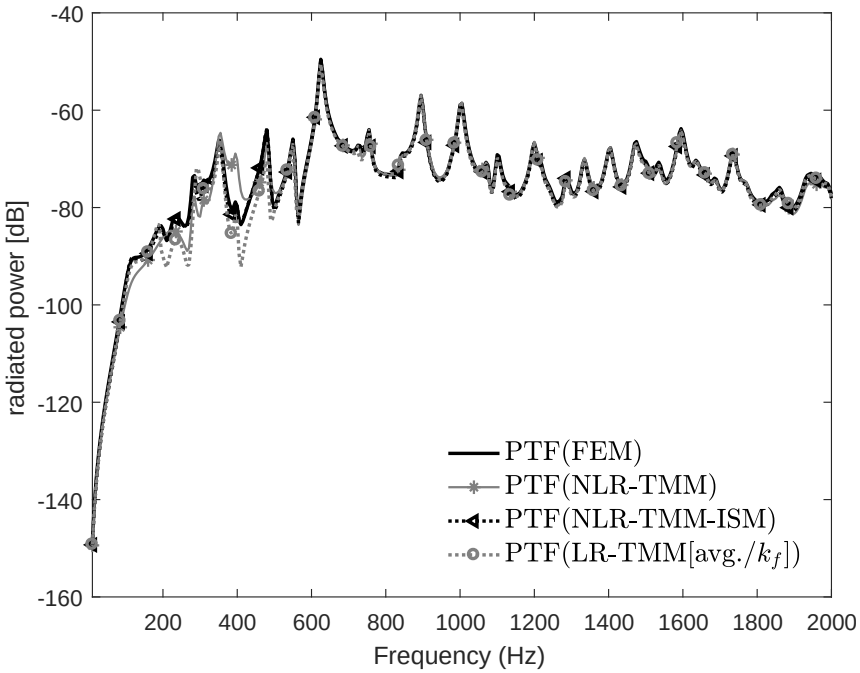

Figure 4.21 Radiated power through the trimmed curved structure excited by a point force. Results relative to the comparison between PTF(FEM), LR-TMM and NLR-TMM with and without finite size correction ($b = 8\%$).

On the other hand, similar observation made in the previous case $b = 4\%$, when the NLR-TMM models are used, are noticed in Figs. 4.20- 4.21. However, in the case of the ratio $b = 20\%$, the NLR-TMM model prediction of the radiated power in Fig. 4.23 exhibits more errors than previous cases $b = 4\%$ and $b = 8\%$. This reduced accuracy may be explained by the fact that by increasing the thickness more energy leaks toward the infinitely extended SP. Hence, ISM correction becomes more important. Indeed, when the reflected field is retrieved by means of ISM using the first and second order of reflections ($N_s = 8$), the NLR-TMM-ISM model prediction compares fairly well with the PTF(FEM) over the whole frequency range expect at the thickness resonance of the SP where an overestimation of about 10 dB is recorded. It can be proved that by tacking into account more virtual images (i.e. increasing the order of reflections), the NLR-TMM model response will be enhanced around and at the thickness resonance of the SP. In order to show this enhancement, Fig. 4.23 shows the radiated power response obtained by the NLR-TMM model where the finite size is obtained by ISM using different order of reflections. It can be observed that the response of the NLR-TMM-ISM model is enhanced when the number of image sources is increased. This proves that the curvature of SP can be neglected. Moreover, it can be concluded that the flat approximation (i.e. the fundamental solution d_{mn} in Eq. 4.6 are provided from the unwrapped SP by the TMM) is mainly acceptable.

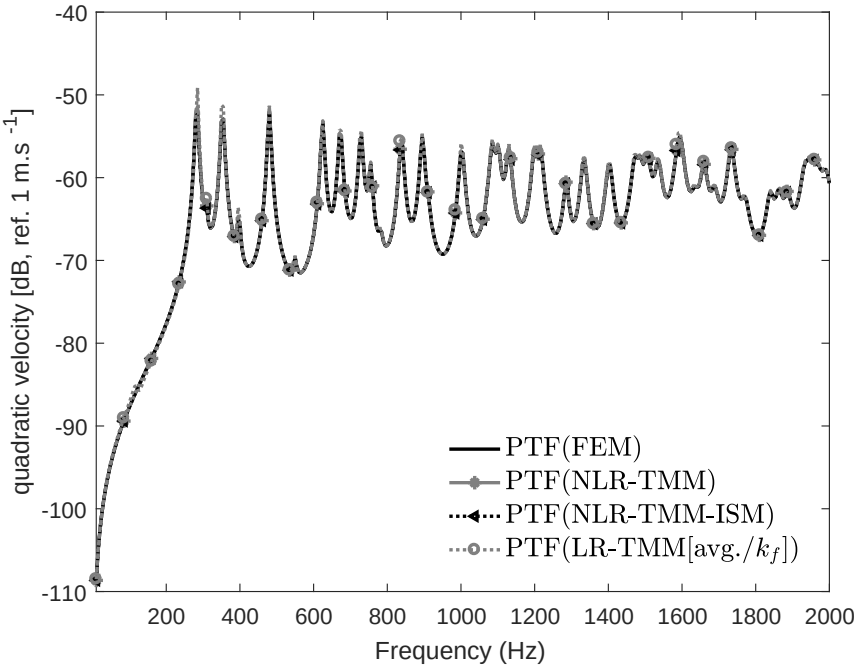

Figure 4.22 quadratic velocity of the trimmed curved structure excited by a point force. Results relative to the comparison between PTF(FEM), LR-TMM and NLR-TMM with and without finite size correction ($b = 20\%$).

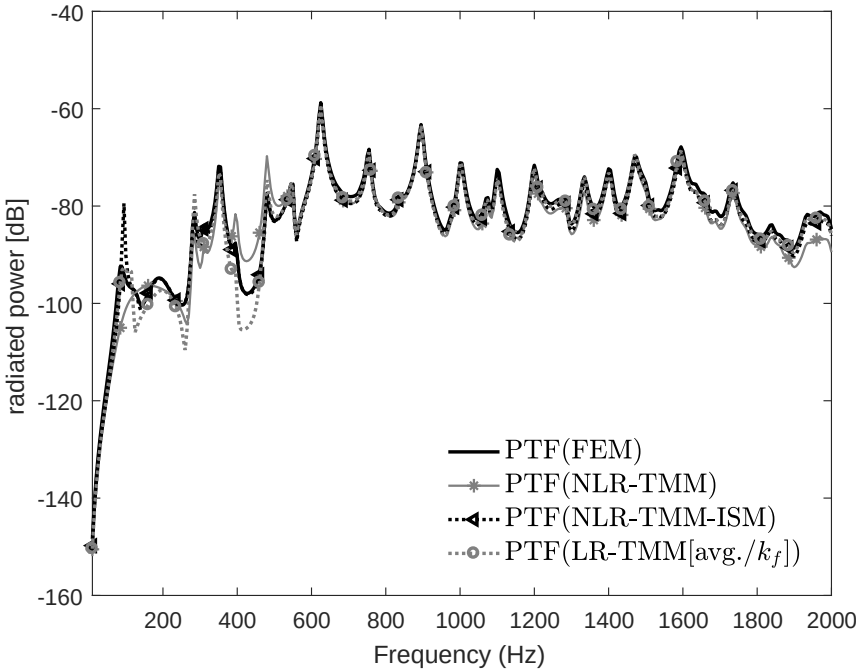

Figure 4.23 Radiated power through the trimmed curved structure excited by a point force. Results relative to the comparison between PTF(FEM), LR-TMM and NLR-TMM with and without finite size correction ($b = 20\%$).

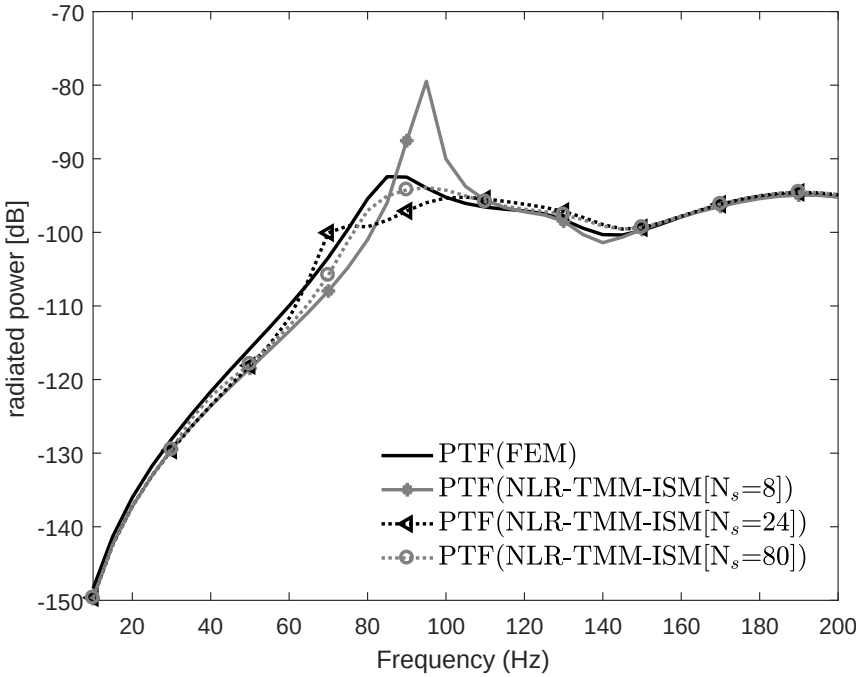

Figure 4.24 Radiated power through the trimmed curved structure excited by a point force. Results relative to the effect of the finite size correction in the NLR-TMM model ($b = 20\%$).

4.5 Conclusion

In this paper, the modeling of SP with flat and curved geometry by a simplified models was investigated. The validity of using the Transfer Matrix based models to approximate the effect of curved spring-mass treatment was studied and analyzed via two parametric studies. The first considers the radius of curvature of the system as a parameter with 20 mm thick SP while the second parametric study uses the SP thickness as a parameter. Indeed, in order to use the TMM based models the curved SP was unwrapped and assumed to be flat, homogeneous and of an infinite lateral extent. Then, the patch transfer approach (PTF) is used to efficiently couple standard finite element schemes (FEM) of the master systems (i.e. structure and the acoustic cavity) with the sound package. The latter was modeled by two different TMM based models, namely : the locally reacting and the non-locally reacting models. Moreover, an exact finite element considering the actual geometry of the SP is also used in order investigate the accuracy of the PTF approach for curved systems. In addition, a convergence study of the PTF approach in a curved system was conducted. This study confirms that a patch size criterion equal to the half of the smallest wavelength $\lambda/2$ can be used in order to predict the dynamic response efficiently of curved vibroacoustic systems.

The results presented throughout this paper confirm that an enhancement of the accuracy of the LR-TMM models can be obtained by using a costless TMM model with adjusted coefficient, i.e. referred to as LR-TMM[avg./k_f]. Indeed, it was found that such a model is able to capture the physics of curved systems at the high portion of the spectrum whereas it has issues around the double wall resonance, especially in the case of strong coupling. This was traced back mainly to the used flexural wavenumber k_f which was not a good approximation for the wavenumber that dominates the coupled response of the system. This is mainly due to the presence of the mass-layer, i.e. the strong coupling between the mass layer and the structure. It should be mentioned that better results may be obtained by properly selecting the wavenumber for the computation of the transfer matrix. However, this is a case-by-case process that depends on the nature of the coupling domains and thus cannot be trusted for general applications. However, such model converges in the high portion of the spectrum to the reference and the PTF(FEM) solutions. This indicates that such models must be used with an ultimate care in the low frequency range, especially around the thickness resonance of the SP.

On the other hand, it was shown the importance of accounting for the non-local behavior of SP, especially in the low frequency range. Indeed, the NLR-TMM model was able to capture accurately the physics of the studied systems even in the case of highly curved

structure. In addition, the effect of the finite size was appreciated in all the cases due to the presence of the mass-layer. The best accuracy is obtained when the size effect is corrected by using the ISM. Nonetheless, when the SP is thick, errors are expected around the SP thickness resonance due to the importance of the reflected field. Therefore, further work is required to fully assess the usefulness and limitations of the NLR-TMM model by studying the effect of other important parameters of the SP such as its nature (felt, screen, complex layup...) and the excitation.

In the light of these results, it can be concluded that for the considered configurations, the curvature of the SP with smaller enough thickness does not much affect the coupled response and it can practically be assumed flat. In addition, by using the NLR-TMM model included in a PTF framework, the sound package can be quickly, easily and accurately accounted for to test different configurations of the SP and excitation type. Such approach allows to speed up parametric and optimization studies making them possible in realistic times and compatible with the efficiency requirements of the industry.

CHAPITRE 5

Extension of the NLR-TMM model to cylindrical sound package

Auteurs et affiliation :

K. Kesour : étudiant au doctorat, Université de Sherbrooke, Faculté de génie, Département de génie mécanique

L. Alimonti : Ph.D. en génie mécanique, ESI US R&D North America, 12555 High Bluff Drive, 92130, San Diego, USA

N. Atalla : professeur, Université de Sherbrooke, Faculté de génie, Département de génie mécanique

Date d'acceptation : En préparation

État de l'acceptation : -

Revue : -

Référence : -

Titre français : Extension du modèle des matrices de transfert à réaction non-locale à des traitements acoustiques cylindriques.

Contribution au document : Cet article contribue à la thèse en proposant une extension du modèle des matrices de transfert à réaction non-locale (NLR-TMM) aux traitements acoustiques cylindriques. Le modèle proposé est validé dans le cas d'une excitation mécanique. De plus, un critère de troncature est proposé afin d'améliorer l'efficacité du modèle NLR-TMM. Ceci répond aux besoins soulignés dans les deux précèdents chapitres où les contributions de sources lointaines ont été nécessaire afin d'obtenir une meilleure approximation aux alentours de la résonance de la double paroi (c.à.d. la résonance masse-air-masse).

Résumé français : Cet article vise à présenter une extension du modèle des matrices de transfert à réaction non-locale aux traitements acoustiques, c.-à-d. *noise control treatment* (NCT), cylindriques. Le modèle NLR-TMM est basé sur une formulation intégrale qui utilise un ensemble de fonctions de Green (c.à.d. solutions fondamentales) du NCT. Ce dernier est supposé homogène, plat et latéralement infini. Dans ces conditions, la TMM est utilisée pour estimer les fonctions de Green. Une telle simplification peut être justifiée par la grande dissipation et les courtes longueurs d'ondes

impliquées dans les matériaux habituellement utilisés dans le NCT. Un maillage nodal est utilisé pour discrétiser la surface du SP et une distance géodésique entre les nœuds est définie afin de respecter la nature hélicoïdale des ondes se propageant à l'intérieur du NCT cylindrique. Le modèle proposé du traitement acoustique est combiné à un modèle d'éléments finis (FEM) de la structure et de la cavité dans le cadre de la *patch transfer functions* (PTF). Une coque cylindrique excitée par une force ponctuelle et couplée à un traitement phonique et à une cavité acoustique est utilisée afin de valider le modèle proposé. Le NCT est constitué d'une couche de mousse de mélamine et d'une couche de masse-lourde. Les résultats sont systématiquement comparés à un modèle FEM standard. On observe que l'approximation du traitement acoustique plat utilisée pour estimer les fonctions de Green par la TMM a un effet négligeable sur la précision du modèle proposé. Cela indique que la courbure est principalement régie par la structure. De plus, les limites des modèles à réaction locale sont également soulignées. Enfin, un critère de troncature itératif dépendant de la fréquence qui permet d'arrêter le calcul intégral impliqué dans le modèle NLR-TMM est présenté et évalué.

Note : -

5.1 Abstract

This paper presents an extension of the non-locally reacting (NLR) model based on the Transfer Matrix Method (TMM) to cylindrical noise control treatment (NCT). The NLR-TMM model is based on an integral formulation that uses a set of Green functions (fundamental solutions) of the NCT. The latter is assumed to be homogeneous, flat and laterally unbounded. Under these conditions, the TMM is employed in order to estimate the Green functions. Such simplification may be justified by the large dissipation and the softness of the materials usually involved in the NCT. A nodal mesh is used to discretize the trimmed surface of the SP and a geodesic distance between nodes is defined in order to respect the helical patterns of the propagating waves inside the cylindrical NCT. The proposed model of the NCT is combined with a Finite Element model (FEM) of the structure and cavity in a Patch Transfer Functions framework. A trimmed cylindrical shell excited by a point force and coupled to an acoustic cavity is used in order to validate the proposed model. The employed NCT is made of a melamine foam layer and a mass-layer. The results are systematically compared with a full FEM model. It is observed that the inherent unwrapped approximation used to estimate the Green functions has a negligible effect on the accuracy of the proposed model. This indicates that the curvature is mainly governed by

the structure. Moreover, the limitations of the locally reacting models are also pointed out. Finally, a frequency dependent iterative truncation criterion that stops the integral calculation involved in the NLR-TMM model is presented and assessed.

5.2 Introduction

Cylindrical structures are widely used in aeronautic and aerospace industries. However, the most effective way to reduce noise is by adding dissipative components (e.g. Sound Package (SP)) between the structure and the acoustic cavity. Nevertheless, materials usually involved in SP have a good performance at high frequencies but their ability to absorb vibrations worsens considerably in the low frequency range due to the long acoustic wavelength. Therefore, several configurations of the noise control treatment are optimized and tested in the early stage of the design process. However, the classical numerical tools used at this stage either are computationally prohibitive (if accuracy is targeted) or lack of accuracy (if efficiency is rather targeted). For these reasons, a new model for parametric studies able to meet the efficiency and the accuracy requirements of the industry is needed.

In literature, a lot of attention was devoted to analytical models [50, 28, 52, 54]. For instance, Magniez et al. [55] suggested a mixed theoretical model and used the model to calculate the sound transmission through an infinite multilayer cylinder using the First-order Shear Deformation Theory for two orthotropic thin skins and the full Biot's theory for the poroelastic core. Although efficient, this class of analytical methods usually involves the introduction of strong assumptions to simplify the modeling of the master structure, the SP as well as the acoustic cavity. Consequently, hybrid methodologies [60, 6, 2, 41] may be the best option to provide the optimal trade-off between efficiency and accuracy. In this context, this paper proposes an extension of the non-locally reacting (NLR) model [6] based on the Transfer Matrix Method (TMM) [8] to cylindrical SP. Moreover, the Patch Transfer Functions (PTF) is employed to couple efficiently the Finite Element Model (FEM) of the cylindrical structure and the cavity to the SP. The latter is modeled using three methods, namely (i) a FEM, (ii) locally reacting (LR) model and NLR based on the TMM. First, the theory of the models is described. Then, the results are presented for two radii of curvature of the structure ($R_{ext} = 0.25$ m and extremely small $R_{ext} = 0.10$ m) in order to show the validity and accuracy of the proposed model. The SP is 2 cm thick and involves a melamine foam and a mass-layer. Moreover, a frequency dependent iterative truncation criterion is proposed and assessed. The truncation criterion aims to stop the integral calculation involved in the NLR-TMM model. Hence, the truncation criterion enhance the

efficiency of the NLR-TMM especially above the thickness resonance by considering only the contributions of close sources to a given receiving node.

5.3 Theory

In this section, the principle of the PTF approach is briefly recalled as well as the coupled equations of the studied vibroacoustic system. Then, the theory of the non-local reacting model is presented.

5.3.1 Patch Transfer Functions approach

The studied vibroacoustic problem involves a cylindrical structure with an attached SP coupled to an acoustic cavity. The PTF approach [62] is a sub-structuring technique. Hence, the coupled system is divided into three subsystems, namely (i) the structure (ii) the acoustic treatment (iii) the cavity. The SP is coupled over one side (i.e. interface 1) to the structure and over the other side (i.e. interface 2) to the cavity. The PTFs relations, mobility or impedance, of each subdomain are defined over the coupling interfaces which are discretized into N_p rectangular patches. Once the PTFs relations of sub-domains are computed, the superposition principle is applied to each subdomain. Then, coupling conditions are used to couple the subsystems leading to the following coupled system equation,

$$\begin{bmatrix} \mathbf{I}_d + \mathbf{Y}^s\mathbf{Z}^a_{11} & \mathbf{Y}^s\mathbf{Z}^a_{12} \\ -\mathbf{Z}^a_{21} & -\mathbf{Z}^a_{22} + \mathbf{Z}^c_{22} \end{bmatrix} \times \begin{bmatrix} \mathbf{V}_1 \\ \mathbf{V}_2 \end{bmatrix} = \begin{bmatrix} \tilde{\mathbf{V}}^s \\ 0 \end{bmatrix}, \tag{5.1}$$

where only the structure is assumed to be excited by an external load. In order to reconstruct the mean quadratic pressure, it is necessary to compute the patch-point impedance vector $\mathbf{Z}^{spl}$ that relates the patches normal velocity $\mathbf{V}_2$ at the SP-cavity interface and the nodal pressure p_r. Thus, the sound pressure level (SPL) at a node r is given by,

$$p_r = \mathbf{Z}^{spl}_r \mathbf{V}_2. \tag{5.2}$$

Note that the Eq. (5.2) is only valid in the case where the patches have the same area. Otherwise, they just have to be scaled with the patch's area. In Eq. (5.1), $\mathbf{I}_d$ is the unit matrix of dimensions $N_p \times N_p$. The superscripts s, a and c stand for the structure, the acoustic treatment and the acoustic cavity, respectively. $\mathbf{Y}^s$ is the structure mobility matrix. Its entries Y^s_{ij} are defined as the ratio of the arithmetical mean of the normal velocity $\langle V_i \rangle$ over a receiving patch i and the mean pressure $\langle P_j \rangle = 1$ Pa of an excited patch j

while using a pressure release condition over the other patches, i.e. $\langle P_{i\neq j}\rangle = 0$ Pa. $\tilde{\mathbf{V}}^s$ is a mobility vector of the in-vacuo structure due to the external excitation. The $\mathbf{Z}_{mn}$ is an impedance matrix. Its entries $Z_{mn_{ij}}$ are defined as the ratio of the mean pressure $\langle P_{m_i}\rangle$ over a receiving patch i belonging to an interface m and the mean normal velocity $\langle V_{n_j}\rangle = 1$ m/s of an excited patch j belonging to an interface n while blocking the other patches, i.e. $\langle V_{n_{i\neq j}}\rangle = 0$ m/s. Detailed derivations of the theory of the PTF technique can be found in [62, 1, 41].

5.3.2 Vibroacoustic indicator calculation

The patches normal velocities at interfaces 1 and 2 of the coupled system are obtained by solving the linear system in Eq. (5.1). Therefore, the averaged quadratic velocity of the structure can be defined as,

$$\langle \mathbf{v}^2 \rangle = \frac{1}{2S} \sum_{i=1}^{N_p} \mathbf{V}_{1_i} \mathbf{V}_{1_i}^* S_i, \tag{5.3}$$

where N_p is the number of patches, S_i is the patch's area and S is the area of the surface at interface 1. The mean quadratic pressure is reconstructed by using the SPL p_i of some microphones inside the cavity using the following equation,

$$\langle \mathbf{p}^2 \rangle = \frac{1}{2N_m} \sum_{i=1}^{N_m} p_i p_i^*, \tag{5.4}$$

where N_m is the number of the considered microphones inside the cavity. The SPL p_i of microphone i is computed from Eq. (5.2).The superscript * indicates the complex conjugate.

5.3.3 Calculation of subsystems PTFs relations

In this subsection, the characterization technique of each subsystem is described. All the PTFs relations of the structure and cavity are computed using the direct FEM. On the other hand, in order to study the validity of the unwrapped approximation, the SP is modeled using three techniques : (i) classical FEM model that considers the cylindrical geometry of the SP, (ii) a locally reacting (LR-TMM) model and (iii) a non-locally reacting model based on the TMM (NLR-TMM). It should be noted that when the FEM is used to provide the PTFs relations of the SP, the operation is done in two steps. First, the SP

is characterized by a hybrid matrix form. Then, the hybrid matrix is reorganized in order to obtain the PTFs relations in the impedance form (see Ref. [69]).

Non-locally reacting cylindrical model

The purpose of this section is to provide the theory behind the NLR-TMM model [5, 6, 40] in the context of homogeneous and isotropic cylindrical noise control treatments modeling. Let's consider the geometry of the homogeneous acoustic treatment at a given radius R as depicted in Fig.5.1. The nodes i and j lie on the cylindrical surface. The waves propagating inside a cylindrical SP have helical patterns. Hence, the nodal transfer functions $D^{\infty}_{mn_{ij}}$ between an excited node x_j and a receiving node x_i in the direct field (i.e. reflections from boundaries are neglected) is provided, in theory, by means of the sum of all contributions from all possible patterns, such as

$$D^{\infty}_{mn_{ij}} = \sum_{l=1}^{\infty} D^{(l)}_{mn_{ij}}. \tag{5.5}$$

With,

$$D^{(l)}_{mn_{ij}} = D_{mn}(r^{(l)}_{ij}, \omega) = \frac{1}{2\pi} \int_0^{\infty} \hat{d}_{mn}(k, \omega) J_0(k r^{(l)}_{ij}) k dk, \tag{5.6}$$

where $r^{(l)}_{ij}$ is the geodesic distance of the pattern (l) between nodes x_i and x_j as depicted in Fig.5.1, k is the wavenumber and $J_0(kr^{(l)}_{ij})$ is the Bessel function of zero order of argument $kr^{(l)}_{ij}$. The notation $\hat{f}(k)$ indicates the Hankel transform of the function $f(r)$. The Green functions $\hat{d}_{mn}$ represents the transfer coefficient of the 2×2 reduced transfer matrix between normal velocities $V_{1,2}$ and pressures $P_{1,2}$ (equivalently, stresses $\sigma_{1,2} = -P_{1,2}$) over the two ends of SP in the wavenumber domain. Therefore, the non-locally reacting model only allows to accounts for the continuity of normal displacements (i.e. velocities) and stresses (i.e. pressures) at the structure and cavity interfaces. It should be noted that in this paper the Green functions $\hat{d}_{mn}$ are obtained from the classical TMM where the SP is assumed to be flat, isotropic, homogeneous in the plane and of infinite lateral extent. However, other methods, like cylindrical TMM, can be used to provide the Green functions $\hat{d}_{mn}$. In practice, the integral is computed between (0, k_s) with k_s is the maximum wavenumber defined by the Nyquist criterion based on the minimum Euclidean distance $r_{min_{ij}}$ between the nodal mesh of the SP surface.

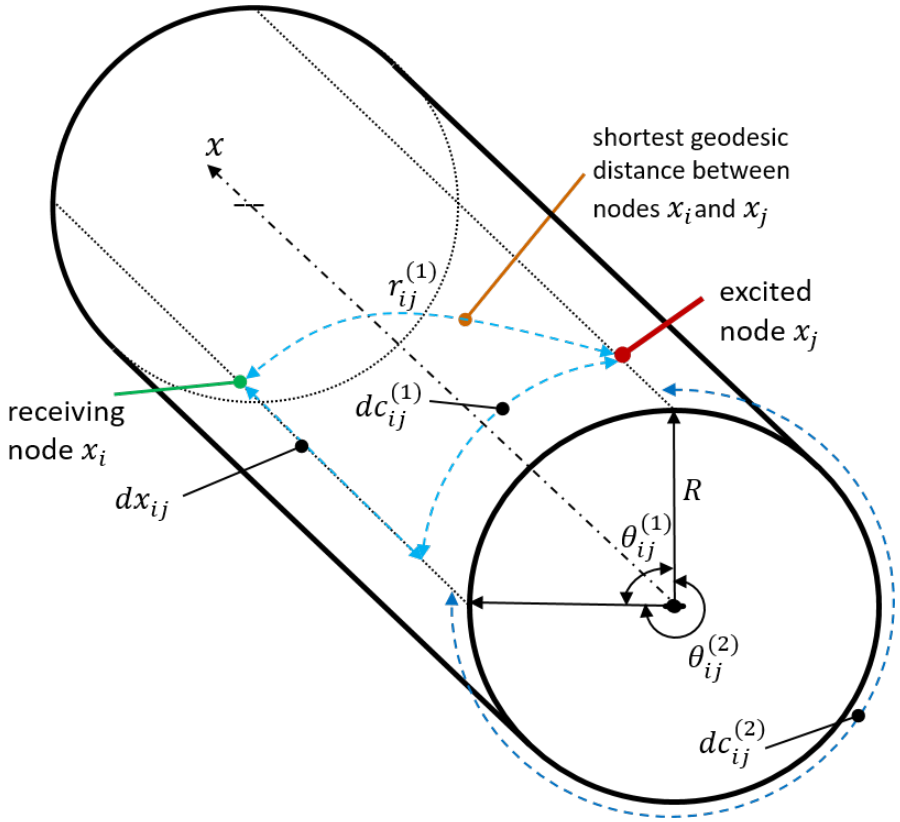

Figure 5.1 Geometry of the cylindrical acoustic treatment. Perspective view of the surface of the SP at a given radius.

The geodesic distance of the pattern (l) is defined as $r_{ij}^{(l)} = \sqrt{dx_{ij}^2 + (dc_{ij}^{(l)})^2}$, where dx_{ij} and $dc_{ij}^{(l)} = R\theta_{ij}^{(l)}$ are, respectively, the longitudinal and circumferential distances of pattern (l) between nodes x_i and x_j. The angles $\theta_{ij}^{(l)}$ are ordered and defined as,

$$\begin{cases} \theta_{ij}^{(l)} & = \min\left(\pi(l-1) + |\theta_i - \theta_j|; \pi(l+1) - |\theta_i - \theta_j|\right), \text{ if } l = 1, 3, 5, ..., \infty \\ \theta_{ij}^{(l)} & = \max\left(\pi(l-2) + |\theta_i - \theta_j|; \pi l - |\theta_i - \theta_j|\right), \text{ if } l = 2, 4, 6, ..., \infty \end{cases}. \tag{5.7}$$

However, one can expect that the first contribution (e.g. the shortest geodesic distance), if the radius of curvature of the cylindrical SP is large enough, to be the most dominant because of the high dissipation and softness of the materials usually involved in the SP (i.e. $D_{mn_{ij}}^{\infty} \approx D_{mn_{ij}}^{(1)}$). On the other hand, the reflected field is may be needed to enhance the prediction of the NLR model. In this case, the Image Source Method (ISM) [3] may be used in order to provide the reflection contributions from the two longitudinal boundaries of the cylinder. Therefore, by assuming a perfect reflection of boundaries, the reflected field contribution is retrieved by means of an equivalent direct field emanating from successive image sources with the same intensity as the original source. Hence, the total transfer function $D_{mn_{ij}}^{Total}$ is defined as the superposition of the direct and reflected field contributions such as

$$D_{mn_{ij}}^{Total} = D_{mn_{ij}}^{\infty} + \sum_{s=1}^{N_w} \sum_{q=1}^{\infty} D_{mn_{ij}}^{\infty}(r_{ij}(s,q), \omega), \tag{5.8}$$

where, $N_w = 2$ represents the two edges of the cylinder and q is the number of successive reflections (in theory an infinite number of reflections is necessary). However, in our case, since the SP often involves highly dissipative and soft materials, it is not necessary to take into account multiple reflections because the reflected field from virtual sources is largely attenuated. Thus, the reflected field, if the length of the cylindrical SP is large enough, can be obtained only from the first reflection at the two edges. Once the transfer functions between all nodes of the nodal mesh are obtained, the methodology explained in Ref. [41] is used in order to average and provide the PTFs relations. An example of the nodal and patch mesh at $R = 0.1$m is depicted in Fig. 5.2.

In this paper, the studied cases consider only the shortest geodesic distance for the direct field and the first order ($q = 1$) of reflections on the two boundaries for the reflected field. To summarize, the shortest geodesic model that account only for the shortest geodesic distance, i.e. $N_l = 1$, is referred to as PTF(NLR-TMM). In addition, the PTF(NLR-

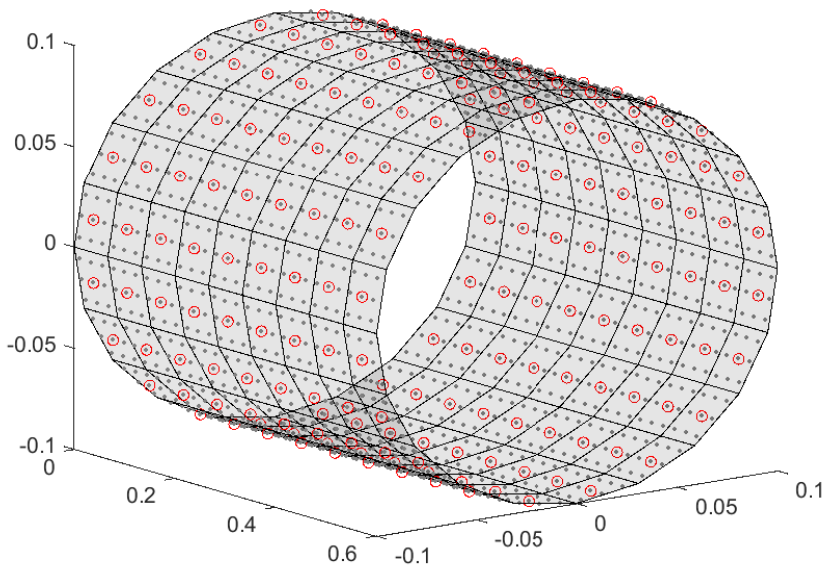

Figure 5.2 An example of the geometry of the cylindrical sound package subdivided into 9×20 patches. The red circles denote the centers of the patches and the dot the used nodal mesh considered in the NLR-TMM model (9 nodes per patch).

TMM-ISM) refers to the case when the reflected field is provided by means of the first order ($q = 1$) of reflections. However, the number of the geodesic distances N_l is also indicated if high order of geodesic contributions are required (i.e. this is the case of the small radius $R_{ext} = 0.1$ m) in the direct field response.

Finally, it should be noted that the transfer functions $D_{mn_{ij}}$ can be computed using the exterior radius R_{ext} (resp. the interior radius R_{in}) of the SP in order to get the structural effect resp. the acoustic effect) of the SP right. In this paper, they are computed using the exterior radius ($R = R_{ext}$) since the structure is excited.

Numerical implementation

The numerical implementation of the non-locally reacting model based on the TMM was first carried out in MATLAB. The parallel toolbox was used for an efficient computation. The implementation steps used in [2] are adopted with some modifications and they are described in the following :

1. Computation of the Green functions $\hat{d}_{mn}(k, \omega)$: The functions $\hat{d}_{mn}(k, \omega)$ are estimated by the TMM at each frequency step over a wavenumber grid between $k = 0$ and

$k = k_s$. The latter grid should be carefully defined in order to guaranty a correct sampling of the oscillatory behavior of the integrand in Eq. 5.6. However, a linear wavenumber grid was adopted in the following results. Moreover, this step can be speed up by using a parallel implementation since a complete independent evaluation of $\hat{d}_{mn}(k, \omega)$ can be handled for different couples (k, ω).

2. Integration of the kernels : The functions $D_{mn}(r_{ij}, \omega)$ are sampled using a grid consisting of N_r distances between $r = 0$ and $r = r_{max}$. $r = r_{max}$ is the maximum distance between two nodes of the nodal mesh and, if used, the added virtual sources. Of course, this step can also benefit from a parallel implementation. Note that a truncating criterion is proposed later (see subsection 5.4.3) in order to stop the expensive integral calculations.

3. Matrices assembly : This step interpolates the previous $D_{mn}(r_{ij}, \omega)$ vector in function of the distance r_{ij} in order to build the matrices (the nodal transfer functions) of the adopted formulation. In this step, the symmetry of the cylindrical surface was exploited in order to enhance the efficiency where only one line of nodes and their virtual images (i.e. geodesic and reflected contributions) was used as sources.

4. Nodal matrices symmetry : In this step, the interaction between all nodes is retrieved thanks to the geometrical symmetry of the cylindrical surface. Of course, the nodal matrices can be included directly in the FEM-TMM model proposed by Alimonti et al. [4].

5. Averaged matrices PTFs : The nodal matrices are reduced by averaging them over patches in order to obtain the PTFs relations (the averaging procedure is given in [41]).

It should be noted that the symmetry can be applied only if a regular nodal and/or patch mesh is used. In this paper a regular mesh is used in order to exploit the symmetry.

Locally reacting model

Recently, a locally reacting model based on the TMM was proposed in Ref. [20]. The model defined in Eq. (5.9) is based on the flexural and acoustic wavenumber of the infinite flat structure and the cavity, respectively. In Ref. [20], it was found that the LR-TMM model

with tuned coefficients was able to provide better predictions compared to the classical LR-TMM with normal incidence for the considered cases.

$$\begin{cases} Z^a_{11_{ii}}(\omega) = \hat{d}_{11}(k_f, \omega) \\ Z^a_{12_{ii}}(\omega) = \left\langle \hat{d}_{12}(k, \omega) \right\rangle_{k_0} = -Z^a_{21_{ii}}(\omega) \\ Z^a_{22_{ii}}(\omega) = \left\langle \hat{d}_{22}(k, \omega) \right\rangle_{k_0} \end{cases}, \tag{5.9}$$

where k_0 is the acoustic wavenumber in the free air and k_f is the structural flexural wavenumber. The $\langle\rangle$ means that the $\hat{d}_{mn}$ is averaged for k between 0 and k_0. It should be noted that the use of flexural wavenumber k_f of the infinite flat structure is hardly justifiable, especially below the ring frequency. However, it was found that such a model gives enhanced results compared to classical locally reacting TMM models (i.e. with normal or averaged incidence), especially above the SP thickness resonance.

5.4 Results

In this section, a parametric study involving a trimmed cylindrical structure-cavity system is conducted. The cylindrical structure is made of 2 mm thick steel with a 0.60 m length, clamped along its edges and excited by a normal point force along the z-axis at (0.3 m, 0.0 m, -R_{ext}) where R_{ext} is the radius of the cylindrical shell (see Fig. 5.3). The acoustic trim involves a 19 mm thick melamine foam modeled as limp with a 1 mm thick mass-layer on top. The acoustic cavity is filled with air. The material properties can be found in [41]. The coupling interface of subsystems are meshed into equal rectangular patches using a conservative criterion as in [41]. The convergence of the full FEM reference is reached by using a $\lambda/9$ criterion. The same FEM mesh is used in order to estimates the PTFs relations of subsystems when FEM is used. The vibroacoustic indicators of interest are the averaged quadratic velocity and pressure of the panel and the cavity, respectively. In addition, the sound pressure level at a microphone inside the cavity is presented.

5.4.1 Case 1 : curvature radius R_{out}=0.25 m

The first studied case considers a cylindrical shell with a radius of curvature $R_{ext} = 0.25$ m. The PTF(FEM) model that considers the real cylindrical geometry of the SP is compared to the reference solution in terms of the quadratic velocity and the pressure of the panel and cavity, respectively, as depicted in Fig. 5.4. The PTF(FEM) approach allows a perfect prediction of the quadratic velocity as well as the quadratic pressure.

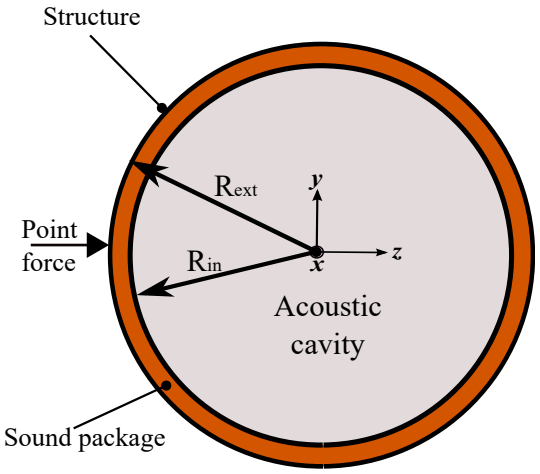

Figure 5.3 Geometry of the cylindrical structure with attached sound package coupled to a cavity. The system is mechanically excited by a normal point force along the z-axis at (0.3 m,0.0 m,$-R_{ext}$).

Figs. 5.5(a) and (b) show the quadratic velocity and pressure of the shell and the panel, respectively, when the TMM simplified models of the sound package, is assumed to be flat, are compared to the FEM model of the cylindrical SP. The quadratic pressure is obtained by averaging over $N_m = 101$ microphones. It can be observed that the LR-TMM model in Eq. (5.9) fails to capture the physics around the double wall resonance leading to large errors in the prediction of the coupled response. These results indicate that the non-local behavior is of main importance in the case of a mechanical excitation, especially around the aforementioned resonance. This is confirmed when the non-local behavior of the unwrapped SP is estimated by means of the direct field NLR-TMM model, considering only the shortest geodesic pattern contribution, where a very good match is observed over the considered frequency range except at the noise control treatment thickness resonance at 270 Hz. Indeed, an almost prefect prediction of the two vibroacoustic indicators is obtained by the NLR-TMM-ISM model when only the shortest geodesic contribution as well as its first order of reflection at the two lateral boundaries are considered. This reveals that the curvature of SP can be simply neglected. On the other hand, in order to give the reader an idea about the accuracy of the compared models in the prediction of local indicators, the absolute value of the pressure inside the cavity at coordinates (0.300 m, 0.076 m, 0.000 m) is recorder in Fig. 5.6. The previous observation can also be made in the case of the SPL.

5.4.2 Case 2 : curvature radius R_{out}=0.10 m

Finally, let's consider the trimmed cylindrical system with a small radius of curvature (R_{ext}=0.10 m). It is observed in Fig. 5.7(a) that the PTF(FEM) model follows perfectly

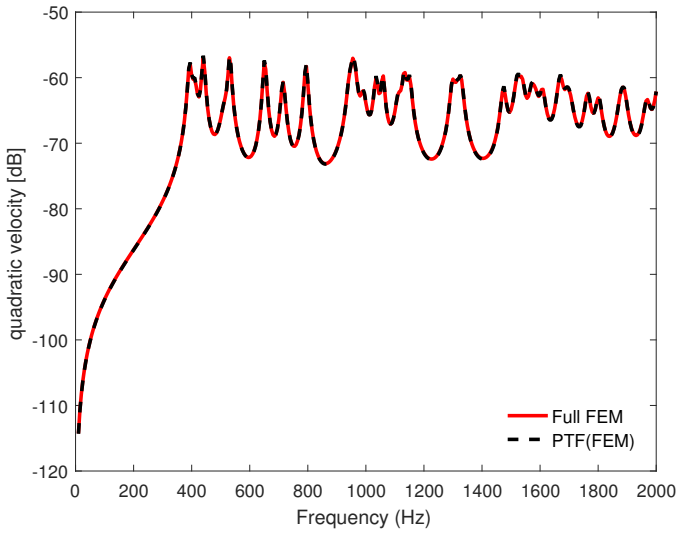

(a)

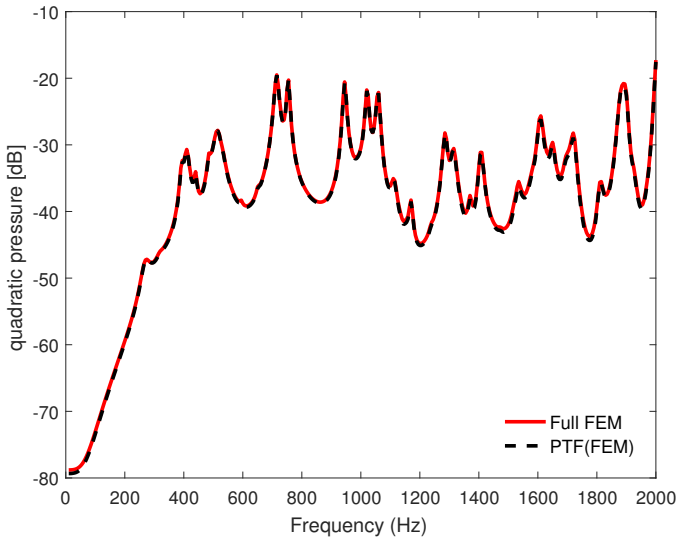

(b)

Figure 5.4 (a) Quadratic velocity of the cylindrical shell. (b) Averaged quadratic pressure inside the acoustic cavity. Results relative to the comparison between PTF(FEM) and reference (R_{ext}=0.25 m).

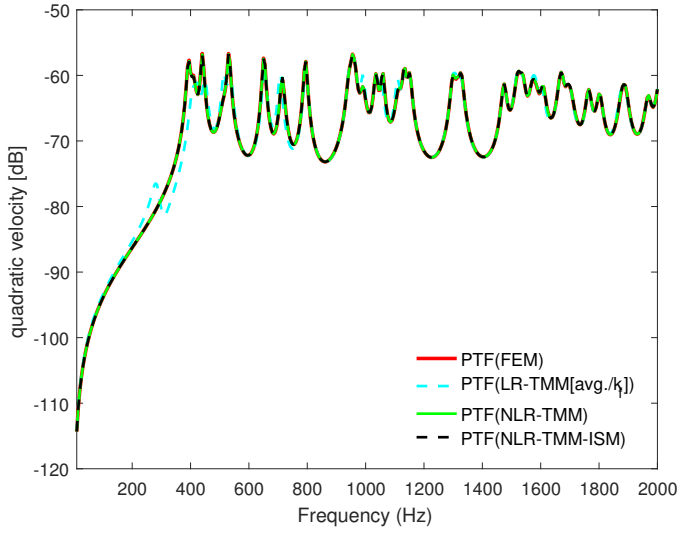

(a)

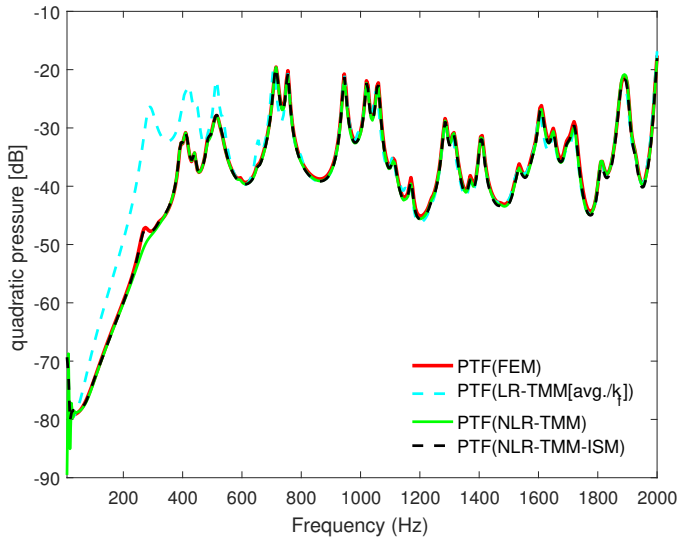

(b)

Figure 5.5 (a) Quadratic velocity of the cylindrical shell. (b) Averaged quadratic pressure inside the acoustic cavity. Results relative to the comparison between PTF(FEM), LR-TMM and NLR-TMM($N_l = 1$) with and without finite size correction (R_{ext}=0.25 m).

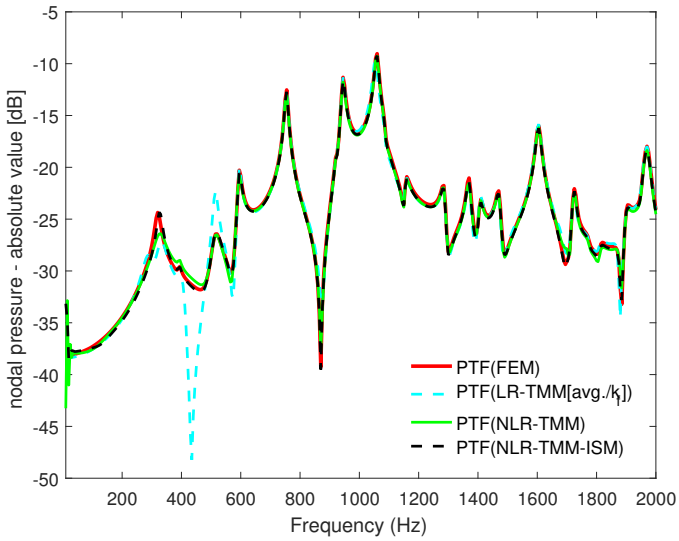

Figure 5.6 Acoustic pressure inside the acoustic cavity at coordinates (0.300 m, 0.076 m, 0.000 m). Results relative to the comparison between PTF(FEM), LR-TMM and NLR-TMM($N_l = 1$) with and without finite size correction (R_{ext}=0.25 m).

the reference prediction of the vibrational response. On the other hand, the physics is well captured in the averaged quadratic pressure response whereas small discrepancies are observed at and below the double wall resonance 375 Hz as depicted in Fig. 5.7(b). These errors are traced back to the averaged scheme and the geometrical approximation within the PTF approach as well as the location where the point force is applied (i.e. the force is applied to a node located at the intersection between patches mesh). Indeed, it could be shown that by applying the force at a node inside a patch and/or by increasing the number of elements in the FEM model, used to compute the mobility vector of the in-vacuo structure, allows to reduce the gap.

Fig. 5.8(a) reports the quadratic velocity of the cylindrical shell computed with the three aforementioned models whereas the averaged quadratic pressure (considering $N_m = 282$ microphones) inside the cavity is depicted in Fig. 5.8(b). On the one hand, the locally reacting model with tuned coefficient referred to as LR-TMM[avg./k_f] does not seem able to capture the acoustic response inside the cavity. On the other hand, fewer errors are observed in the structural response due to stiffness provided by the curvature of the cylindrical shell. Nonetheless, an enhancement of the accuracy of the TMM based model is appreciated when the non-local behavior of the SP is estimated by means of the NLR-TMM model using only the shortest geodesic pattern contribution $N_l = 1$. Indeed, the same observations made in the previous studied case are observed here where small errors are recorded at the double wall resonance and an underestimation of the quadratic pressure

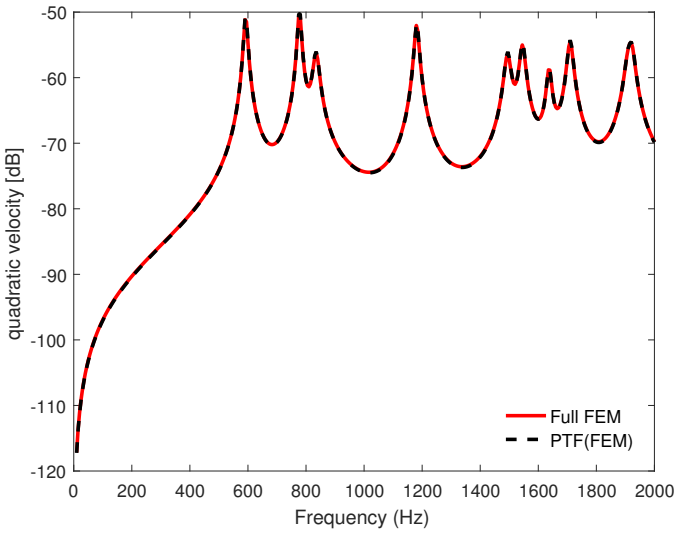

(a)

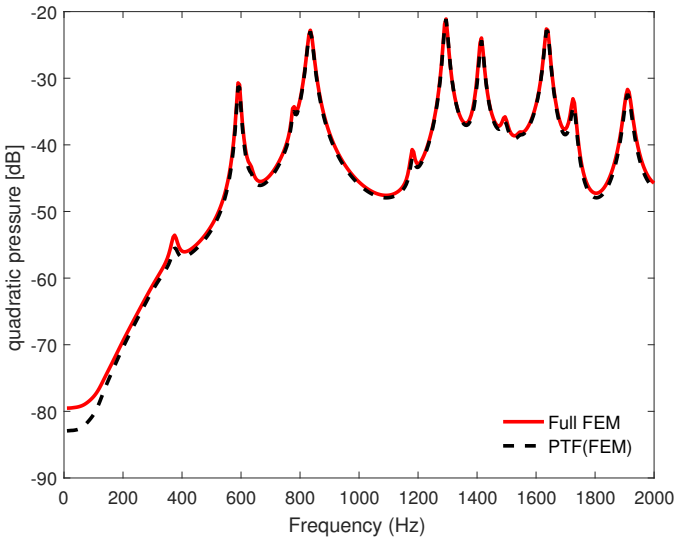

(b)

Figure 5.7 (a) Quadratic velocity of the cylindrical shell. (b) Averaged quadratic pressure inside the acoustic cavity. Results relative to the comparison between PTF(FEM) and reference (R_{ext}=0.10 m).

at the higher portion of the spectrum in Fig. 5.8(b). The observed underestimation is may due to the estimation of the Green functions $\hat{d}_{mn}$ in Eq.5.6 by the TMM that considers a flat SP, i.e. this can be investigated by using a cylindrical TMM. As expected, due to the small radius, no enhancement of the accuracy of the NLR-TMM-ISM model was observed at the aforementioned resonance when the finite size correction was retrieved. This is in line with the results of previous works[41, 40].

Of course, the accuracy of the NLR-TMM model is enhanced, as depicted in Fig.5.9, when the direct field was provided by two shortest geodesic contributions ($N_l = 2$) as well as the finite size using only the first order of reflections at the two lateral boundaries. Similar tendencies are observed in the nodal acoustic pressure inside the cavity in Fig. 5.10.

Finally, it should be mentioned that the LR-TMM model converges in the higher frequency range for all the vibroacoustic indicators presented in this paper. Moreover, the results of the NLR-TMM model with or without finite size correction exhibit errors at very low frequency. It was found that these errors are due to the linear wavenumber grid used to sample the $\hat{d}_{mn}$ functions (i.e. see step 1 on the numerical implementation). It can be proved that the prediction of the NLR-TMM can be enhanced by using a logarithmic scale or by using a wavenumber grid that guaranty a correct sampling of the oscillatory behavior of the $\hat{d}_{mn}$ functions.

5.4.3 Iterative truncation criterion

In this section, a further truncation criterion is introduced to fully take advantage of the large damping and the short wavelength within poroelastic materials. The iterative truncation rule is proposed in order to tackle some open issues of the NLR-TMM such convergence and the computational cost due to the added virtual sources. Indeed, computational cost of the added virtual sources can be expensive if high order of reflections are needed. This is the case when the SP surface area is small and/or when the SP thickness resonance is located at low frequencies as shown in previous chapters 3 and 4. For example, Alimonti and Atalla [3] proposed a truncation rule based on the dimension of the SP (i.e. the mean free path [43]). This truncation rule stops the image source generation process without considering the material properties or the thickness of the SP. Moreover, such criterion is static and deal with all the frequency range using the same rule where only the low frequencies have to consider the contribution of far sources. In the high frequency range, only contributions from sources that are relatively close to the receiving node should be considered (i.e. the waves that propagate inside the SP die quickly). To summarize, the distance r increases when the frequency decreases. Consequently, a truncation rule

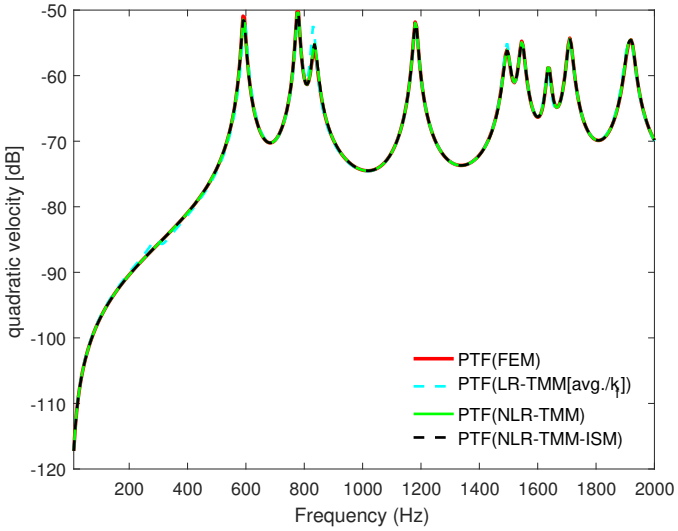

(a)

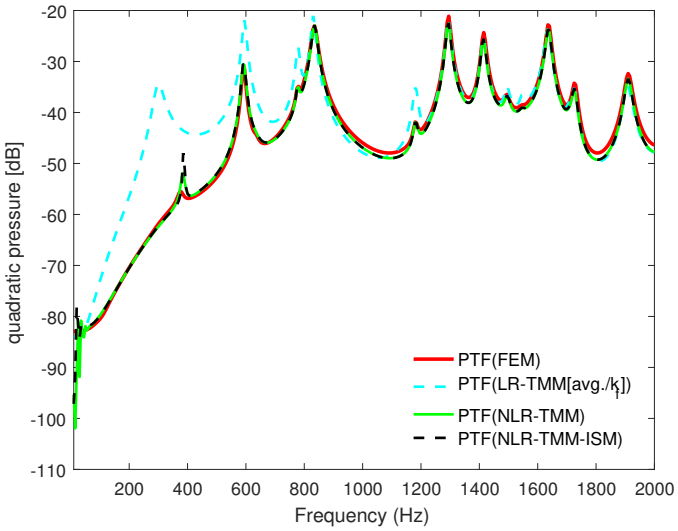

(b)

Figure 5.8 (a) Quadratic velocity of the cylindrical shell. (b) Averaged quadratic pressure inside the acoustic cavity. Results relative to the comparison between PTF(FEM), LR-TMM and NLR-TMM($N_l = 1$) with and without finite size correction (R_{ext}=0.10 m).

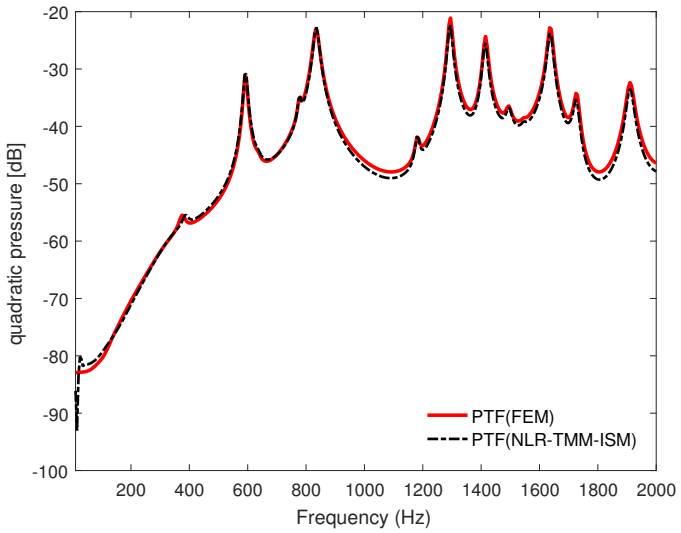

Figure 5.9 Averaged quadratic pressure inside the acoustic cavity. Results relative to the comparison between PTF(FEM), and NLR-TMM-ISM when the $N_l = 2$ shortest geodesic patterns were used to account for the direct field with the finite size correction (R_{ext}=0.10 m).

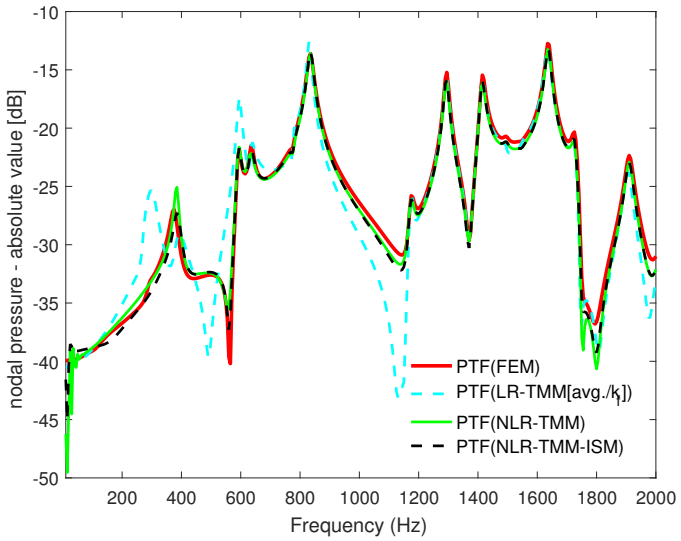

Figure 5.10 Acoustic pressure inside the acoustic cavity at coordinates (0.288 m, 0.03 m, 0.008 m). Results relative to the comparison between PTF(FEM),LR-TMM, NLR-TMM($N_l = 1$) and NLR-TMM-ISM when the $N_l = 2$ shortest geodesic patterns were used to account for the direct field with the finite size correction (R_{ext}=0.10 m).

that considers only the sources that have a significant contribution to the receiving node is needed.

In this context, a frequency dependent iterative truncation criterion that aims to stop the integral calculation is presented. As indicated previously, in step 2 of the numerical implementation, the functions $D_{mn}(r_{ij}, \omega)$ are sampled using a grid consisting of N_r distances between $r_1 = 0$ and $r_{N_r} = r_{max}$ and noted as $r = [r_1, r_2, ...r_{N_r}]$. The iterative truncation criterion is evaluated at each distance r_t of the distance grid for each frequency and truncates sources that have an insignificant contribution. For a given frequency ω and distance iteration r_t, the criterion is defined by

$$\left| \frac{\|D_{mn}(1 : r_t, \omega)\| - \|D_{mn}(1 : r_{t-1}, \omega)\|}{\|D_{mn}(1 : r_{t-1}, \omega)\|} \right| \leq \varepsilon, \text{ with, } t = 2, ..., N_r, \tag{5.10}$$

where, $\|D_{mn}(1 : r_t, \omega)\|$ is the Euclidean norm of the functions vectors D_{mn} considering distances between r_1 and r_t. ε is the tolerance criterion. The integral calculation is stopped once the truncation criterion is verified otherwise the calculation continues until the maximum distance $r_{N_r} = r_{max}$ provided by the considered number of the shortest geodesic distances for the direct field and the order of reflections for the reflected field.

On the other hand, it's expected that the needed distance r_t will increase when the frequency decreases. Hence, a decreasing frequency vector is defined in order to fully take advantage of the nature of materials usually involved within SP and to avoid the evaluation of the truncation criteria at each distance r_t. Such procedure aims to exploit the parallel computation. The tolerance criterion is studied in the case of the previous considered cases. Fig. 5.11(a) shows the error between the averaged quadratic pressure inside the cylindrical cavity obtained with the converged NLR-TMM-ISM of the lattice in Fig. 5.5(b) and that obtained with the proposed truncation rule for different values of tolerance ε. The results indicate that more errors are observed below 1200 Hz, especially when the tolerance values are $\varepsilon = 10^{-6}$ and $\varepsilon = 10^{-9}$. That confirms that the contributions of far virtual sources are needed in the low frequency range. In addition, the errors disappear when greater values of tolerance ε are considered. It could be argued that a value of the tolerance ε around 10^{-10} already gives a good solution with an error below 0.5 dB over the whole studied frequency range. Fig. 5.11(b) exhibits similar observations when the error between the averaged quadratic pressure inside the cylindrical cavity obtained with the converged NLR-TMM-ISM of the lattice in Fig. 5.9 and that obtained with the proposed truncation rule for different values of tolerance ε. However, the results obtained by the

truncation criterion are difficult to interpret due to the oscillatory behavior of the D_{mn} functions.

On the other hand, for the sake of conciseness only the maximal distances r_t considered in the calculation of each D_{mn} function vector at each frequency in the $R_{ext} = 0.25$ m configuration are depicted in Fig. 5.12. It shows that, in the high portion of the spectrum, only the contributions relatively close to the receiving node should be considered as well as the presence of an asymptotic shape of the considered distances r at the low frequency. This confirms that in theory infinitely far sources are needed in order to predict accurately the low frequency aspect. It should be mentioned that the efficiency provided by the proposed criterion will be more appreciated in the case of SP with large dimensions.

5.5 Conclusion

In this paper an extension of the NLR-TMM model to cylindrical SP was proposed. The limitations of the LR-TMM model are confirmed. However, the LR-model uses the flexural wavenumber of an infinite plate which is hardly justifiable in the studied cases. The considered frequency range is under the ring frequency in both cases $R_{ext} = 0.25$ m and 0.10 m. Then, the importance of the non-locally behavior of the SP was shown through a parametric study using the radius of curvature as a parameter, especially when the structure is excited by a mechanical force. For the considered cases, these obtained results reveal that for SP with a sufficiently large radius (i.e. greater than 0.25 m) and length only the shortest geodesic is necessary to capture its dynamic accurately. Conversely, high order of geodesic distance contributions on the direct field as well as reflections may be needed if the dimensions of the SP are small and/or if its thickness resonance is located at low frequency. In order to enhance the efficiency of the NLR-TMM model only the sources with significant contributions should be considered. For this purpose, frequency dependent iterative truncation criterion was proposed in order to stop the integral calculation in Eq. (5.6). A preliminary assessment of the proposed truncation rule was conducted by considering different values of tolerance ε. Moreover, the considered distance at each frequency in the D_{mn} functions was presented in order to show the efficiency added when such a criterion is exploited. The main conclusion, for the considered cases, is that the curvature of the considered SP can be simply neglected and that the curvature effect is mainly governed by the structure. However, this can't be a general conclusion and a cylindrical TMM is needed in order to assess the curvature effect (this work is initiated in the next chapter). In addition, more studies are needed in order to fully assess the proposed NLR-TMM (e.g. thickness of SP, nature of SP, acoustic excitation). Also, the proposed

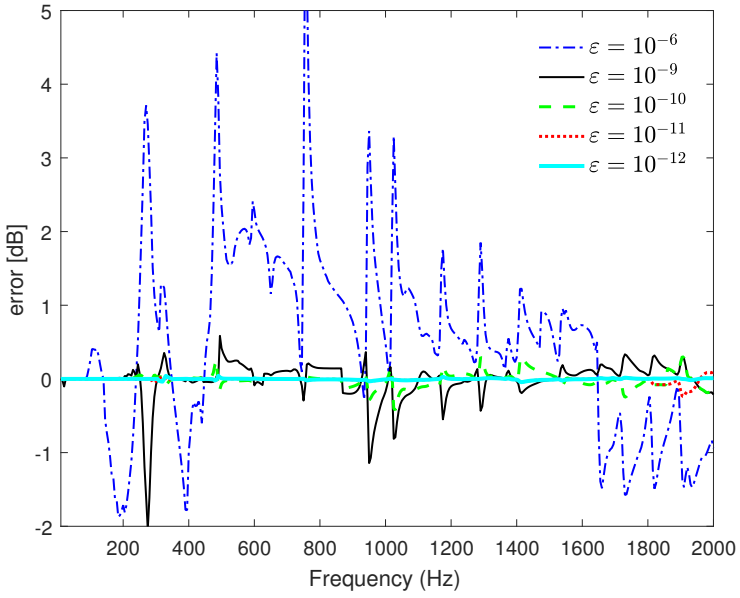

(a)

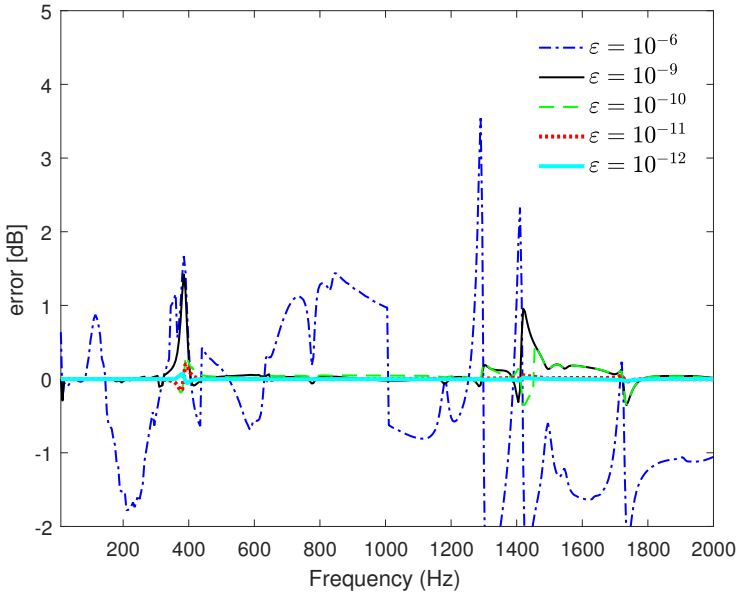

(b)

Figure 5.11 Effect of the tolerance ε in the frequency independent iterative truncation rule for a treated cylindrical structure-cavity system in two configurations : (a)R_{ext} = 0.25 m and (b) R_{ext} = 0.10 m. The error refers to the decibel difference between the averaged quadratic pressure inside the cylindrical cavity obtained with the converged NLR-TMM-ISM and that obtained with the proposed truncation rule for different values of tolerance ε.

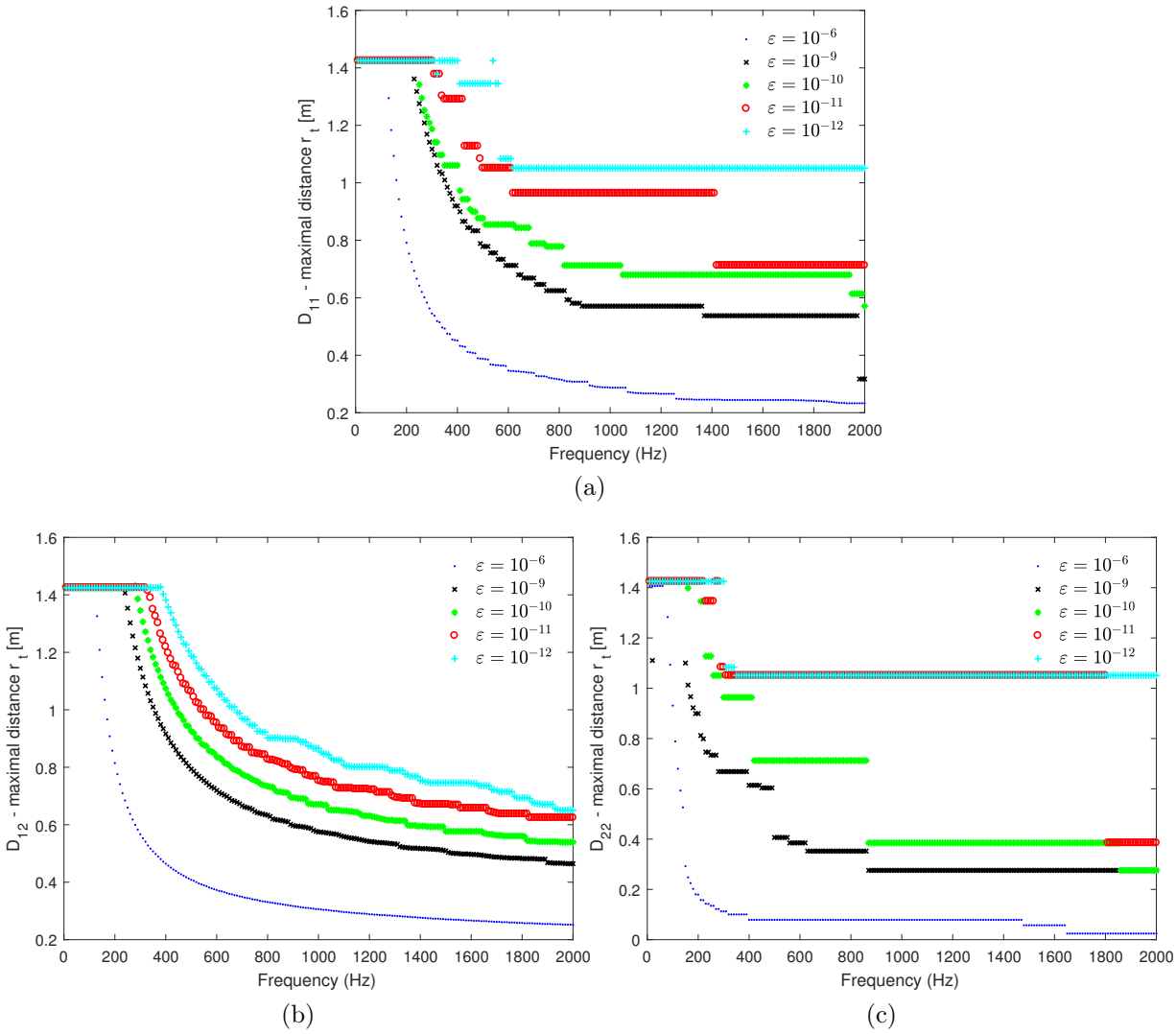

Figure 5.12 Maximal distances r considered in the calculation of each D_{mn} function vector at each frequency for the configuration with $R_{ext} = 0.25$ m : (a) D_{11}, (b) D_{12} and (c) D_{22}.

model can be applied to different axisymmetric geometries like, for example, conical and elliptical geometries. However, geodesic distance calculation may be more challenging for complex geometries.

CHAPITRE 6

Diffuse field sound transmission through infinite multiphysical cylinders using WFEM

Auteurs et affiliation :

K. Kesour : étudiant au doctorat, Université de Sherbrooke, Faculté de génie, Département de génie mécanique

N. Atalla : professeur, Université de Sherbrooke, Faculté de génie, Département de génie mécanique

Date d'acceptation : En préparation

État de l'acceptation : -

Revue : -

Référence : -

Titre français : La modélisation de la transmission sonore à travers un cylindre multiphysique infini à l'aide de la méthode des éléments finis ondulatoires.

Contribution au document : Dans les chapitres précédents, nous avons montré le besoin d'une matrice de transfert cylindrique afin d'étudier rigoureusement l'effet de la courbure d'un traitement acoustique. Dans ce contexte, ce travail est initié dans ce chapitre qui propose un modèle pour calculer la perte par transmission à travers un cylindre multiphysique infini en utilisant la méthode des éléments finis ondulatoires. Dans le future, ce modèle sera utilisé afin de développer une matrice de transfert cylindrique afin d'estimer judicieusement les fonctions de Green d'un traitement acoustique cylindrique infini.

Résumé français : Cet article s'intéresse à la modélisation de la transmission sonore à travers un cylindre périodique multiphysique infini. Le modèle proposé est basé sur la méthode des éléments finis ondulatoires (WFEM) qui combine les éléments finis standards et la théorie de la propagation des ondes en structures périodiques. La méthode utilise la matrice de rigidité dynamique d'une petite cellule cubique droite ainsi qu'une modélisation analytique de l'excitation et du couplage entre la structure cylindrique et les milieux fluides interne et externe. Tout d'abord, la théorie derrière la méthode proposée est présentée en détail. Ensuite, le modèle WFEM est validé dans le cas d'un cylindre sandwich orthotrope infini avec un coeur en matériau

polymère et poroélastique. Enfin, le couplage entre la mousse poroélastique et les deux peaux est étudié en considérant une excitation par une onde plane oblique ainsi que par un champ acoustique diffus.

Note : -

6.1 Abstract

This paper is concerned with the modeling of the sound transmission through an infinite multiphysical periodic cylinder. The proposed model is based on the Wave finite element method (WFEM) which combines conventional finite elements and wave propagation theory into periodic structures. The method uses the dynamic stiffness matrix of a small right cubic unit cell as well as analytical modeling of the excitation and of the coupling between the cylindrical structure and the internal and external fluid media. First, the theory behind the proposed method is presented in detail. Then, the WFEM is validated in the case of an infinite orthotropic sandwich cylinder with a polymer core and a poroelastic core. Finally, the coupling effect of the skeleton of the poroelastic foam with the two skins is studied under an oblique plane wave excitation as well as an excitation by a diffuse acoustic field.

6.2 Introduction

The sound transmission through infinite cylindrical structures is of main importance in many industrial applications, e.g. pipes, launchers, aircraft fuselages and submarines. For instance, lightweight poroelastic materials are usually employed in order to reduce the acoustic transmission inside the interior cabin yielding to an enhancement of passengers' comfort in the transport industry or to the acoustic protection of payloads in the space industry. Indeed, such acoustic materials are known to be very good acoustic absorbent in high frequency range. The poroelastic materials are composed of a solid phase, i.e. skeleton, containing air-filled pores. Their acoustic absorption comes from losses due to viscous effects (friction of the air against the skeleton) and thermal effects (absorption of excess heat from the fluid by the skeleton) as well as the skeleton elasticity effects (if the skeleton is in motion). However, their ability to absorb decrease with frequency due to the long wavelength. For these reasons, design and optimization tools are increasingly needed in order to enhance the acoustic performance of cylindrical structures with attached sound packages.

In this context, several works have studied the sound transmission through cylindrical structures using analytical models. For instance, Koval modeled analytically the sound transmission through a single isotropic as well as orthotropic cylindrical shell [44, 45] and extended the analysis to laminate composite shells [46] in the presence of an external mean flow. However, transverse shearing and rotational inertia were neglected in his studies. In addition, in his works, the significance of the ring and coincidence frequencies was pointed out. Later, Blaise and Lesueur [16, 17, 18] proposed an extension of Koval's work to handle acoustic transmission of generic oblique incidence through isotropic and multilayered orthotropic cylindrical structures in order to compute the diffuse field transmission. Ghinet and Atalla [34] later proposed a more general alternative for modeling the transmission loss (TL) through infinite laminated and sandwich composite shells. In their model, the transverse shearing and rotational inertia as well as the orthotropic ply angle were considered. In a recent paper, Magniez et al. [54] proposed a mixed 3D-shell analytical model successfully applied to a cylinder composed of two thin orthotropic skins and a thick isotropic core. Later, they developed a Biot-shell model which take into account the elasticity effect of a poroelastic core by means of a Biot model [15]. However, the coupling effect between the poroelastic material and the two skins was not studied in their work. Other recent works studied the aforementioned coupling effect in the case of an oblique incidence angle [28, 84, 85, 70] as well as a diffuse acoustic field (DAF) [52]. However, the poroelastic material was modeled as an equivalent fluid based on the methodology proposed by Lee et al. [50].

In this context, this paper proposes a simple approach that overcomes the complex algebra expressions involved in the development of analytical models by exploiting the flexibility of the well established finite element method (FEM). The proposed approach is based on the Wave finite element method (WFEM)[59] that combines conventional FEM and the theory of wave propagation in periodic structures. The method uses the dynamic stiffness matrix (DSM) of a small right cuboid that represents the periodic unit cell (UC) as well as an analytical modeling of the excitation and of the coupling between the infinite cylinder with the internal and external fluid media. In literature, the characteristics of wave propagation in complex structures using WFEM has received a lot of attention. For instance, Mencik and Ichchou [61] used a one-dimensional WFEM to find the dispersion curve and the forced response of an infinite cylinder filled with acoustic fluid. Manconi and Mace [56], based on previous work [53], developed a two-dimensional WFEM to compute the dispersion curve of curved and cylindrical structures. Later, Renno and Mace [71] extended the two-dimensional WFEM to calculate a forced response of a cylinder in vacuo. The cylinder's axisymmetry was exploited. Chronopoulos [24] proposed a 2D WFEM to

predict the dispersion characteristics of composite orthotropic curved panels and cylindrical shell structures as well as the TL within a SEA framework. In addition, Errico et al. [33] used a 1D axisymmetric WFEM, within a transfer matrix framework, to model the flow-induced vibrations of periodic and axial-symmetric structures when random spatially correlated loads act on the external surface. Droz et al. [31] used small-scale resonators combined with poroelastic foam to improve the TL around the ring frequency. Recently, Kingan et al. [42] modeled the sound transmission through cylindrical structures using a two-dimensional WFEM. In their work, the infinite cylindrical structure is excited by a point source. The excitation is modeled analytically as well as the coupling with outer and inner fluid media. Indeed, more general modeling approach is developed in this paper. In addition, the infinite cylinder is excited by an oblique plane wave and a DAF.

This paper is composed of three sections. First, the theory on the basis of the proposed approach is derived. The oblique plane wave excitation and the coupling with external and internal fluid media are modeled analytically. Then, the WFEM is detailed for a generic system. The second section presents the validation of the proposed approach with previous works in literature [54, 55]. Finally, in the third section, the coupling effect between a poroelastic foam and the two skins of the infinite sandwich cylinder is studied. The results are presented in the case of an oblique plane wave as well as a DAF acting on the external surface of the sandwich cylinder.

6.3 Theory

In this section, the analytical modeling of the incident and transmitted fields is presented. Then, the WFEM based on the DSM of a generic system is briefly derived. Finally, the vibroacoustic indicators are presented, namely, the transmission loss under oblique and a diffuse field as well as radiated power.

6.3.1 Analytical modeling of sound fields

Let us consider an infinite cylindrical structure, possibly layered, surrounded and filled by acoustic media. The outer surface of the infinite cylinder at $r = r_1$ is excited by an oblique plane wave of an amplitude p_0 with an incident angle θ and a heading angle Ψ as depicted in Fig. 6.1. In the following, the subscripts 1 and 2 refer to external and internal fluid media, respectively. The incident pressure can be expressed and expanded in cylindrical

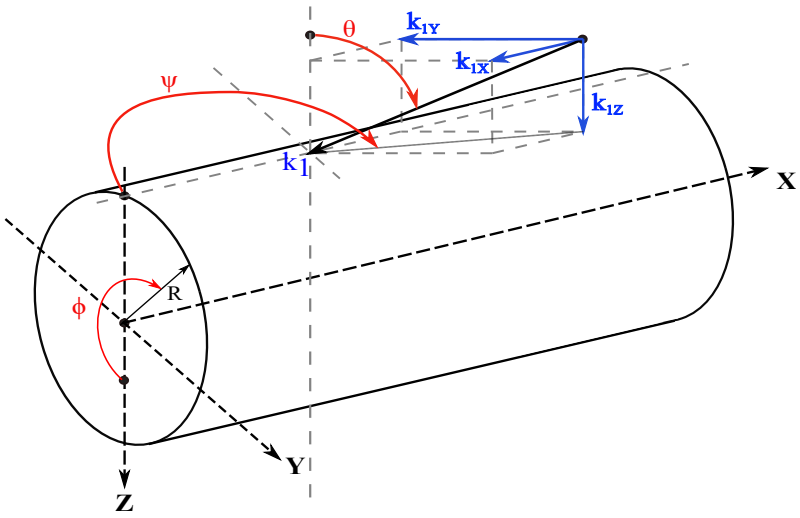

Figure 6.1 Infinite cylindrical surface excited by an oblique plane wave.

harmonics using the Jacobi-Anger expansion [16, 34, 52] as

$$\begin{aligned} P_1^I(r,\theta,x,t) &= p_0 e^{j(\omega t - k_{1x}x - k_{1r}r\cos(\phi+\beta))} \\ &= p_0 e^{j(\omega t - k_{1x}x)} \sum_{n=0}^{\infty} \varepsilon_n (-j)^n J_n(k_{1r}r)\cos(n(\phi+\beta)), \end{aligned} \tag{6.1}$$

where the longitudinal k_{1x} and the radial k_{1r} components of the wavenumber are

$$\begin{cases} k_{1x} = k_1 \sin\theta \cos\Psi \\ k_{1r} = \sqrt{k_1^2 - k_{1x}^2} = k_1 \cos\theta / \cos\beta \end{cases}, \tag{6.2}$$

$k_1 = \omega/c_1$ is the acoustic wavenumber, c_1 is the speed of sound on the exterior fluid, and the auxiliary angle β is defined as

$$\tan\beta = \tan\theta \sin\Psi, \tag{6.3}$$

n is the circumferential mode number, $J_n(k_{1r}r)$ is the Bessel function of order n and of argument $k_{1r}r$. The Neumann factor ε_n is given by

$$\varepsilon_n = \begin{cases} 1 & \text{for} \quad n = 0 \\ 2 & \text{for} \quad n \geq 1 \end{cases}. \tag{6.4}$$

On the other hand, the pressure scattered by the surface of the infinite cylinder into the external fluid medium is given by

$$P_1^S(r,\theta,x,t) = e^{j(\omega t - k_{1x}x)} \sum_{n=0}^{\infty} p_{1n}^S H_n^2(k_{1r}r)\cos(n(\phi+\beta)), \tag{6.5}$$

while pressure in the non-resonant interior cavity is expressed as

$$P_2^T(r,\theta,x,t) = e^{j(\omega t - k_{2x}x)} \sum_{n=0}^{\infty} p_{2n}^T H_n^1(k_{2r}r)\cos(n(\phi+\beta)), \tag{6.6}$$

where p_{1n}^S and p_{2n}^T are, respectively, the unknown amplitudes of the diffracted wave and the transmitted wave of circumferential mode n. H_n^1 and H_n^2 are the Hankel functions of order n of the first and second kinds, respectively. Moreover, since the axial wavenumber k_{1x} remains the same throughout the system, the axial wavenumber k_{2x} in the internal fluid medium is simply given by

$$k_x = k_{1x} = k_{2x}. \tag{6.7}$$

While the radial wavenumber k_{2r} in the inner fluid is defined as

$$k_2 = \sqrt{k_{2r}^2 + k_{2x}^2}, \tag{6.8}$$

where $k_2 = \omega/c_2$ and c_2 are the acoustic wavenumber and the speed of sound in the interior fluid medium, respectively.

Boundary conditions - external fluid

It should be noted that the total pressure on the exterior fluid domain is given by

$$P_1(r,\theta,x,t) = P_1^I(r,\theta,x,t) + P_1^S(r,\theta,x,t) \qquad r \geq r_1. \tag{6.9}$$

As a consequence, the "blocked-wall" pressure P^b (i.e. the real excitation seen by the infinite cylinder) is obtained by assuming a Neumann boundary at $r = r_1$ (i.e. the surface of the cylinder is assumed to be rigid). Hence, the acoustic particle normal displacement must vanish on the rigid surface of the cylinder as

$$\left.\frac{\partial P_1}{\partial r}\right|_{r=r_1} = \left.\frac{\partial (P_1^I + P_1^S)}{\partial r}\right|_{r=r_1} = 0. \tag{6.10}$$

Therefore, once the amplitude of the scattered wave p_{1n}^S is known, the "blocked-wall" pressure is expressed as

$$P^b = p_0 e^{j(\omega t - k_{1x}x)} \sum_{n=0}^{\infty} \varepsilon_n (-j)^n \left[J_n(k_{1r}r) - \frac{J_n^{'}(k_{1r}r_1)}{H_n^{2'}(k_{1r}r_1)} H_n^2(k_{1r}r) \right] \cos(n(\phi+\beta)), \quad (6.11)$$

where this equation can be reduced to

$$P^b = p_0 e^{j(\omega t - k_{1x}x)} \sum_{n=0}^{\infty} \frac{2\varepsilon_n (-j)^{n+1}}{\pi k_{1r} r_1} \left[\frac{1}{H_n^{2'}(k_{1r}r_1)} \right] \cos(n(\phi+\beta)), \quad (6.12)$$

using the following Wronskian relation

$$J_n(k_{1r}r_1) H_n^{2'}(k_{1r}r) - J_n^{'}(k_{1r}r_1) = -\frac{2j}{\pi k_{1r} r_1} H_n^2(k_{1r}r). \quad (6.13)$$

The radiated acoustic pressure p_1^{rad} into the external fluid medium due to the cylinder motion is obtained by using continuity of radial velocity between the fluid and the structure, i.e. $\frac{\partial P_1^S}{\partial r}\Big|_{r=r_1} = \rho_1 \omega^2 \mathrm{w}_{1n}$, and is given by

$$p_1^{rad} = \rho_1 \omega^2 e^{j(\omega t - k_{1x}x)} \sum_{n=0}^{\infty} \frac{H_n^2(k_{1r}r)}{k_{1r} H_n^{2'}(k_{1r}r_1)} \mathrm{w}_{1n} \cos(n(\phi+\beta)), \quad (6.14)$$

Boundary conditions - internal fluid

In a similar way, the radiated pressure p_2^{rad} from the inner surface of the cylinder at $r = r_2$in the interior fluid is expressed as,

$$p_2^{rad} = \rho_2 \omega^2 \mathrm{e}^{j(\omega t - k_{1z}z)} \sum_{n=0}^{\infty} \frac{H_n^1(k_{2r}r)}{k_{2r} H_n^{1'}(k_{2r}r_2)} \mathrm{w}_{2n} \cos(n(\phi+\beta)). \quad (6.15)$$

Cylindrical harmonics

In order to couple the structure and the surrounding fluids, the spectral forms of the above pressures are needed and they are given by

$$p_n^b = p_0 \frac{2\varepsilon_n (-j)^{n+1}}{\pi k_{1r} r_1} \left[\frac{1}{H_n^{2'}(k_{1r}r_1)} \right], \quad (6.16)$$

$$p_{1n}^{rad} = D_{1n}\mathrm{w}_{1n} = \frac{\rho_1\omega^2 H_n^2(k_{1r}r_1)}{k_{1r}H_n^{2'}(k_{1r}r_1)}\mathrm{w}_{1n}, \tag{6.17}$$

$$p_{2n}^{rad} = D_{2n}\mathrm{w}_{2n} = \frac{\rho_2\omega^2 H_n^1(k_{2r}r_2)}{k_{2r}H_n^{1'}(k_{2r}r_2)}\mathrm{w}_{2n}. \tag{6.18}$$

Note that the D_{1n} and D_{2n} are the dynamic spectral stiffness of the external and internal fluids, respectively.

6.3.2 WFEM of the vibroacoustic system

In this part, the theory behind the employed WFEM is described. Let's consider a generic unit cell (UC) with structural and fluid degrees of freedom (DOFs). The first step consists in computing the (DSM) of the UC using a FEM solver. The coupling conditions between the structural and fluid phases involved in the UC are handled within the FEM. The in-house NOVAFEM solver is used to provide the DSM of the UC. For time harmonic motion at frequency ω, the governing equation of the UC finite element system is given by [9],

$$\begin{pmatrix} [K]-\omega^2[M] & -[C] \\ -[C]^T & \frac{[H]}{\omega^2}-[Q] \end{pmatrix} \begin{Bmatrix} \{\mathrm{u}\} \\ \{\mathrm{p}\} \end{Bmatrix} = \begin{Bmatrix} \{\mathrm{F}\} \\ \frac{1}{\rho_f\omega^2}\{\Phi\} \end{Bmatrix}, \tag{6.19}$$

where ρ_f is the fluid density, matrices $[M]$ and $[K]$ (resp. $[H]$ and $[Q]$) are the mass and stiffness matrices of the structure (resp. the fluid). Matrix $[C]$ is a surface coupling matrix between the solid and the fluid domains. The vectors $\{u\}$ and $\{p\}$ contain the structural displacement and pressure DOFs, respectively. $\{F\}$ presents the external nodal force vector acting on the structure at external boundaries. $\{\Phi\}$ denotes the normal external pressure gradient nodal vector acting on the fluid phase at external boundaries. Not that $\{\Phi\}$=0 if only solid domain is located at the external boundaries and $\{F\}$=0 if only fluid domain is located at the external boundaries. On the other hand, the dynamic equilibrium equation of the UC can be rewritten by splitting boundary forces as

$$\mathbf{D}_{loc}(\omega)\mathbf{q} = \mathbf{f} + \mathbf{e}, \tag{6.20}$$

where $\mathbf{D}_{loc}$ denotes the dynamic stiffness matrix of the right cuboid unit cell, the vector $\mathbf{q}$ involves the structural displacements and pressures, the vector $\mathbf{f}$ represents the internal forces due to adjacent unit cells and the vector $\mathbf{e}$ contains external forces imposed on the unit cell external boundaries. In this paper, $\{\Phi\}$=0 since an acoustic excitation acting only on the structural domain is considered. Hence, $\mathbf{e}$ contains forces imposed on the

cylindrical structure by the acoustic pressure fields on each side. The second step consists in partitioning the unit cell into nine parts, namely, an internal region (I), surfaces S_1, S_2, S_3, S_4 and corner lines C_1, C_2, C_3, C_4 as depicted in Fig. 6.2. Hence, the DOFs vector $\mathbf{q}$ is partitioned as

$$\mathbf{q} = [\mathbf{q}_{C_1} \quad \mathbf{q}_{C_2} \quad \mathbf{q}_{C_3} \quad \mathbf{q}_{C_4} \quad \mathbf{q}_{S_1} \quad \mathbf{q}_{S_2} \quad \mathbf{q}_{S_3} \quad \mathbf{q}_{S_4} \quad \mathbf{q}_I]^T, \tag{6.21}$$

where the subscript T denotes transposition. In a similar way, the vector of internal and external forces are partitioned as

$$\mathbf{f} = [\mathbf{f}_{C_1} \quad \mathbf{f}_{C_2} \quad \mathbf{f}_{C_3} \quad \mathbf{f}_{C_4} \quad \mathbf{f}_{S_1} \quad \mathbf{f}_{S_2} \quad \mathbf{f}_{S_3} \quad \mathbf{f}_{S_4} \quad \mathbf{f}_I]^T, \tag{6.22}$$

$$\mathbf{e} = [\mathbf{e}_{C_1} \quad \mathbf{e}_{C_2} \quad \mathbf{e}_{C_3} \quad \mathbf{e}_{C_4} \quad \mathbf{e}_{S_1} \quad \mathbf{e}_{S_2} \quad \mathbf{e}_{S_3} \quad \mathbf{e}_{S_4} \quad \mathbf{e}_I]^T. \tag{6.23}$$

It is assumed that opposite surfaces and the four corner lines have the same number of DOFs. The local coordinates of the structural domain must be rotated in order to account for the desired curvature. For this purpose, in the third step, a rotation matrix **ROT** is built so that the DSM of the curved unit cell is defined as [56, 71]

$$\mathbf{D} = \mathbf{ROT}^T \mathbf{D}_{loc} \mathbf{ROT}. \tag{6.24}$$

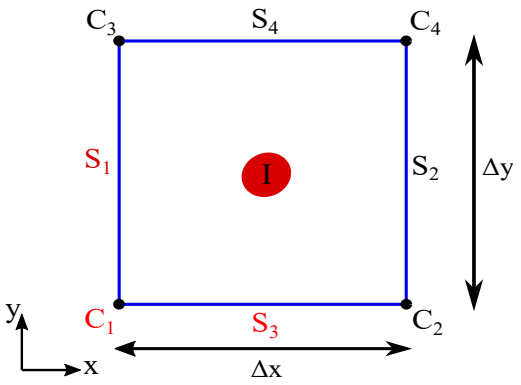

Figure 6.2 Unit cell (in local coordinates (x, y, z)) partitioning into nine parts, namely, an internal region (I), surfaces S_1, S_2, S_3, S_4 and corner lines C_1, C_2, C_3, C_4. The reduced problem considers only the parts in red.

The rotation matrix **ROT** is a block diagonal where the i-th block is related to the i-th node. Solid DOFs are rotated using unitary sub-matrices $\mathbf{r}_i^s$ defined as

$$\mathbf{r}_i^s = \begin{bmatrix} 1 & 0 & 0 \\ 0 & \cos(\alpha_i) & \mp\sin(\alpha_i) \\ 0 & \pm\sin(\alpha_i) & \cos(\alpha_i) \end{bmatrix}. \tag{6.25}$$

where the angle $\alpha_i = \frac{y_i - y_{mid}}{R}$, y_i is the y-axis coordinate the i-th node, y_{mid} is the median coordinate of the unit cell on the y-axis, $R = \frac{r_1+r_2}{2}$ is the median curvature radius. The fluid DOFs are rotated using unitary sub-matrices $\mathbf{r}_i^f$ defined as

$$\mathbf{r}_i^f = \begin{bmatrix} 1 \end{bmatrix}. \tag{6.26}$$

In the contexte of the $(u,\ p)$ mixed formulation [10], the poroelastic DOFs are rotated using unitary sub-matrices $\mathbf{r}_i^{ps}$ defined as

$$\mathbf{r}_i^s = \begin{bmatrix} 1 & 0 & 0 & 0 \\ 0 & \cos(\alpha_i) & \mp\sin(\alpha_i) & 0 \\ 0 & \pm\sin(\alpha_i) & \cos(\alpha_i) & 0 \\ 0 & 0 & 0 & 1 \end{bmatrix}. \tag{6.27}$$

Periodic boundary conditions

Applying Bloch's theorem to the displacement and pressure vectors at the boundaries leads to the following relations :

$$\mathbf{q}_{C_2} = \mathbf{q}_{C_1}\lambda_x, \qquad \mathbf{q}_{C_3} = \mathbf{q}_{C_1}\lambda_y, \qquad \mathbf{q}_{C_4} = \mathbf{q}_{C_1}\lambda_x\lambda_y, \qquad \mathbf{q}_{S_2} = q_{S_1}\lambda_x, \qquad \mathbf{q}_{S_4} = \mathbf{q}_{S_3}\lambda_y, \tag{6.28}$$

with

$$\lambda_x = \exp(-jk_x\Delta x), \qquad \lambda_y = \exp(-jk_y\Delta y), \tag{6.29}$$

where Δy and Δy are the dimension of the flat rectangular segment as depicted in 6.2. The longitudinal wavenumber is defined in Eq.6.2. The tangential wavenumber k_y is given by as

$$k_y = \frac{n}{R}, \tag{6.30}$$

where n is the circumferential mode number and R is the median curvature radius. Therefore, the DOFs vector of the unit cell in Eq. 6.21 using periodicity relations can be written as

$$\mathbf{q} = \mathbf{\Lambda}\widetilde{\mathbf{q}}, \quad \mathbf{\Lambda} = \begin{pmatrix} I & 0 & 0 & 0 \\ I\lambda_x & 0 & 0 & 0 \\ I\lambda_y & 0 & 0 & 0 \\ I\lambda_x\lambda_y & 0 & 0 & 0 \\ 0 & I & 0 & 0 \\ 0 & I\lambda_x & 0 & 0 \\ 0 & 0 & I & 0 \\ 0 & 0 & I\lambda_y & 0 \\ 0 & 0 & 0 & I \end{pmatrix}, \quad \widetilde{\mathbf{q}} = \begin{Bmatrix} \mathbf{q}_{c_1} \\ \mathbf{q}_{S_1} \\ \mathbf{q}_{S_3} \\ \mathbf{q}_I \end{Bmatrix}. \tag{6.31}$$

Moreover, similar periodicity relations can be applied to the external forces vector as

$$\mathbf{e} = \mathbf{\Lambda}\widetilde{\mathbf{e}}. \tag{6.32}$$

Hence, the dynamic equilibrium equation in Eq.6.20 can be reduced as

$$\mathbf{\Lambda}^H\mathbf{D}(\omega)\mathbf{\Lambda}\widetilde{\mathbf{q}} = \mathbf{\Lambda}^H(\mathbf{f}+\mathbf{e}), \tag{6.33}$$

where H denotes the Hermitien transpose. The internal forces can be removed from the previous equation thanks to periodicity and it can be shown that [30, 66]

$$\mathbf{\Lambda}^H\mathbf{f} = 0. \tag{6.34}$$

Hence, the reduced dynamic problem can be written as

$$\widetilde{\mathbf{D}}(\omega,\theta,\Psi,n)\widetilde{\mathbf{q}} = \mathbf{\Lambda}^H\mathbf{e} = \mathbf{\Lambda}^H\mathbf{\Lambda}\widetilde{\mathbf{e}}. \tag{6.35}$$

Coupling with fluid media and acoustic excitation

As assumed, only structural elements of the unit cell are in contact with the external fluid (i.e. the incident side and referred to as 1) and with the internal fluid (i.e. the transmission side and referred to as 2). Moreover, the only non-zero terms on the reduced vector of external forces will be those relatives to DOFs in z-direction on both sides in local coordinates (equivalently, the radial direction in the global coordinates as in Fig. 6.1). For

this purpose, two Boolean operators $\widetilde{\mathbf{u}}_1$ and $\widetilde{\mathbf{u}}_2$ are used in order to gather the z-DOFs of nodes on the reduced problem belonging to interfaces 1 and 2. Hence, the acoustic loads due to the spectral blocked pressure and the coupling with the internal and internal fluids are simply lumped on DOFs using the Boolean operators, and the reduced external forces vector is defined as

$$\widetilde{\mathbf{e}} = -S_1(\mathbf{p}_n^b + p_{1n}^{rad})\widetilde{\mathbf{u}}_1 + S_2 p_{2n}^{rad}\widetilde{\mathbf{u}}_2, \tag{6.36}$$

with,

$$\mathbf{p}_n^b = p_n^b \exp(-j(k_x x + k_y y), \tag{6.37}$$

where x, y are the nodal coordinates while S_1 and S_2 are the nodal areas at interfaces 1 and 2, respectively. If a uniform mesh is used, then S_1 and S_2 are defined as the ratio of the unit cell area $S = \Delta x \Delta y$ and the number of nodes at interface 1 and interface 2, respectively. The spectral forms of p_n^b, p_{1n}^{rad} and p_{2n}^{rad} are given in Eqs. 6.16-6.18. Moreover, the radial displacements w_{1n} and w_{2n} can be defined as [42]

$$\mathrm{w}_{1n} = \widetilde{\mathbf{u}}_1^T\widetilde{\mathbf{q}}, \qquad \mathrm{w}_{2n} = \widetilde{\mathbf{u}}_2^T\widetilde{\mathbf{q}}. \tag{6.38}$$

Therefore, the forced coupled spectral dynamic system is given as

$$\widetilde{\mathbf{D}}(\omega, \theta, \Psi, n)\widetilde{\mathbf{q}} = -\mathbf{\Lambda}^H\mathbf{\Lambda}(S_1\mathbf{p}_n^b\widetilde{\mathbf{u}}_1 + (D_{1n}\widetilde{\mathbf{u}}_1^T\widetilde{\mathbf{u}}_1 - D_{2n}\widetilde{\mathbf{u}}_2^T\widetilde{\mathbf{u}}_2)\widetilde{\mathbf{q}}. \tag{6.39}$$

Hence, the pressures and the displacements are obtained as

$$\widetilde{\mathbf{D}}_{tot}\widetilde{\mathbf{q}} = (\omega, \theta, \Psi, n)(-\mathbf{\Lambda}^H\mathbf{\Lambda}(S_1\mathbf{p}_n^b\widetilde{\mathbf{u}}_1)), \tag{6.40}$$

with

$$\widetilde{\mathbf{D}}_{tot}(\omega, \theta, \Psi, n) = \widetilde{\mathbf{D}}(\omega, \theta, \Psi, n) + (D_{1n}\widetilde{\mathbf{u}}_1^T\widetilde{\mathbf{u}}_1 - D_{2n}\widetilde{\mathbf{u}}_2^T\widetilde{\mathbf{u}}_2) \tag{6.41}$$

Once the reduced DOFs vector $\widetilde{\mathbf{q}}$ is obtained by means of Eq. 6.40, displacements along the z-direction at interfaces 1 and 2 are averaged and noted as $\langle \mathrm{w}_{1n} \rangle$ and $\langle \mathrm{w}_{2n} \rangle$ respectively.

6.3.3 Sound Transmission Loss

The cylindrical structure is excited by an oblique plane wave with (θ, Ψ). Hence, the incident acoustic power per unit length on the external surface of the cylinder at $r = r_1$ is given by [52]

$$W^I(\omega, \theta, \Psi) = \frac{r_1 p_0^2}{\rho_1 c_1} \cos\theta / \cos\beta. \tag{6.42}$$

Note that this equation is consistent with previous works, since with $\Psi = 0$ the simplified incident power used in previous works is obtained. On the other hand, the transmitted sound power per unit length of the internal surface of the vibroacoustic system is

$$\begin{aligned} W^T(\omega,\theta,\Psi) &= \sum_{n=0}^{\infty} \frac{r_2}{2} \mathrm{Re}[D_{2n} \langle \mathrm{w}_{2n} \rangle (j\omega \langle \mathrm{w}_{2n} \rangle)^*] \int_0^{2\pi} \cos^2(n(\alpha+\beta)) \mathrm{d}\theta \\ &= \sum_{n=0}^{\infty} \frac{r_2 \pi}{\varepsilon_n} \mathrm{Re}[D_{2n} \langle \mathrm{w}_{2n} \rangle (j\omega \langle \mathrm{w}_{2n} \rangle)^*]. \end{aligned} \tag{6.43}$$

Thus, the acoustic transparency is defined as

$$\tau(\omega,\theta,\Psi) = \frac{W^T(\omega,\theta,\Psi)}{W^I(\omega,\theta,\Psi)} = \frac{r_2 \pi \rho_1 c_1}{r_1 p_0^2 \cos\theta / \cos\beta} \sum_{n=0}^{\infty} \frac{\mathrm{Re}[D_{2n} \langle \mathrm{w}_{2n} \rangle (j\omega \langle \mathrm{w}_{2n} \rangle)^*]}{\varepsilon_n}, \tag{6.44}$$

In the case of a diffuse field excitation (i.e. sounds waves are randomly incident from all directions with equal probability), the acoustic transparency is expressed as

$$\tau_d(\omega) = \frac{\int_0^{2\pi} \int_{\theta_{min}}^{\theta_{max}} \tau(\omega,\theta,\Psi) \cos\theta \sin\theta \, \mathrm{d}\theta \, \mathrm{d}\Psi}{\int_0^{2\pi} \int_{\theta_{min}}^{\theta_{max}} \cos\theta \sin\theta \, \mathrm{d}\theta \, \mathrm{d}\Psi}. \tag{6.45}$$

Finally, the TL is defined by the following equation :

$$\mathrm{TL} = -10 \log_{10}(\tau). \tag{6.46}$$

It should be noted that the TL must be corrected by the constant $10 \log_{10}(\pi)$ in order to represent the total surface of the cylinder [51, 34]. However, such constant is not used in the following presented results.

6.4 Validation

The main concern of this section is the validation of the WFEM developed in this paper. The results obtained with the WFEM are compared with those provided by an analytical model proposed by Magniez et al. [54, 55]. The TL obtained with the two methodologies are compared in the case of an infinite orthotropic sandwich with thick polymer core and poroelastic core excited by a plane wave (θ=45°, Ψ=0°). The two orthotropic skins have identical thickness and material properties. The DSM of the right cuboid UC used in the WFEM is obtained using an in-house FEM code (i.e. NOVAFEM). The external and

internal fluid medium properties are $c_1 = c_2 = 340$ m/s and $\rho_1 = \rho_2 = 1.284$ kg/m^3. The material properties used in the numerical simulations are presented in Table 6.1.

6.4.1 Sandwich cylinder with a thick polymer core

The first case concerns the transmission loss through an infinite orthotropic sandwich cylinder with a thick isotropic polymer core. The proposed curved UC model is compared to the analytical model developed by Magniez et al. [54]. As in their work, an external radius $r_1 = 2.164$ m and an internal radius $r_2 = 2.148$ m are considered.

The result obtained by the WFEM uses a periodic unit cell with dimensions $1 \times 1 \times 16$ mm^3. The finite element mesh of the 2 mm thick skins use $2 \times 2 \times 6$ eighth-brick solid elements while the polymer core involves $2 \times 2 \times 12$ eighth-brick solid elements. Fig. 6.3 presents the comparison of the TL predicted by the proposed model and Mangiez et al. analytical model. It's observed that the predicted TL by the WFEM is in an excellent agreement with the analytical model over the whole frequency range.

6.4.2 Sandwich cylinder with a thick poroelastic core

The second case is more challenging where the polymer core is replaced by a poroelastic core with a thickness of 50 mm. The external radius remains the same $r_1 = 2.164$ m while the internal radius is now $r_2 = 2.110$ m. The same air properties are filling the pores of the poroelastic material. The DSM is provided by a FEM of a right cuboid UC with dimensions $1 \times 1 \times 54$ mm^3. The two skins are modeled as a solid with the same mesh as in the previous case. On the other hand, the poroelastic core is modeled with Biot's model using 36 eighth-brick element through the thickness.

It should be noted that rigid and limp equivalent fluid were also used to model the poroelastic material and similar results were obtained as published by Magniez et al. [55]. However, for the sake of conciseness, these results are not presented. Fig. 6.4 shows a perfect match between the proposed approach and the analytical model, except at the first resonance which is mainly due to the frequency resolution. Indeed, the ring frequency is well captured and is located around 160 Hz. Moreover, interesting resonances are observed due to the coupling between the skins and the skeleton of the porous material. For this purpose, the next section will study the effect of the coupling between the skeleton of the poroelastic material and the skins on the transmission loss.

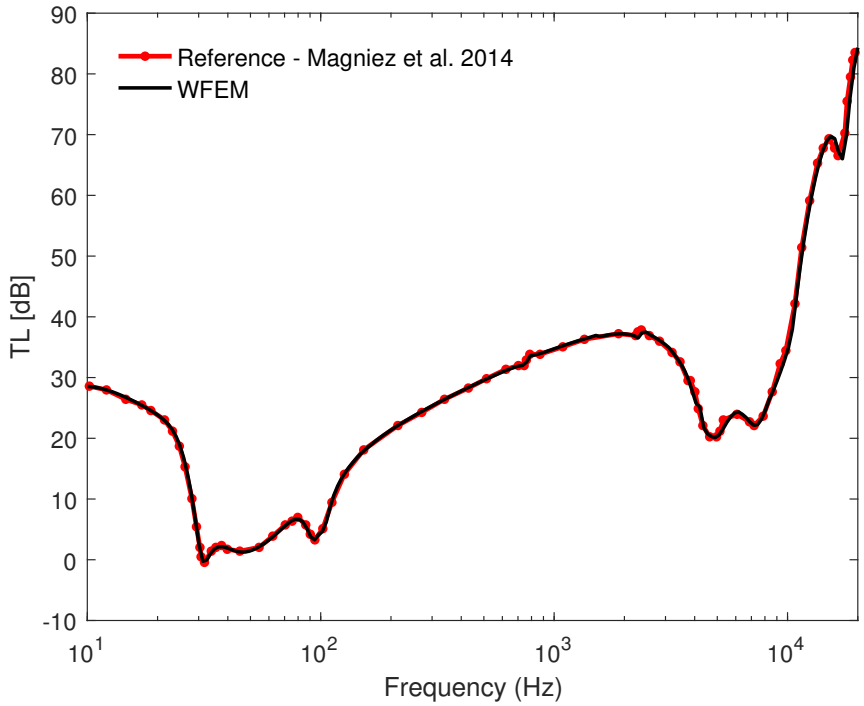

Figure 6.3 TL through an infinite cylindrical orthotropic sandwich with a polymer core at the incidence angle θ= 45° and azimuthal angle Ψ= 0°.

Tableau 6.1 Material properties for the validation cases [27, 54, 55].

Layer (material)	skins (Graphite/Epoxy)	core (polymer)	core (poroelastic)
Density (kg/m^3)	1600	1000	8.43
Young modulus E_x (GPa)	137.9	0.001	1.949e-4
Young modulus E_y=E_z (GPa)	8.96	0.001	1.949e-4
Shear modulus G_{xy} (GPa)	7.1	3.4e-4	6.863e-5
Shear modulus G_{xz} (GPa)	7.1	3.4e-4	6.863e-5
Shear modulus G_{yz} (GPa)	6.2	3.4e-4	6.863e-5
Poisson's ratio $\nu_{xy} = \nu_{xz}$ (-)	0.3	0.49	0.42
Damping μ (%)	0	5	5
Porosity ϕ (-)	-	-	0.994
Tortuosity α_∞ (-)	-	-	1.02
Flow resistivity σ (N s/m^4)	-	-	9045
Viscous characteristic length Λ (μm)	-	-	103
Thermal characteristic length Λ' (μm)	-	-	197
Thickness h (mm)	2	12	50

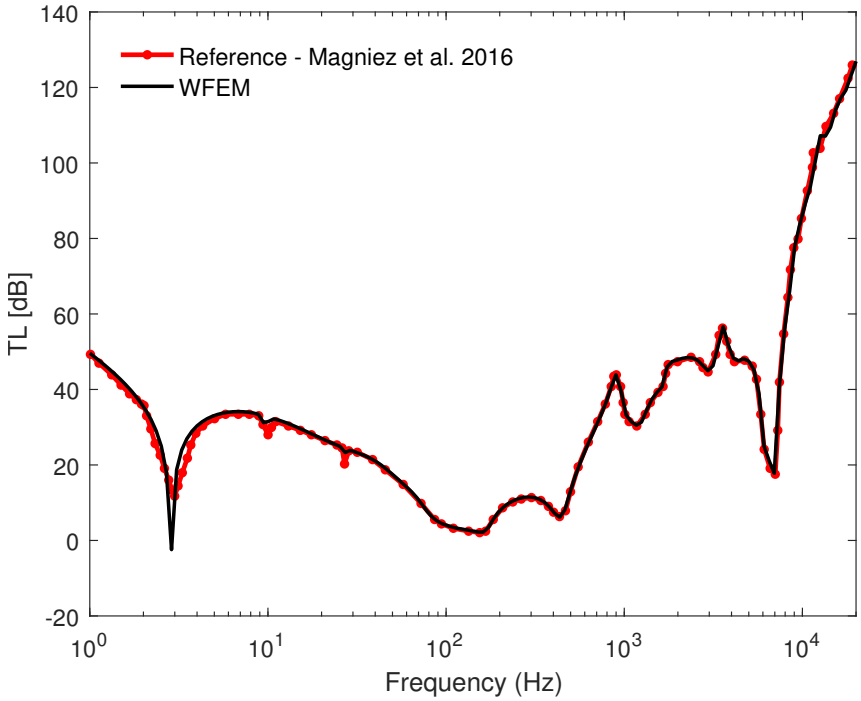

Figure 6.4 TL through an infinite cylindrical orthotropic sandwich with a poroelastic core at the incidence angle θ= 45° and azimuthal angle Ψ= 0°.

6.5 Effect of the coupling between the porous material and the two skins

In this section, the effect of the coupling between the poroelastic material and the two skins on the sound transmission loss is studied. First, an oblique plane wave (θ=45°, Ψ=0°) excitation is employed. Then, a DAF is considered with θ_{min}=0° and θ_{max}=90° in Eq. 6.45. In order to study the coupling effect, the validation case 2 (i.e referred to as **BB** configuration) when where the 50 mm thick poroelastic foam fills the gap between the two skins is compared to four configurations. The distance L between the two skins remains constant L=50 mm while the thickness of the foam is reduced to h=40 mm for the other configuration with air gaps (**UB**, **BU** and **UU**). In addition, another configuration where the foam is replaced by air, referred to as "**Air gap**", is also presented to highlight the enhancement of TL when a poroelastic foam is used. Air gaps of δ_1=10 mm, δ_2=10 mm and δ_1=δ_2=5 mm are used, respectively, in the **UB**, **BU** and **UU** configurations as depicted in Fig. 6.5. The material properties employed in this study are the same of the validation case 2. In addition, the considered FEM mesh of the right cuboid unit cell respect the criterion of eighth wavelength.

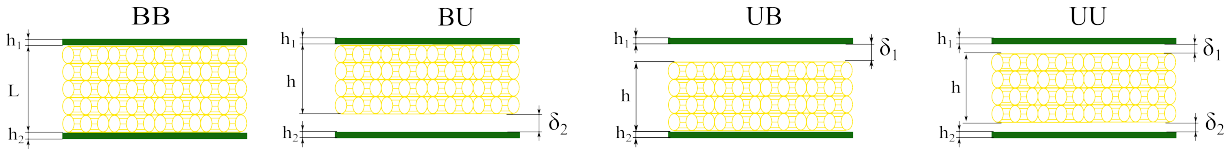

Figure 6.5 The configurations considered in the study of the coupling effect between the porous material and the two skins.

6.5.1 Oblique plane wave

Fig. 6.6 shows the TL through the infinite cylindrical configurations when the outer skin is excited by an oblique plane wave (45°,0°). As found in previous works, [52], below the ring frequency located around 160 Hz, the coupling effect between the foam and the skins is negligible due to the negligible stiffness added by the poroelastic foam. On the other hand, above the ring frequency, it is observed an enhancement of the TL when the air gap between the two skins is filled with a foam (**BB**). Indeed, resonances due to the coupling between the elastic skeleton of the porous foam and the skins are noticed especially above the ring frequency. Moreover, the TL is enhanced above the ring frequency when configurations **UB**, **BU** and **UU** are considered. Indeed, the configurations **UB** and **BU** give similar results revealing that the TL enhancement is only due to the decoupling added by the air gap. In addition, the TL result is better than all other configurations between 200 Hz and 900 Hz due to the skeleton resonances. Nevertheless, the **UU** configuration exhibits almost the best TL between 1000 Hz and 5000 Hz. This is mainly due to the acoustic absorption and multiple reflections provided by the air gaps placed between the poroelastic foam and the two skins. To this end, in the case of a double wall, it can be concluded that one of the configurations **UB**, **BU** and **UU** can be chosen according to the targeted TL.

6.5.2 Diffuse acoustic field

Now, a diffuse acoustic field is considered as an excitation. Fig. 6.7 presents the TL results. The same observations made in the previous figure are recorded in the case of a DAF excitation. The curves exhibit two mainly dips located around the ring frequency and the critical zone frequency. It is confirmed that the **UB** and **BU** configurations provide the best TL level between 200 Hz and 900 Hz (up to 5 dB at 500 Hz). The TL level is so poor at this frequency range that the gain provided by the resonance of the elastic skeleton in the case of **UB** and **BU** configurations is so valuable. For this reason, the **UB** and **BU** configurations should be preferred rather than the **UU** configuration. On the other hand, it is confirmed that classical sound package using poroelatsic material in

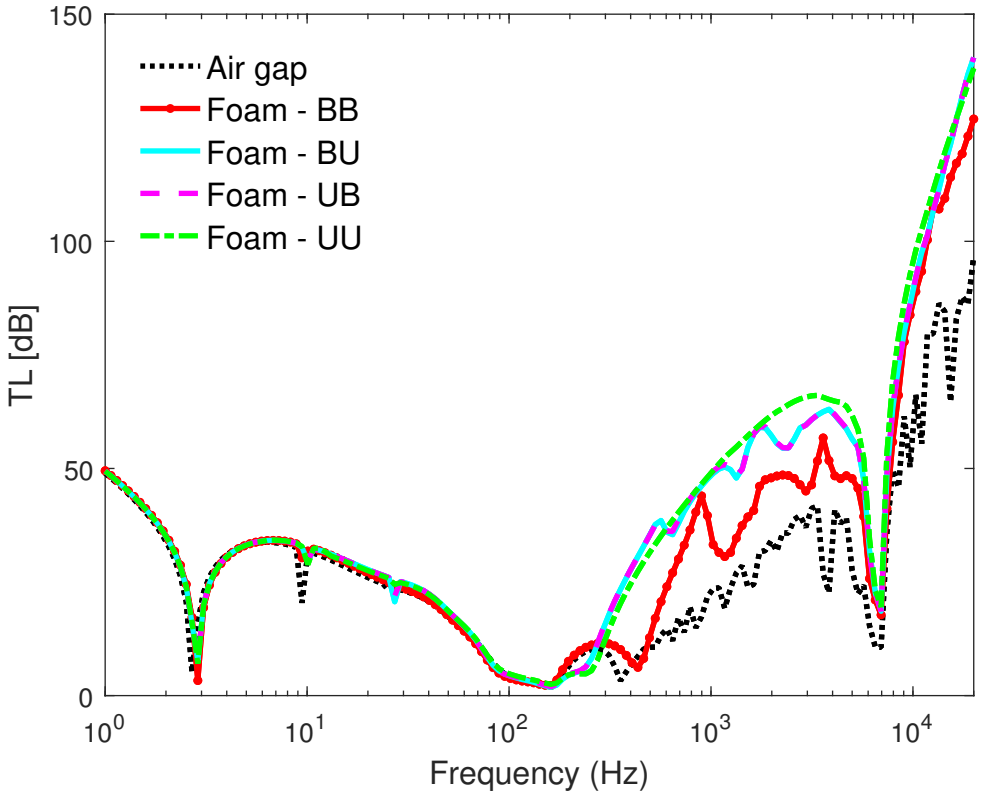

Figure 6.6 TL through an infinite cylindrical orthotropic sandwich with a poroelastic core at the incidence angle $\theta = 45°$ and azimuthal angle $\Psi = 0°$. Effect of the coupling between the poroelastic foam and the two skins.

multilayered fashion have limited ability to enhance the TL around the ring frequency due to their negligible added stiffness.

6.6 Conclusion

In this paper, a WFEM was proposed in order to model the sound transmission through infinite cylindrical system. This paper presents a preliminary assessment of the proposed model. The results obtained by the proposed model were compared with those of an analytical model where a very good agreement was observed. Moreover, Infinite orthotropic cylindrical sandwich configurations, with a polymer core and a poroelastic core, were studied in the case of oblique plane wave as well as a DAF. It is shown through the presented results that the TL is enhanced, especially above the ring frequency, when the poroelastic core is considered. In addition, the coupling effect study confirms that the poroelastic core should be decoupled at least from one of the two skins. It should be noted that the proposed numerical tool can be used to design periodic locally resonant meta-materials able to enhance the TL at the two major dips observed in the TL curves, namely, the ring and coincidence frequencies.

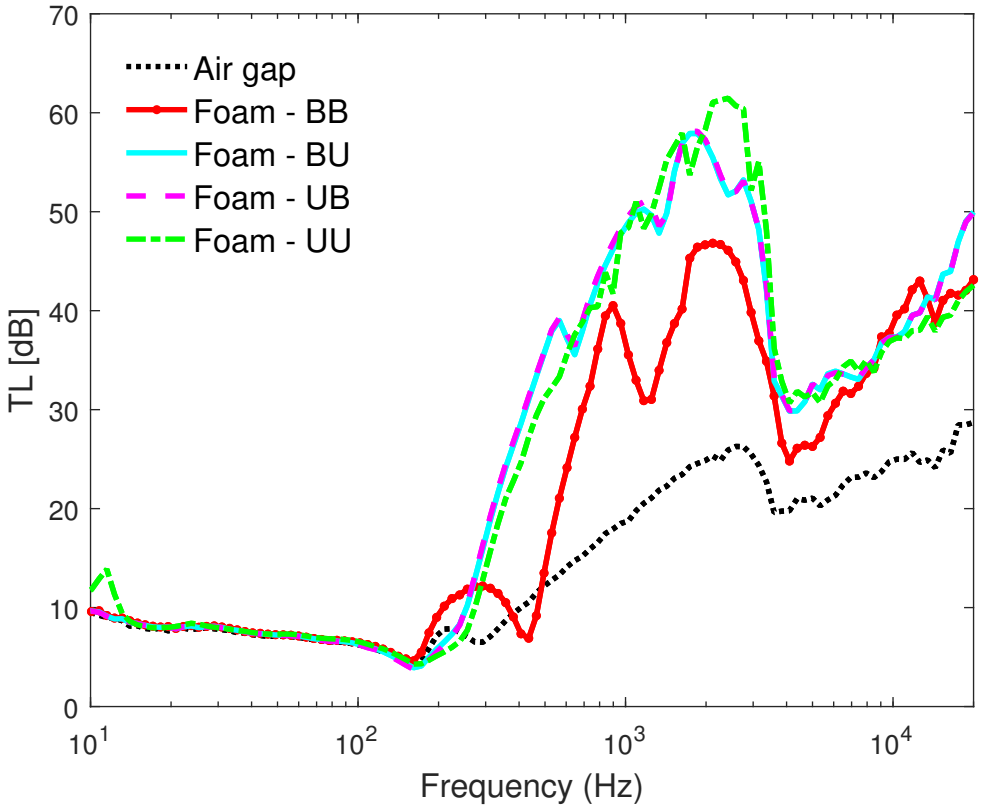

Figure 6.7 TL through an infinite cylindrical orthotropic sandwich with a poroelastic core due to a diffuse acoustic field. Effect of the coupling between the poroelastic foam and the two skins.

CHAPITRE 7

CONCLUSION

Dans ce travail de thèse, nous nous sommes intéressés à la prédiction de la réponse vibroacoustique des structures planes, courbes et cylindriques avec des traitements acoustiques.

Nous avons positionné le problème dans le chapitre 1. Celui-ci met en évidence le besoin d'optimiser les composants dissipatifs en basse fréquence par l'agencement de plusieurs couches et la nécessité d'effectuer des études paramétriques en utilisant des outils de simulation numérique rapides et précis.

Le chapitre 2 a présenté les matériaux poroélastiques, suivi des méthodes existantes concernant la modélisation des systèmes vibroacoustiques en basses fréquences. Ces derniers sont listés par type d'approche (déterministe, analytique et hybride). À travers cette étude de littérature, nous avons mis l'accent sur les inconvénients et le caractère ambitieux à développer de chaque méthode.

Les chapitres 3 à 6 constituaient les contributions originales de la thèse.

Nous avons proposé et développé dans le chapitre 3 une nouvelle méthode hybride efficace et précise pour évaluer les performances acoustiques des traitements de contrôle du bruit attachés à des structures planes à parois simple et double. Cette méthode hybride utilise la procédure PTF pour coupler efficacement, à travers des surfaces élémentaires, les modèles par éléments finis des systèmes maitres (structure et cavité acoustique) avec un modèle TMM à réaction non locale du traitement acoustique. Le couplage entre les sous-systèmes est réalisé par des relations de mobilités et d'impédances moyennées sur les surfaces élémentaires appartenant à l'intersection de leurs interfaces physiques. Puisque le cadre analytique de la TMM considère le traitement acoustique homogène, plat et latéralement infini, une correction par la méthode des sources images (ISM) avec le nombre approprié de sources virtuelles est utilisée pour tenir compte du champ réfléchi. Après une étude de convergence de la procédure PTF, nous avons évalué les performances de l'approche proposée pour différents problèmes de transmission (p. ex. configurations à parois simple et double) avec différents traitements acoustiques attachés (une mousse de mélamine et un traitement de type masse-ressort). Les résultats obtenus ont été systématiquement comparés, d'abord avec une solution exacte FEM/BEM et ensuite plusieurs comparaisons ont été réalisées avec les modèles suivants (dans un cadre PTF) : (i) un

modèle TMM à réaction non locale sans correction de la taille finie, (ii) un modèle TMM à réaction locale et (iii) un modèle FEM du traitement acoustique dans un cadre PTF. Les résultats ont montré que la méthode développée a une précision comparable à celles de la solution exacte FEM/BEM et du modèle FEM du traitement acoustique dans un cadre PTF. Toutefois, ces derniers ont un cout computationnel élevé par rapport à la méthode développée. D'autre part, le modèle à réaction locale présente des limites quant à la prédiction de la réponse dynamique des traitements acoustiques pratiques (p. ex. traitement de type masse-ressort).

Le chapitre 4 présentait quant à lui l'évaluation des performances acoustiques des traitements de contrôle du bruit attaché à des structures courbes en se basant sur la méthode hybride FE-TMM-PTF développée dans le chapitre 3. Toutefois, la méthode TMM ne peut pas considérer un traitement acoustique courbe à cause de l'hypothèse simplificatrice liée à son cadre analytique : le traitement phonique est considéré plat. Dans ce contexte, nous avons proposé de dérouler le traitement acoustique courbe pour estimer les fonctions de Green avec la TMM. Pour évaluer l'approximation proposée, une étude qualitative de l'effet du rayon de courbure et de l'épaisseur d'un traitement acoustique pratique de type masse-ressort en forme demi-cylindrique sur la précision de la méthode développée a été réalisée après une étude de convergence de la procédure PTF. De la même manière, les résultats de l'étude ont été comparés à l'approche standard (une solution FEM/BEM exacte), à un modèle TMM à réaction non locale sans correction de la taille finie, à un modèle TMM à réaction locale et un modèle FEM du traitement acoustique dans un cadre PTF. D'une part, les résultats obtenus par la solution exacte FEM/BEM et par le modèle FEM du traitement acoustique dans un cadre PTF sont en accord, alors que les performances de la méthode de sous-structuration considérant un modèle TMM à réaction locale dépendent de la nature des domaines de couplage, de la nature de l'excitation et ne peuvent donc pas être considérés comme fiables pour des applications générales. D'autre part, les résultats ont montré que la méthode développée permet une très bonne approximation de la solution exacte FEM/BEM. Le rayon de courbure et l'épaisseur du traitement acoustique ont un effet négligeable sur la précision de la méthode proposée dans les cas considérés, tandis que le nombre des sources virtuelles augmente d'une manière significative dans les deux cas spécifiques suivants :

- le cas d'un traitement acoustique de petite taille,
- le cas d'une résonance double parois située à très basse fréquence ($<$100Hz).

Ces deux cas de figure détériorent la performance computationnelle de la méthode proposée.

Pour améliorer les performances computationnelles du modèle TMM à réaction non locale, nous avons proposé, dans le chapitre 5, un critère de troncature dynamique permettant de considérer seulement les sources à contribution significative à la réponse dynamique du traitement acoustique. Le critère de troncature a été étudié et a montré sa performance computationnelle dans le cadre d'une extension du modèle TMM à réaction non locale pour des traitements acoustiques cylindriques après validation de sa précision. La validation du modèle proposé a été réalisée en utilisant les mêmes bases de comparaison considérées dans le chapitre précédent.

Finalement le chapitre 6 a proposé un modèle basé sur les éléments finis ondulatoires pour calculer la transmission acoustique à travers des structures cylindriques multicouches. L'approche développée a permis de surmonter la complexité des expressions algébriques utilisées dans le développement des modèles analytiques ainsi que d'exploiter la flexibilité de la méthode FEM.

Perspectives

La présente thèse ouvre une fenêtre vers plusieurs travaux futurs complémentaires. D'une part, les aspects suivants peuvent encore être évalués pour que le modèle de la matrice de transfert à réaction non locale soit entièrement généralisé :

1. Considérer d'autres natures de traitements acoustiques et différents types d'excitation (p. ex. monopole, champ diffus ...) afin d'évaluer entièrement son domaine de validité.

2. Extension du modèle NLR-TMM à des géométries axisymétriques plus complexes comme, par exemple, les géométries coniques et elliptiques. Cependant, le calcul de la distance géodésique peut s'avérer plus difficile.

3. Évaluer quantitativement des configurations hétérogènes. Une attention particulière doit être consacrée à l'effet de la taille finie et à sa correction au moyen du ISM. En effet, une étude préliminaire a montré que les sources virtuelles utilisées pour tenir compte de la taille finie du patchwork devraient être considérées en respectant les dimensions de la surface totale de la configuration.

4. Étudier la faisabilité d'une correction alternative pour mieux prendre en compte le champ réfléchi dans des matériaux qui ne se comportent pas comme des fluides équivalents (p. ex. solides ou matériaux poroélastiques avec des propriétés mécaniques non négligeables).

D'autre part, le calcul des PTFs des sous-systèmes maitres (la structure et la cavité) par les éléments finis peut être considérablement accéléré par l'utilisation du modèle de réduction d'ordre comme le *Matrix-Free Krylov Model* [38, 77, 78].

En ce qui concerne la procédure PTF, nous l'avons utilisée avec des maillages en patchs rectangulaires uniformes. Cependant, d'autres types de maillage peuvent être étudiés pour étendre l'approche à des applications complexes.

Finalement, la méthode WFEM développée est limitée à un couplage solide-fluide. Les principales perspectives à développer se résument alors par les points suivants :

1. Utiliser cette méthode pour modéliser et optimiser des traitements acoustiques avec des inclusions résonantes périodiques.
2. Étendre le modèle WFEM développé à d'autres types de couplage (fluide-fluide et poroélastique-fluide).
3. Développer une matrice de transfert cylindrique à partir de ce modèle suivant l'approche proposée dans [66] et l'utiliser pour estimer les fonctions de Green dans le cadre du modèle à réaction non locale.

ANNEXE A

Radiation impedance

This appendix presents a simple approach for calculating the radiation impedance based on Rayleigh's integral [9, 22]. Let us consider a vibrating surface $\partial\Gamma_\omega$ embedded in a rigid baffle and radiating in an unbounded fluid domain.

$$p(M) = i\omega\rho_0 \int_{\partial\Gamma_\omega} V_n(Q)G(M,Q)dS_Q, \tag{A.1}$$

where the baffled Green's function is given by

$$G(M,Q) = \frac{\exp(-\mathbf{i}kr)}{2\pi r}. \tag{A.2}$$

The vibrating surface $\partial\Gamma_\omega$ is discretized into elementary areas called patches such that $\partial\Gamma_\omega = \cup_{i=1}^{N}\partial\Gamma_{\omega,i}$. Hence, the nodal pressure at a given point M_i can be expressed by

$$p(M_i) = i\omega\rho_0 \sum_{j=1,j\neq i}^{N} \int_{\partial\Gamma_{\omega,j}} V_n(Q)G(M_j,Q)dS_Q + i\omega\rho_0 \int_{\partial\Gamma_{\omega,i}} V_n(Q)G(M_i,Q)dS_Q. \tag{A.3}$$

The patch dimensions are considered to be small enough, so that the normal velocity V_n can be assumed constant over each patch. Thus, the integral can be approximated by its value using the distance r_{ij} between patches central points.

$$p(M_i) = i\omega\rho_0 \sum_{j=1,j\neq i}^{N} \bar{V}_{n,j}\frac{\exp(-\mathbf{i}kr_{ij})}{2\pi r_{ij}}\partial\Gamma_{\omega,i} + i\omega\rho_0\bar{V}_{n,i}\int_{\partial\Gamma_{\omega,i}} \frac{\exp(-\mathbf{i}kr)}{2\pi r}dS_Q. \tag{A.4}$$

In order to avoid the Green's function singularity, the cylindrical coordinates are used to calculate Cauchy's principal value integral and the patch is considered with an equivalent

circular surface of a radius a such that $a = \sqrt{\partial\Gamma_{\omega,i}/\pi}$. Equation A.4 can be written such as

$$p(M_i) = \sum_{j=1, j\neq i}^{N} \bar{V}_{n,j} Z_{rad,ij} + \bar{V}_{n,i} Z_{rad,ii}, \tag{A.5}$$

where,

$$Z_{rad,ii} = i\omega\rho_0 \int_{\partial\Gamma_{\omega,i}} \frac{\exp(-\mathbf{i}kr)}{2\pi r} dS_Q \approx \rho_0 c_0 (1 - \exp(-\mathbf{i}ka)), \tag{A.6}$$

$$Z_{rad,ij} = i\omega\rho_0 \frac{\exp(-\mathbf{i}kr_{ij})}{2\pi r_{ij}} \partial\Gamma_{\omega,i}. \tag{A.7}$$

LISTE DES RÉFÉRENCES

[1] Christopher G. Albert, Giorgio Veronesi, Eugène Nijman, and Jan Rejlek. Prediction of the vibro-acoustic response of a structure-liner-fluid system based on a patch transfer function approach and direct experimental subsystem characterisation. *Applied Acoustics*, 112 :14–24, 2016.

[2] L Alimonti and N Atalla. Efficient modeling of flat and homogeneous acoustic treatments for vibroacoustic finite element analysis. direct field formulations. *Journal of Sound and Vibration*, 367 :84–100, 2016.

[3] L. Alimonti and N. Atalla. Efficient modeling of flat and homogeneous acoustic treatments for vibroacoustic finite element analysis. finite size correction by image sources. *Journal of Sound and Vibration*, 388 :201–215, 2017.

[4] Luca Alimonti. *Développement D'une Méthode Hybride Éléments Finis-matrice de Transfert Pour la Prédiction de la Réponse Vibroacoustique de Structures Avec Traitements Acoustiques*. PhD thesis, Université de Sherbrooke, 2015.

[5] Luca Alimonti, Noureddine Atalla, Alain Berry, and Franck Sgard. Assessment of a hybrid finite element-transfer matrix model for flat structures with homogeneous acoustic treatments. *The Journal of the Acoustical Society of America*, 135(5) :2694–2705, 2014.

[6] Luca Alimonti, Noureddine Atalla, Alain Berry, and Franck Sgard. A hybrid finite element-transfer matrix model for vibroacoustic systems with flat and homogeneous acoustic treatments. *The Journal of the Acoustical Society of America*, 137(2) :976–988, 2015.

[7] Luca Alimonti and B. Gardner. Practical noise control modeling for full spectrum vibroacoustic analysis. In *Proceedings of ISMA2016 Including USD2016*, pages 3883–3894. ISMA2016, 2016.

[8] Jean Allard and Noureddine Atalla. *Propagation of sound in porous media : modelling sound absorbing materials 2e*. John Wiley & Sons, 2009.

[9] N. Atalla and F. Sgard. *Finite Element and Boundary Methods in Structural Acoustics and Vibration*. CRC Press, 2015.

[10] Noureddine Atalla, Mohamed A Hamdi, and Raymond Panneton. Enhanced weak integral formulation for the mixed (u_, p_) poroelastic equations. *The Journal of the Acoustical Society of America*, 109(6) :3065–3068, 2001.

[11] Noureddine Atalla, Raymond Panneton, and Patricia Debergue. A mixed displacement-pressure formulation for poroelastic materials. *The Journal of the Acoustical Society of America*, 104(3) :1444–1452, 1998.

[12] M. Aucejo, L. Maxit, N. Totaro, and J.-L. Guyader. Convergence acceleration using the residual shape technique when solving structure-acoustic coupling with the patch transfer functions method. *Computers & Structures*, 88(11) :728–736, 2010.

[13] Maurice A Biot. Theory of propagation of elastic waves in a fluid-saturated porous solid. ii. higher frequency range. *The Journal of the acoustical Society of america*, 28(2) :179–191, 1956.

[14] Maurice A Biot. Theory of propagation of elastic waves in a fluid-saturated porous solid. ii. higher frequency range. *The Journal of the acoustical Society of america*, 28(2) :179–191, 1956.

[15] Maurice A Biot. Generalized theory of acoustic propagation in porous dissipative media. *The Journal of the Acoustical Society of America*, 34(9A) :1254–1264, 1962.

[16] A Blaise and C Lesueur. Acoustic transmission through a 2-d orthotropic multilayered infinite cylindrical shell. *Journal of Sound and Vibration*, 155(1) :95–109, 1992.

[17] A Blaise and C Lesueur. Acoustic transmission through a" 3-d" orthotropic multilayered infinite cylindrical shell, part i : Formulation of the problem. *Journal of sound and vibration*, 171(5) :651–664, 1994.

[18] A Blaise and C Lesueur. Acoustic transmission through a" 3-d" orthotropic multilayered infinite cylindrical shell, part ii : validation and numerical exploitation for large structures. *Journal of Sound and Vibration*, 171(5) :665–680, 1994.

[19] Christian Cacciolati and Jean-Louis Guyader. Acoustic mobility for vibroacoustic prediction. In *Procedings ICSV 7, Gaermische-Partenkirchen, Ger.*, 2000.

[20] Arnaud Caillet, Luca Alimonti, and Willem Van Hal. Efficient trim modelling simulation method for vehicle design phase. In *SAE Technical Paper*. SAE International, 06 2018.

[21] Yvan Champoux and Jean-F Allard. Dynamic tortuosity and bulk modulus in air-saturated porous media. *Journal of applied physics*, 70(4) :1975–1979, 1991.

[22] Jean-Daniel Chazot and Jean-Louis Guyader. Prediction of transmission loss of double panels with a patch-mobility method. *The Journal of the Acoustical Society of America*, 121(1) :267–278, 2007.

[23] Jean-Daniel Chazot and Jean-Louis Guyader. Transmission loss of double panels filled with porogranular materials. *The Journal of the Acoustical Society of America*, 126(6) :3040–3048, 2009.

[24] D. Chronopoulos, B. Troclet, M. Ichchou, and J.P. Lainé. A unified approach for the broadband vibroacoustic response of composite shells. *Composites Part B : Engineering*, 43(4) :1837 – 1846, 2012.

[25] Corentin Coguenanff, Arnaud Duval, and Mickael Goret. A spectral method for fast broadband insertion loss modeling of curved sound packages : correlation with

poroelastic finite elements. In *Proceedings of the 47th International Congress and Exposition on Noise Control Engineering*. Chicago, Illinois, USA, 2018.

[26] Theophane Courtois, Claudio Bertolini, and Juergen Ochs. A procedure for efficient trimmed body fe simulations, based on a transfer admittance model of the sound package. *SAE Int. J. Passeng. Cars - Mech. Syst.*, 3 :1–13, 06 2010.

[27] K. Daneshjou, A. Nouri, and R. Talebitooti. Analytical model of sound transmission through orthotropic cylindrical shells with subsonic external flow. *Aerospace Science and Technology*, 13(1) :18 – 26, 2009.

[28] K Daneshjou, H Ramezani, and R Talebitooti. Wave transmission through laminated composite double-walled cylindrical shell lined with porous materials. *Applied Mathematics and Mechanics*, 32(6) :701–718, 2011.

[29] J-F Deü, Walid Larbi, and Roger Ohayon. Vibration and transient response of structural–acoustic interior coupled systems with dissipative interface. *Computer Methods in Applied Mechanics and Engineering*, 197(51-52) :4894–4905, 2008.

[30] C Droz, C Zhou, MN Ichchou, and J-P Lainé. A hybrid wave-mode formulation for the vibro-acoustic analysis of 2d periodic structures. *Journal of Sound and Vibration*, 363 :285–302, 2016.

[31] Christophe Droz, Olivier Robin, Mohamed Ichchou, and Noureddine Atalla. Improving sound transmission loss at ring frequency of a curved panel using tunable 3d-printed small-scale resonators. *The Journal of the Acoustical Society of America*, 145(1) :EL72–EL78, 2019.

[32] Arnaud Duval, Ludovic Dejaeger, Julien Baratier, and Jean-François Rondeau. Structureborne and airborne insertion loss simulation of trimmed curved and flat panels using rayon-vtm-tl : implications for the 3d design of insulators. *Congrès SIA Confort automobile et ferroviaire - November 19-20, Le Mans, France, 2008*, 2008.

[33] F Errico, M Ichchou, S De Rosa, O Bareille, and F Franco. The modelling of the flow-induced vibrations of periodic flat and axial-symmetric structures with a wave-based method. *Journal of Sound and Vibration*, 424 :32–47, 2018.

[34] Sebastian Ghinet, Noureddine Atalla, and Haisam Osman. Diffuse field transmission into infinite sandwich composite and laminate composite cylinders. *Journal of sound and vibration*, 289(4-5) :745–778, 2006.

[35] Jean-Louis Guyader, Christian Cacciolati, and D Chazot. Transmission loss prediction of double panels filled with porous materials and mechanical stiffeners. In *Proceedings of ICA 2010, Sydney, Australia*, 2010.

[36] MA Hamdi, N Atalla, L Mebarek, and A Omrani. Novel mixed finite element formulation for the analysis of sound absorption by porous materials. In *Proceedings of Internoise*, 2000.

[37] David Linton Johnson, Joel Koplik, and Roger Dashen. Theory of dynamic permeability and tortuosity in fluid-saturated porous media. *Journal of fluid mechanics*, 176 :379–402, 1987.

[38] Stijn Jonckheere, Xianhui Li, and Wim Desmet. A matrix-free model order reduction scheme for vibro-acoustic problems with complex damping treatments. In *Proceedings of the 2016 International Conference on Noise and Vibration Engineering*, volume 1, pages 3521–3534, 2016.

[39] K Kesour and N Atalla. Transmission loss prediction through a curved structure-cavity system with attached sound packages by means of a hybrid patch transfer-green functions approach. In *Proceedings of the 47th International Congress and Exposition on Noise Control Engineering*. Chicago, Illinois, USA, 2018.

[40] Kamal Kesour and Noureddine Atalla. Assessment of a hybrid patch transfer-green functions method for predicting the vibroacoustic response of curved systems with attached noise control treatments. In *10th International Styrian Noise, Vibration & Harshness Congress : The European Automotive Noise Conference*. SAE International, jun 2018.

[41] Kamal Kesour and Noureddine Atalla. A hybrid patch transfer-green functions method to solve transmission loss problems of flat single and double walls with attached sound packages. *Journal of Sound and Vibration*, 429 :1 – 17, 2018.

[42] Michael J Kingan, Yi Yang, and Brian R Mace. Sound transmission through cylindrical structures using a wave and finite element method. *Wave Motion*, 2018.

[43] C.W. Kosten. The mean free path in room acoustics. *Acustica*, 10 :245–250, 1960. cited By 31.

[44] Leslie Robert Koval. On sound transmission into a thin cylindrical shell under "flight conditions". *Journal of Sound and Vibration*, 48(2) :265–275, 1976.

[45] Leslie Robert Koval. On sound transmission into an orthotropic shell. *Journal of Sound and Vibration*, 63(1) :51–59, 1979.

[46] Leslie Robert Koval. Sound transmission into a laminated composite cylindrical shell. *Journal of Sound and Vibration*, 71(4) :523–530, 1980.

[47] Denis Lafarge, Pavel Lemarinier, Jean F Allard, and Viggo Tarnow. Dynamic compressibility of air in porous structures at audible frequencies. *The Journal of the Acoustical Society of America*, 102(4) :1995–2006, 1997.

[48] RS Langley. Numerical evaluation of the acoustic radiation from planar structures with general baffle conditions using wavelets. *The Journal of the Acoustical Society of America*, 121(2) :766–777, 2007.

[49] Walid Larbi, J-F Deü, and Roger Ohayon. A new finite element formulation for internal acoustic problems with dissipative walls. *International journal for numerical methods in engineering*, 68(3) :381–399, 2006.

[50] Joon-H. Lee, J. Kim, and Han-J. Kim. Simplified method to solve sound transmission through structures lined with elastic porous material. *The Journal of the Acoustical Society of America*, 110(5) :2282–2294, 2001.

[51] Claude Lesueur. *Rayonnement acoustique des structures : vibroacoustique, interactions fluide-structure*. Eyrolles, 1988.

[52] Yu Liu and Chuanbo He. Diffuse field sound transmission through sandwich composite cylindrical shells with poroelastic core and external mean flow. *Composite Structures*, 135 :383 – 396, 2016.

[53] Brian R Mace and Elisabetta Manconi. Modelling wave propagation in two-dimensional structures using finite element analysis. *Journal of Sound and Vibration*, 318(4-5) :884–902, 2008.

[54] Julien Magniez, Jean-Daniel Chazot, Mohamed Ali Hamdi, and Bernard Troclet. A mixed 3d-shell analytical model for the prediction of sound transmission through sandwich cylinders. *Journal of Sound and Vibration*, 333(19) :4750–4770, 2014.

[55] Julien Magniez, Mohamed Ali Hamdi, Jean-Daniel Chazot, and Bernard Troclet. A mixed biot–shell analytical model for the prediction of sound transmission through a sandwich cylinder with a poroelastic core. *Journal of Sound and Vibration*, 360 :203 – 223, 2016.

[56] Elisabetta Manconi and Brian R Mace. Wave characterization of cylindrical and curved panels using a finite element method. *The Journal of the Acoustical Society of America*, 125(1) :154–163, 2009.

[57] Laurent Maxit, Mathieu Aucejo, and J-L Guyader. Improving the patch transfer function approach for fluid-structure modelling in heavy fluid. *Journal of Vibration and Acoustics*, 134(5), 2012.

[58] Laurent Maxit, Christian Cacciolati, and Jean-Louis Guyader. Airborne noise prediction using patch acoustic impedance. In *Proceedings of ICSV 9, Orlando, United-States*, 2002.

[59] DJ Mead. Wave propagation and natural modes in periodic systems : Ii. multi-coupled systems, with and without damping. *Journal of Sound and Vibration*, 40(1) :19–39, 1975.

[60] Abderrazak Mejdi, Franck Sgard, and Noureddine Atalla. Validity of transfer matrix method for prediction of the transmission loss of curved panels. In *Proceedings of Meetings on Acoustics ICA2013*, volume 19. ASA, 2013.

[61] J.-M. Mencik and M.N. Ichchou. Wave finite elements in guided elastodynamics with internal fluid. *International Journal of Solids and Structures*, 44(7) :2148 – 2167, 2007.

[62] Morvan Ouisse, Laurent Maxit, Christian Cacciolati, and Jean-Louis Guyader. Patch transfer functions as a tool to couple linear acoustic problems. *Journal of vibration and acoustics*, 127(5) :458–466, 2005.

[63] Raymond Panneton. Modélisation numérique tridimensionnelle par éléments finis des milieux poroélastiques. *These, Université de Sherbrooke, Canada*, 1996.

[64] Raymond Panneton. Comments on the limp frame equivalent fluid model for porous media. *The Journal of the Acoustical Society of America*, 122(6) :EL217–EL222, 2007.

[65] Raymond Panneton and Noureddine Atalla. An efficient finite element scheme for solving the three-dimensional poroelasticity problem in acoustics. *The Journal of the Acoustical Society of America*, 101(6) :3287–3298, 1997.

[66] Andrea Parrinello and GL Ghiringhelli. Transfer matrix representation for periodic planar media. *Journal of Sound and Vibration*, 371 :196–209, 2016.

[67] Goran Pavić. Mechanical noise synthesis by sub-structuring. *Diagnostyka*, pages 9–15, 2009.

[68] Allan D Pierce et al. *Acoustics : an introduction to its physical principles and applications*, volume 678. McGraw-Hill New York, 1981.

[69] Markus Polanz, Eugene Nijman, and Martin Schanz. The patch-transfer-function (ptf) method applied to numerical models of trim materials including poro-elastic layers. In *10th International Styrian Noise, Vibration & Harshness Congress : The European Automotive Noise Conference*. SAE International, jun 2018.

[70] H Ramezani and A Saghafi. Optimization of a composite double-walled cylindrical shell lined with porous materials for higher sound transmission loss by using a genetic algorithm. *Mechanics of Composite Materials*, 50(1) :71–82, 2014.

[71] Jamil M Renno and Brian R Mace. Calculating the forced response of cylinders and cylindrical shells using the wave and finite element method. *Journal of Sound and Vibration*, 333(21) :5340–5355, 2014.

[72] Dilal Rhazi. *Numerical modeling and experimental validation of the acoustic transmission of aircraft's double-wall structures including sound package*. PhD thesis, Université de Sherbrooke, 2012.

[73] Dilal Rhazi and Noureddine Atalla. A simple method to account for size effects in the transfer matrix method. *The Journal of the Acoustical Society of America*, 127(2) :EL30–EL36, 2010.

[74] Dilal Rhazi and Noureddine Atalla. Transfer matrix modeling of the vibroacoustic response of multi-materials structures under mechanical excitation. *Journal of Sound and Vibration*, 329(13) :2532 – 2546, 2010.

[75] Dilal Rhazi and Noureddine Atalla. Transfer matrix modeling of the vibroacoustic response of multi-materials structures under mechanical excitation. *Journal of Sound and Vibration*, 329(13) :2532 – 2546, 2010.

[76] Jean-François Rondeau, Armaud Duval, Julien Monet-Descombey, and Ludovic Dejaeger. Equivalent curvatures broadband insertion loss simulation technique coupling virtual sea and bem/fem approaches. In *INTER-NOISE and NOISE-CON Congress and Conference Proceedings*, volume 247, pages 3978–3987. Institute of Noise Control Engineering, 2013.

[77] Nicolas Schaefer, Bart Bergen, Stijn Jonckheere, and Wim Desmet. Application of a matrix-free model order reduction scheme to automotive treated panels. In *Proceedings of the 2016 International Conference on Noise and Vibration Engineering*, volume 1, pages 3863–3872, 2016.

[78] Nicolas Schaefer, Bart Bergen, Tomas Keppens, and Wim Desmet. A design space exploration framework for automotive sound packages in the mid-frequency range. Technical report, SAE Technical Paper, 2017.

[79] P Shorter and S Mueller. Modeling the mid-frequency response of poroelastic materials in vibro-acoustics applications. *in : Proceedings of SAPEM 2008, Bradford, UK*, pages 1–32, December 2008.

[80] Michel A Tournour, Fumihiko Kosaka, and Hirotaka Shiozaki. Fast acoustic trim modeling using transfer admittance and finite element method. Technical report, SAE Technical Paper, 2007.

[81] Kévin Verdière, Raymond Panneton, Saïd Elkoun, Thomas Dupont, and Philippe Leclaire. Transfer matrix method applied to the parallel assembly of sound absorbing materials. *The Journal of the Acoustical Society of America*, 134(6) :4648–4658, 2013.

[82] Giorgio Veronesi, Christopher Albert, Eugène Nijman, Jan Rejlek, and Arnaud Bocquillet. Patch transfer function approach for analysis of coupled vibro-acoustic problems involving porous materials. In *8th International Styrian Noise, Vibration & Harshness Congress : The European Automotive Noise Conference*. SAE International, jun 2014.

[83] T. Yamamoto, S. Maruyama, S. Nishiwaki, and M. Yoshimura. Thickness optimization of a multilayered structure on the coupling surface between a structure and an acoustic cavity. *Journal of Sound and Vibration*, 318(1) :109–130, 2008.

[84] Jie Zhou, Atul Bhaskar, and Xin Zhang. The effect of external mean flow on sound transmission through double-walled cylindrical shells lined with poroelastic material. *Journal of Sound and Vibration*, 333(7) :1972–1990, 2014.

[85] Jie Zhou, Atul Bhaskar, and Xin Zhang. Sound transmission through double cylindrical shells lined with porous material under turbulent boundary layer excitation. *Journal of Sound and Vibration*, 357 :253–268, 2015.